

Experimental Blade Research - phase 2



Department of Wind Energy E Report 2015

M.A. Eder, K. Branner, P. Berring, F. Belloni, H.S. Toft,
J.D. Sørensen, A. Corre, T. Lindby, A. Quispitupa &
T.K. Petersen

Edited by K. Branner

DTU Wind Energy E-0083

March 2015

DTU Vindenergi
Institut for Vindenergi



Authors: M.A. Eder, K. Branner, P. Berring, F. Belloni, H.S. Toft, J.D.

Sørensen, A. Corre, T. Lindby, A. Quispitupa & T.K. Petersen

Title: Experimental Blade Research - phase 2

Department: Department of Wind Energy

Summary (max 2000 characters):

The following persons have contributed to the project and their contributions are highly appreciated.

LM Wind Power A/S: Torben Lindby, Hank McShane, Cornelis van Beveren & Adrien Corre

SSP Technology A/S: Claus Burchardt, Flemming Sørensen & Christopher Stanley

Vestas Wind Systems A/S (until 2012): Tomas Vronsky & Jakob Wedel-Heinen

DNV GL AS: Christer Eriksson, Dayton Griffin, Tomasz Sieradzan, Ole Kjær, Bente Vestergaard, Amilcar Quispitupa & Thomas Karl Petersen

Dong Energy: Bernt Pedersen & Jacob Kronborg Andersen

Blade Test Centre A/S: Carsten Skamris

Bladena ApS: Find Mølholt Jensen, Mikkel Lagerbon & Andrei Buliga

Baumer A/S: Anders Rosborg Hjulmann, Martin Jørgensen & Michael Weigel

German Aerospace Center (DLR): Alexander Kling & Tobias Wille

Swerea SICOMP AB: Sören Nilsson

Aalborg University: John Dalsgaard Sørensen & Henrik Stensgaard Toft

DTU Mechanical Engineering: Christian Berggreen & Jacob Herold Høgh

DTU Wind Energy (alphabetic order): Andreas Waage Borgen, Angelo Tesauro, Basel Hayatleh, Christen Malte Markussen, Christian Pavese, Claus

Brian Munk Pedersen, Erik Vogeley, Federico Belloni, Gilmar Ferreira

Pereira, Jan Sjølin, Jonas Kreutzfeldt Heininge, Jonathan Shmueli Alvarado,

José Pedro Blasques, Kim Branner, Magda Kirstine Nielsen, Mahmoud

Jabbari, Malcolm Mcgugan, Martin A. Eder, Per Hørlyk Nielsen, Peter

Berring, Philipp Ulrich Haselbach, Robert David Bitsche, Taeseong Kim,

Thomas Buhl, Tom Løgstrup Andersen & Vladimir A. Fedorov

DTU Wind Energy E-0083

March 2015

Contract no.:

J.nr. 64011-0006

Project no.:

Sponsorship:

Energiteknologisk udvikling og demonstration (EUDP)

Front page:

Pages: 108

Tables: 13

References: 23

Danmarks Tekniske Universitet

DTU Vindenergi

Nils Koppels Allé

Bygning 403

2800 Kgs. Lyngby

Telephone 46775470

kibr@dtu.dk

www.vindenergi.dtu.dk

Project details

Project title	Experimental Blade Research - phase 2
Project identification (program abbrev. and file)	J.nr. 64011-0006
Name of the programme which has funded the project	Energiteknologisk udvikling og demonstration (EUDP)
Project managing company/institution (name and address)	DTU Vindenergi, Risø Campus, Frederiksborgvej 399, 4000 Roskilde
Project partners	LM Wind Power A/S, SSP Technology A/S, Vestas Wind Systems A/S (until 2012), DNV GL AS, Dong Energy, Blade Test Centre A/S, Bladena ApS, Baumer A/S, German Aerospace Center (DLR), Swerea SICOMP AB & Aalborg University
CVR (central business register)	30060946
Date for submission	March 31, 2015

Content

- Summary 6

- 1. Project overview 7
 - 1.1 Project details..... 7
 - 1.2 Short description of project objective and results 7
 - 1.3 Executive summary 7
 - 1.4 Project objectives 8
 - 1.5 Project results and dissemination of results 10
 - 1.6 Utilization of project results 11
 - 1.7 Project conclusion and perspective 13

- 2. Blade road map 13
 - 2.1 Design challenges and short-term and long-term goals for blades 14
 - 2.2 Capabilities of different methods and tools..... 18
 - 2.3 Using project results in certification requirements and design guidelines..... 21

- 3. Load envelope and load carrying capacity 24
 - 3.1 The 3D load envelope 24
 - 3.2 Load carrying capacity and failure modes 26

- 4. Full-scale blade testing..... 30
 - 4.1 Blade testing methodology 32
 - 4.2 Blade test results..... 42

- 5. Numerical analysis methods 52
 - 5.1 3D-modelling methodology..... 53
 - 5.2 3D-modelling results..... 54
 - 5.3 Slice model methodology 57
 - 5.4 Slice modelling results..... 60

- 6. Analytical method 62
 - 6.1 Analytical methodology 63
 - 6.2 Analytical results 65

- 7. Sub-component test 67
 - 7.1 Sub-component testing methodology 67
 - 7.2 Development of a framework for reliability analysis of wind turbine blades 71
 - 7.3 Sub-component tests focusing on failure of trailing edge bonds 77
 - 7.4 Trailing edge strength..... 80

- 8. Discussion 94

- References 99
 - Publications from current project 99

Other publications	100
Appendix A Manufacturing the trailing edge specimens	101
Appendix B Trailing edge test setup and methodology.....	102
Appendix C Trailing edge test results	104
Acknowledgements	107

Summary

This report is a summary of the results obtained in the project: Experimental Blade Research – phase 2 (EBR2). The project was supported by the Danish Energy Authority through the 2010 Energy Technology Development and Demonstration Program (EUDP 2010-II) and has journal no. 64011-0006. The project has been running from spring 2011 to the end of 2014.

Being a summary report, this report only contains a collection of the research topics and the major results. For more details, see the publications listed at the end of this report.

1. Project overview

In this chapter of this final report, a project overview is given, which can be used for general dissemination purposes. In the rest of this report a summary of the technical and scientific results are presented, which can be used for more technical dissemination purposes.

Being a summary report, this report only contains a collection of the research topics and the major results. For more details, see the publications listed at the end of this report.

1.1 Project details

See page 3 for project details.

1.2 Short description of project objective and results

English version

The objective of this project is to develop the experimental platform needed to obtain better structural design of wind turbine blades. This is achieved by developing new test and measuring methods. It is also achieved by developing numerical and analytical design tools that model the structural behaviour observed in experiments. A design framework that gives guidance on how to choose the appropriate numerical analyses and structural tests needed to obtain the optimal design at a certain level of reliability is also developed. Three blades have been tested to failure and special focus in the project has been on understanding failure in adhesive bonds and improvement of design methods for these.

Danish version

Formålet med dette projekt er at udvikle den eksperimentelle platform der behøves for at opnå bedre strukturelt design af vindmøllevinger. Dette er nået ved udvikling af nye test og måle metoder. Det er også nået ved udvikling af numeriske og analytiske design værktøjer som modellerer den strukturelle opførelse som observeres ved forsøg. Et design rammeværktøj er også udviklet. Dette giver vejledning i, hvilke numeriske analyser og strukturelle tests der er nødvendige for at opnå et optimalt design på et vist niveau af pålidelighed. Tre vinger er blevet testet til svigt i projektet og særligt fokus har været på at forstå svigt i limsamlinger og forbedring af designmetoderne for disse.

1.3 Executive summary

The objective of this project was to develop the experimental platform needed to obtain better structural design of wind turbine blades. This is a long term goal and this project has contributed significantly to this goal. However, there is still much to do as the blade roadmap in chapter 2 illustrates. New test and measuring methods have been developed. New numerical and analytical design tools that model the structural behaviour observed in experiments have been developed. And a design framework that guides on how to choose the appropriate numerical analyses and structural tests needed to obtain the optimal design at a certain level of reliability has also been developed. Most of the project has evolved around the three full-scale tests to

ultimate failure and understanding failure in trailing edge adhesive bonds and improvement of design methods for these has also been a red thread through the project.

The project was organized in 4 work packages (WP) in which the following activities were covered:

- WP1 - Development of a road map based on different tools.
- WP2 - Full scale blade tests.
- WP4 - Failure modes
- WP5 - Sub component tests.

The purpose of these activities was to ensure that wind turbine manufacturers and blade manufacturers can obtain higher reliability and reduce development costs and time for new blade designs, thereby realizing shorter time to market and competitive positioning opportunities.

The project has contributed to improving the quality of the wind turbine blades manufactured at the project partner LM Wind Power, as the project has provided insight into the failure modes and structural mechanisms in the blades. Furthermore, the project has contributed to understanding how test of blades and components can be performed.

Project results like, use of sub-component test data for blade design, design of bonded joints based on a fracture mechanics approach and blade testing under combined loading are currently being examined and assessed internally at another project partner DNV GL. DNV GL is working on developing a blade standard and these project results are on the agenda. The DNV GL blade standard is foreseen to be ready by end of 2015. DNV GL states that this project has produced research results that are relevant for the wind turbine blade industry. We are confident that the project results will make it into certification requirements and design guidelines and therefore provide a positive quality improvement for the whole wind turbine blade industry.

The blade roadmap presented in chapter 2 is also intended to serve the wind turbine blade industry and the research and development community as a guide for the near future development within wind turbine blade research, development and demonstration. Future research, development and demonstration project applications will be based on this roadmap.

1.4 Project objectives

The need for more fast and cost effective design tools has been addressed by several of the major players in the Danish wind power industry. Thus, to meet the demands from the wind turbine manufactures it is necessary to constantly focus on ways to increase profitability and reliability of wind turbines and to realize these ambitions without compromising time and cost.

The project was organized in 4 work packages (WP) in which the following activities were covered:

- WP1 - Development of a road map based on different tools.

- WP2 - Full scale blade tests.
- WP4 - Failure modes
- WP5 - Sub component tests.

The purpose of these activities was to ensure that wind turbine manufacturers and blade manufacturers can obtain higher reliability and reduce development costs and time for new blade designs, thereby realizing shorter time to market and competitive positioning opportunities.

Originally the project had a WP3 on down-scale testing. However, this work package was dropped as it early in the project became possible to have three 34m SSP-blades for full scale testing instead of the two load-carrying SSP-box-girders and two down-scaled box-girders that originally were intended to be tested.

Testing three full-scale blades has shown to be good decision. Much has been learned from the three tests, different measuring techniques and equipment has been used, new measuring techniques developed and the tests have triggered the development of promising new numerical, experimental and analytical methods as described in the rest of the report.

The milestones shown in Table 1 were agreed with EUDP.

Table 1 Overview of milestone status.

Technical milestones	Status
M1 (WP2): Complete test of 1 st blade	Completed
M2 (WP2): Complete test of 2 nd blade	Completed
M3 (WP2): Complete test of 3 rd blade	Completed
M4 (WP4): Complete failure analysis of blade and comparison with full-scale tests	Completed
M5 (WP5): Comparison of results from sub-component and full-scale tests	Completed
M6 (WP5): Recommendations for future sub component tests	Completed
M7 (WP1): Recommendations for future design and test standards	Completed
Commercial milestones	
M8 (WP5): DNV guideline for accepting smaller design modifications using sub-component testing and demonstration at an industry partner	Ongoing*
M9 (WP4): DNV guideline for choosing full-scale static tests in combined loading based on 3D load envelope	Ongoing*

* DNV are in the process of meeting these commercial milestones, by implementing project results into a new blade standard (see section 2.3)

The completion of milestones M1, M2 and M3 is documented in chapter 3 and 4. The completion of M4 is documented in chapter 3. The completion of M5 and M6 is documented in chapter 7. The completion of M7 is documented in chapter 2. Finally, the completion of the commercial milestones M8 and M9 has come as far as possible within the timeframe of this

project as documented in section 2.3. Implementing new knowledge into certification requirements and design guidelines is not strait forward and it takes time.

The project had two university partners (DTU & Aalborg University) and 8 industrial partners (LM Wind Power A/S, SSP Technology A/S, Vestas Wind Systems A/S (until 2012), DNV GL AS, Dong Energy, Blade Test Centre A/S, Bladena ApS & Baumer A/S) and two non-Danish research institution partners (German Aerospace Center (DLR) & Swerea SICOMP AB). All partners have contributed to the discussions and workshops throughout the project, but not all partners have been as active as originally planned.

From a technology point of view it has also turned out to be more difficult than anticipated to develop a sub-component test for larger blade parts. The technology of applying intelligent boundary conditions on larger sub-component specimens is in general not mature yet.

1.5 Project results and dissemination of results

Most of the project has evolved around the three full-scale tests to ultimate failure and understanding failure in trailing edge adhesive bonds and improvement of design methods for these has also been a red thread through the project.

Some of the main results obtained in the project are:

- A method for obtaining a 3D load envelope based on aeroelastic simulations has been developed and demonstrated for the full-scale blades tested in the project.
- The load carrying capacity of the full-scale blades in different load directions has been computed based on the governing failure modes. The failure modes considered are material failure criterion Tsai-Wu, nonlinear Eigenvalue buckling analysis and shear distortion failure (lateral buckling).
- The results from the ultimate blade tests are compared with the expected failure predicted by the numerical simulations. The failure modes observed in all three tests were very similar and was in very good agreement with the numerical predictions in this project.
- Small Displacement Measurement System (SDMS) has been developed in order to perform reliable measurements of trailing edge adhesive joint deformations during the full-scale tests. The SDMS offers a wide variety of different applications because of its versatility.
- A fully automatic image processing software (AIPS) was developed with the capability to automatically process a large number of images from SDMS avoiding the introduction of human error.
- SDMS measurements revealed that the trailing edge opens and closes for different loading directions. In the present report it could be shown experimentally that the trailing edge opened under +30 degree loading and closed under -30 degree loading. These insights were an essential starting point for further investigations which eventually led to a deep understanding of trailing edge deformation behaviour on a theoretical level.
- SDMS and AIPS were used on a larger scale with success to measure the global deformations i.e. buckling wave of the trailing edge.
- Local buckling analysis conducted on two different models showed that local buckling can have a significant influence on the integrity of adhesively bonded joints. Once local buckling is present in the trailing edge pretty much all fracture modes appear depending on the location along the wave.

- Fiber optical strain gauges were used to measure both longitudinal and transversal surface strains along the trailing edge of the blade. The measurement methodology was tailor made to pick up the occurrence of the buckling wave at an early loading stage.
- The double cantilever beam tests conducted on three different flow front geometries showed that mitigation of the singularity due to rounded flow front shapes increases the initiation fracture energy. On the other hand in 50% of the investigated cases the crack initiated in the rounded region and propagated a long way in the adhesive. Considering the low critical energy release rate of the adhesive compared to interface cracks this behaviour is considered unsatisfactory.
- Based on the probabilistic framework developed within the project it is possible for wind turbine manufacturers to quantify the information obtained from coupon, sub-component and full-scale testing, and in some cases to combine the information obtained using a Bayesian approach. This information can be used for reliability assessment and calibration of partial safety factors, and for decision making on which types of tests to perform and how many tests.

For a more detailed description of the results obtained in the project then consult chapter 2 to 8 in this report.

The objective of this project was to develop the experimental platform needed to obtain better structural design of wind turbine blades. This is a long term goal and this project has contributed significantly to this goal. However, there is still much to do as the blade roadmap in chapter 2 illustrates. New test and measuring methods have been developed. New numerical and analytical design tools that model the structural behaviour observed in experiments have been developed. And a design framework that guides on how to choose the appropriate numerical analyses and structural tests needed to obtain the optimal design at a certain level of reliability has also been developed.

Project results been disseminated during the project to the project partners by workshops for all participants, steering committee meetings and different meetings between two or more of the project partners.

Project results have also been disseminated by publications in international journals and by oral presentations at national meetings and at international conferences in Europe, Asia and America. More journal and conference publications are in the pipeline.

A video from the full-scale test to failure of the first blade was shown on TV2 Lorry August 27, 2013 in a program about green energy in the program-series "Region Hovedstaden: En international metropol".

Further disseminated of project results to the industry and broader public is currently under planning.

1.6 Utilization of project results

Some of the results obtained in the project are already being utilized by some of the industrial project partners.

LM Wind Power is working with many of the same subjects that have been part of this project and therefore there have throughout the project been a natural interest in the developed methods. The project has contributed to improving the quality of the wind turbine blades manufactured at LM Wind Power as the project has provided insight into the failure modes and structural mechanisms in the blades. Furthermore, the project has contributed to understanding how test of blades and components can be performed.

In particular, design of bonded joints based on a fracture mechanics approach is an interest by LM Wind Power. As part of this project LM Wind Power has performed component tests on a trailing edge as well as several series of coupon tests, where two types of specimens were tested to measure the mode I fracture toughness of the interface laminate adhesive and to investigate the effect of crack front on strength, respectively.

DNV GL is currently reviewing results from the project and is planning to incorporate the following in the coming blade standard:

- Use of sub-component test data for blade design
- Design of bonded joints based on a fracture mechanics approach
- Blade testing under combined loading

The procedures for including sub-component test data have been outlined in WP5. DNV GL will explicitly define a reliability index and a failure probability for blades. In this manner, when incorporating sub-component test data for blade designs, the reliability index and probability of failure shall be kept or improved. By defining a reliability index and probability of failure for wind turbine blades, it would also allow performing calibration of material safety factors. This might also lead to, reduction of the extent of full-scale blade testing.

Published scientific literature suggests that fracture mechanics data of cracked bonded joints exhibits large scatter. Current design standards assume that test data follows a normal distribution which may not necessarily fit bonded joints data. This calls for more sophisticated statistical models to analyse the data and to determine characteristic design values. The new DNV GL standard will also define and recommend number of specimens to be tested, loading conditions, mixed mode ratios and test methods. In connection to using advanced fracture mechanics methods, the DNV GL material safety factor might be re-evaluated.

As an outcome of this project it has been demonstrated that the maximum bending moments for ultimate limit state does not happen at flap or edgewise direction, but at a given angle with respect to the flapwise direction. This angle introduces a combined flap and edgewise loading. DNV GL is considering how this can be implemented in the coming blade standard. However, further research is needed in the area of fatigue testing under combined loading.

The results obtained in the project have also attracted interest from industry outside the project group.

The results from the project are also partly used in teaching of future engineers at DTU. Knowledge and results from the project have been used in at least the following courses at DTU Wind Energy:

- 46000 - Introduction to Wind Energy
- 46300 - Wind Turbine Technology and Aerodynamics
- 46411 - Design of Large Composite Structures

Project results are also used in PhD projects.

1.7 Project conclusion and perspective

The project has to a large extent met the objectives.

The project has contributed to improving the quality of the wind turbine blades manufactured at LM Wind Power as the project has provided insight into the failure modes and structural mechanisms in the blades. Furthermore, the project has contributed to understanding how test of blades and components can be performed. We are confident that the project results also will improve the quality of wind turbine blades made by other blade manufacturers.

Project results like, use of sub-component test data for blade design, design of bonded joints based on a fracture mechanics approach and blade testing under combined loading are currently being examined and assessed internally at DNV GL. DNV GL is working on developing a blade standard and these project results are on the agenda. The DNV GL blade standard is foreseen to be ready by end of 2015. DNV GL states that this project has produced research results that are relevant for the wind turbine blade industry. We are confident that the project results will make it into certification requirements and design guidelines and therefore provide a positive quality improvement for the whole wind turbine blade industry.

We also believe that the industry will benefit from other project results that not yet are proper implemented in the industry.

The blade roadmap presented in chapter 2 is also intended to serve the wind turbine blade industry and the research and development community as a guide for the near future development within wind turbine blade research, development and demonstration. Future research, development and demonstration project applications will be based on this roadmap.

2. Blade road map

A technology roadmap is a **plan** that matches short-term and long-term **goals** with specific **technology solutions** to help meet those goals.

The goal for this blade roadmap is that it will lead to better structural design of wind turbine blades.

2.1 Design challenges and short-term and long-term goals for blades

Based on several discussions and workshops during the project period, a number of design challenges for wind turbine blades has been identified and listed here. The blade road map is then a plan that set these design challenges as goals and matches them with specific technology solutions that can solve the design challenges.

Design challenges:

- Sufficient blade stiffness and strength
- Robust adhesive joints
- Predicting strength reduction due to manufacturing defects and damage
- Predicting fatigue life
- Reliable repair methods
- Reducing erosion and wear

The following technology solutions are then considered to find areas where research and development is needed in order to meet the design challenges:

- Test at different scales
- Numerical, analytical and optimization tools
- Reliability methods

Challenge: Sufficient blade stiffness and strength

Experimental solutions

- Identify and test most critical load directions in combined loading.
- Account for torsional loading to make sure blades are loaded realistically in torsion.
- Improve load application method so it comes closer to real loading, more load points and loading clamps to not restrict blade deformations (anchor plates is a possible solution).
- Develop cutting edge technologies to monitor blade structures and materials both statically and dynamically
- Develop a reliable method for performing down-scaled testing of wind turbine blades and mapping the possibilities and limitations of this test method.

Numerical solutions

- Base analysis on non-linear finite element methods.
- Predict static strength based on load and capacity envelopes in combined loading.
- Develop and implement better methods to predict buckling strength of blades.
- Developing multi-scale design methods.

Reliability methods

- Stochastic modelling of stiffness and strength parameters at various scales for reliability assessment and probabilistic design.

Challenge: Robust adhesive joints

Experimental solutions

- Measuring what local loading adhesive joints experience.

- Developing sub-component methods to test adhesive bonds under realistic loading conditions.

Numerical solutions

- Implementing fracture mechanical models from material level at structural design level.
- Development of a fracture mechanics approach for adhesive joints in blades.

Reliability methods

- Develop a more damage tolerant design procedure.
- Develop stochastic models for the adhesive material and geometrical properties (size) after manufacturing for use in probabilistic design.

Challenge: Predicting strength reduction due to manufacturing defects and damage

Experimental solutions

- Understanding how imperfections introduce failure. In situ measurements.
- Testing imperfection such as wrinkles and delaminations under realistic loading and in realistic structures. This could maybe be done by developing appropriate sub-component test methods.

Numerical solutions

- Developing models to include imperfections in the design process.

Reliability methods

- Stochastic modelling of manufacturing defects.
- Reliability assessment including random manufacturing defects.
- Reliability based planning of inspections and operation & maintenance with respect to random defects.

Challenge: Predicting fatigue life

Experimental solutions

- Understanding the degradation of composite materials in fatigue. In situ measurements.
- Understanding the effect of loading history.
- Develop more realistic methods for testing blades in fatigue. Can be based on dual axis test methods or done in combined loading.

Numerical solutions

- Going beyond Miners rule and rainflow counting.
- Developing advanced fatigue models based on the real physical fatigue mechanisms.
- Developing methods to predict remaining lifetime and possible lifetime extension.

Reliability methods

- Accurate estimation of reliability as function of time and of the remaining lifetime with reliability larger than the target reliability level.
- Calibration of partial safety factors in order to obtain the target reliability level.

Challenge: Reliable repair methods

Experimental solutions

- Developing reliable repair procedures and methods for experimental validation of their soundness.

Numerical solutions

- Developing methods to predict static and fatigue strength of repaired composite structures.

Reliability methods:

- Stochastic models for the quality of a repair which can be implemented in the operation & maintenance strategy for cost optimal decision making.

Challenge: Reducing erosion and wear

Experimental solutions

- Establish relevant test methods to understand erosion and wear mechanisms.
- Identify damage initiation for different coating types.

Numerical solutions

- Developing finite element method for predicting the effect of impact on coating and substrate.

Target

The target for the blade roadmap is that the plan with the suggested specific technology solutions will lead to reduced rotor weight per MW, reduction in rotor manufacturing time per MW, reduction in rotor manufacturing cost per MW, reduction in O & M cost for blades, reduction in blade damage incidents and reduction in blade damage repair cost.

The blade roadmap is presented in Figure 1.

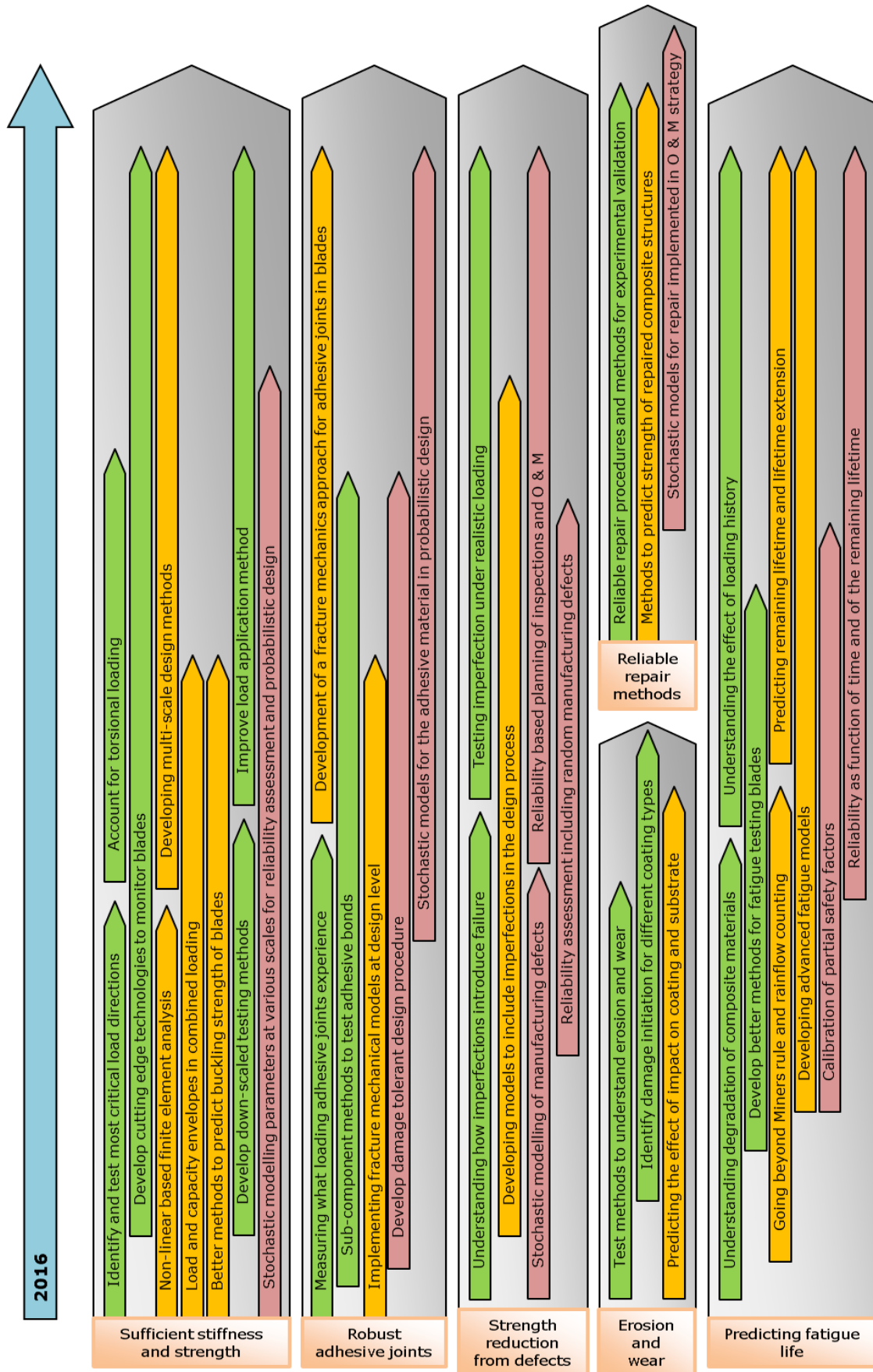


Figure 1 Blade roadmap. Green arrows represent experimental solutions, orange numerical solutions and reddish brown reliability methods.

2.2 Capabilities of different methods and tools

This section describes the tools that are currently used for blade design at the project partners. Also tools that can be used in the future are described. The positive features and shortcomings of the tools are listed. It is also listed how the tools depends on or interact with other tools and finally how the tools are viewed by the certifying bodies.

2.2.1 Experimental tools

Coupon tests

Coupon tests are routinely used to establish the stress/strain limits for composite failure criteria used in the design process. The number and type of tests required will depend on the composite failure criteria chosen. Coupon test are also used to establish S-N-curves for fatigue life predictions. Fracture mechanics tests can be used to measure the fracture toughness of interfaces. If the influence of parameters like fiber volume fraction and temperature on the test results should be investigated, the number of tests required can be very large.

Coupon tests including manufacturing defects and structural details

Testing specimen containing manufacturing defects (e.g. wrinkles) or structural details (e.g. ply drops) offers several advantages:

- The results are more representative of the real blade.
- The size of acceptable manufacturing defects can be determined.

A research project could standardize manufacturing defects and structural details and establishes a database comparable to the OptiDAT database. Such a database would be of great value to the industry. Of course, in order to fully benefit from the idea, certification rules (safety factors) would have to be adapted accordingly.

Sub-component tests

Sub-component tests are today mainly used to test the strength of adhesive connections and the strength of the root inserts. The tests result in critical forces and moments that can be compared to the results obtained from three dimensional finite element models. A downfall of these tests is that is difficult to apply realistic boundary conditions to the sub-components. Another major downfall is that the so-called edge effects will often lead to very conservative results.

An attractive alternative to using sub-component tests directly (as described above) is using them for the verification or calibration of advanced numerical models. This strategy mitigates the problems associated with boundary conditions and edge effects. On the other hand the complexity of the numerical models involved may pose an additional challenge.

Full-scale tests

Static full-scale tests are usually performed by applying concentrated loads at certain cross-sections of the blade. Dynamic (fatigue) full scale tests are usually performed by exciting one of the natural frequencies of the blade. Both tests are part of the normal certification process of a wind turbine blade. These tests are very realistic in the sense that the real structure is tested and may be able to capture some failure modes that other tests and models did not capture. There are, however, a number of disadvantages:

- The tests are very expensive and time-consuming. Therefore, they can usually only be performed at a very late stage of the design process as a last verification step.
- Usually only a single blade is tested. Therefore, the results are statistically insignificant.
- For the static tests load application poses a challenge.
- For the fatigue tests achieving the required test load level in a big part of the blade poses a challenge.
- The concept of “fatigue equivalent loads” is known to be problematic.

Down-scaled tests

It has been suggested that some of the downfalls of full-scale tests described above could be mitigated by performing these tests on geometrically down-scaled blades.

Advantages:

- The costs for down-scaled blades are much lower. Therefore a larger number of tests could be performed yielding statistically significant results. Moreover, the tests could be performed at an earlier stage of the design process.
- As the natural frequencies of the down-scaled blade are higher, more load cycles could be reached in a given time.

Disadvantages / open questions:

- How well would a geometrically down-scaled blade represent the real blade?
- It is far from obvious how to down-scale the composite layup. Example: How to downscale a sandwich which has only 1 ply of composite material as face layers?
- Can we make sure that the manufacturing errors of the down-scaled blades are representative of the manufacturing errors of the real blade?
- New moulds would have to be manufactured for the down-scaled blades.

The list of disadvantages and open questions above indicates that a lot of basic research would be required before down-scaled tests can become a tool used by the industry and accepted by certification bodies. An improved understanding of scaling-effects in large composite structures would also provide additional advantages: It would allow blade designers to more efficiently transfer the know-how gained when designing a blade to the next generation of (larger) blades.

2.2.2 Numerical tools

Aeroelastic Turbine Models

Aeroelastic models of wind turbines capture the two-way interaction between the aerodynamics and the deformation of the turbine. Examples are: Bladed, FLEX and HAWC2. Aeroelastic models are necessary to analyze the dynamics of the wind turbine and compute realistic loads that act on the individual components of the turbine. As these models need to be computationally efficient, the structural part of the model is usually based on beam theory.

Advantages:

- Model of the entire turbine / turbine dynamics.
- Computationally efficient

- Simulation results can be compared to measurements from real turbines
- Can predict whether the blades hit the tower (tip clearance)
- Can predict the loads that act on individual components of the turbine

Disadvantages:

- The models are based on a strong simplification of reality, both in terms of aerodynamics and structural mechanics.
- Input parameters can be difficult to obtain (e.g. the input parameters for a beam model that correctly represents a bend-twist coupled blade)

Cross Section Analysis Tools

Cross section analysis tools can compute the cross section stiffness and inertia properties of wind turbine blades based on a two-dimensional description of the cross sections. Examples are VABS, BECAS and LMBlades. The cross section stiffness and inertia properties serve as input parameters for beam theory based models (e.g. aeroelastic simulation tools). Optionally, cross section analysis tools can also recover local stress and strain fields from the cross section forces and moments computed using a beam model. Some tools can also perform preliminary buckling analysis.

Advantages:

- Efficient computation of cross section stiffness properties required as input for other tools
- Only a two-dimensional description of blade cross sections is required as input.
- Efficient computation of local stress and strain fields
- Efficient strength and fatigue life analysis
- Efficient preliminary buckling analysis
- The two-dimensional description of the cross section may contain a very high level of detail.

Disadvantages:

- Some tools disregard the taper and twist of the blade.
- Usually limited to linear analysis (e.g. the Brazier effect cannot be modeled).
- Buckling analysis is only approximate.

Three dimension finite element models

Three dimensional finite element models discretize the entire blade using shell elements or solid (continuum) elements. While models using shell elements are easier to generate and are computationally efficient, continuum elements generally allow for a more detailed description of the actual blade. The two modelling strategies may also be mixed. Models using shell elements with nodes offset from the mid-surface are known to yield inaccurate results in several commercial finite element programs. It seems however to be solved in more recent versions of the finite element programs.

The models are usually loaded by applying concentrated forces to certain groups of nodes in order to achieve a certain distribution of cross section forces in the blade (e.g. the ultimate bending moments). Buckling loads can be determined using eigenvalue buckling analysis and

non-linear static analysis. Fracture mechanics based methods (e.g. Cohesive elements, VCCT, contour integral methods) allow for the analysis of adhesive joints and delaminations. Sub-modelling techniques can be used to obtain an accurate solution in a local region. Cross section stiffness properties can be derived based on the predicted deformation of the blade. Alternatively, the predicted dynamic mode shapes and natural frequencies may serve as input for the aeroelastic simulation.

Advantages:

- Very realistic model (few simplifying assumptions are made)
- Possibility to predict local buckling phenomena
- The consideration of geometrical or material non-linearities is usually straight forward.

Disadvantages:

- Computationally expensive
- Usually only a limited number of load cases is considered (as the model is computationally expensive)
- Model generation may be time-consuming

Optimization Tools

Various mathematical optimization tools are usually used in conjunction with other tools described in this section. An example would be the minimization of blade mass with restrictions regarding strain, tip deflection, fatigue, buckling loads and manufacturability. In the future topology optimization methods may be used to find the optimum material distributions in a given design space.

Consistency between different numerical tools

Besides the advantages and disadvantages of the different numerical tools listed in this section, the consistency between these tools also deserves attention. Examples:

- Are the beam model used in the aeroelastic model and the three-dimensional finite element model consistent?
- Are the loads (cross-section forces and moments) computed using the aero-elastic model applied to the three-dimensional finite element model in a consistent way?

2.3 Using project results in certification requirements and design guidelines

DNV, now DNV GL is the leading certification body within the wind industry. As partner on the “Experimental Blade Research – Phase II (EBR-II)” research project, DNV GL has acted as collector of the research outcomes in order to translate them into certification requirements and/or design guidelines. The certification requirements will assist the wind industry in order to have more reliably blade designs. At the moment, DNV GL is in the process of developing and writing a standard addressing design, manufacturing and testing of wind turbine blades. The EBR-II research outcomes are relevant for the wind industry and will be used as input for the

DNV GL blade standard. The following topics were addressed within EBR-II and are planned to be incorporated in the blade standard:

1. Use of sub-component test data for blade design
2. Design of bonded joints based on a fracture mechanics approach
3. Blade testing under combined loading

The listed items are further discussed below.

2.3.1 Use of sub-component test data for blade design

Wind turbine blades are regarded as the most complex and critical components of a wind turbine. It is generally composed by several sub-components. Typical sub-components are:

- Thick root sections with embedded or bonded steel insert for connecting the blade to the blade bearing. The design of this sub-component is a complex task and in general, the design values are derived from representative sub-component testing. Characteristic design values are derived from static and fatigue tests.
- Spar cap to web bonded joint. This bonded joint can be subjected to a combined loading of mode I, mode II, mode III, or a combination of them. Due to different elastic properties of materials being joined and mixed mode loading, complex failure modes are expected.
- Trailing edge bonded joint, i.e. joint between lower and upper blade shells at the blade's trailing edge. This is similar to the case above. The out-of-plane deformations at the trailing edge may introduce a significant mode I loading reducing the strength of the bonded joint dramatically.

The use of sub-component test data for blade design is a topic that is receiving a lot of attention by blade manufactures. Current design standard or/and guidelines do not clearly define a method or process for incorporating sub-component testing on blade design procedures. In order to use sub-component test data for blade design, the end safety level of the blade has to be the same or better than when using coupon test data. The safety level of a blade is defined by a reliability index and failure probability. The DNV-DS-J102 blade standard does not specifically prescribes these parameters, but refers to DNV-OS-C501 for defining a base material safety factor for composites with a probability of failure of $< 10^{-4}$, low safety class and brittle failure mode.

The DNV GL will explicitly define a reliability index and a failure probability for blades. In this manner, when incorporating sub-component test data for blade designs, the reliability index and probability of failure shall be kept or improved. By defining a reliability index and probability of failure for wind turbine blades, it would also allow performing calibration of material safety factors.

The procedures for including sub-component test data have been outlined in EBR-II Work Package 5. This might also lead to, reduction of the extent of full-scale blade testing.

2.3.2 Design of bonded joints based on a fracture mechanics approach

Bonded joints may exhibit complex failure modes depending on local loading and manufacturing defects. Local loading depends on blade geometrical details (e.g. trailing edges) and materials

being joined. In general, design of bonded joints is based on a simplified and inaccurate assumption of average shear stresses. This may potentially lead to non-conservative designs; as such there is a strong need for more accurate and realistic design methods. It is known that manufacturing defects may turn into cracks at an early stage of the design life. Those cracks may propagate and reach critical crack sizes that may lead to catastrophic failure of blades. Fracture mechanics is a method that incorporates cracks and can also be used to develop lifetime prediction methodologies.

One of the challenges of employing fracture mechanics methods for composite materials, specifically for bonded joints, is that there are no standardized methods. There are, however, methods such as the ASTM D 6671/D 6671M – 06, DBC-UBM (Double cantilever beam-uneven bending moments) and MMB (mixed mode bending for sandwich specimens) that can be used (perhaps in a modified formulation) for bonded joints characterization. The last two methods are being used in the scientific community for dealing with interface cracks and have potential to become accepted methods for bonded joints.

Published scientific literature suggests that fracture mechanics data of cracked bonded joints exhibits large scatter. Current design standards assume that test data follows a normal distribution which may not necessarily fit bonded joints data. This calls for more sophisticated statistical models to analyse the data and to determine characteristic design values. The new DNV GL standard will also define and recommend number of specimens to be tested, loading conditions, mixed mode ratios and test methods. In connection to using advanced fracture mechanics methods, the DNV GL material safety factor might be re-evaluated.

2.3.3 Blade testing under combined loading

Traditional flapwise and edgewise full scale testing loads the blade in these two main directions. The intention of the testing is to validate design assumptions and verify static and fatigue strength. The testing may also help to identify critical design details. Full scale blade testing is a compulsory requirement for blade certification as per IEC 61400-23 and IEC 61400-22. The simplified flap and edgewise testing might not be very representative of the loading seen by the blade during operation. On top of this, experience showed that fatigue testing of large blades is a challenging and time consuming task. Fatigue testing puts blade manufacturers under constant pressure to complete blade test programs at reasonable time and cost.

As an outcome from EBR-II, it has been demonstrated that the maximum bending moments for ultimate limit state does not happen at flap or edgewise direction, but at a given angle with respect to the flapwise direction. This angle introduces a combined flap and edgewise loading. As such, the extreme static test to verify ultimate limit state should be carried out at a combined loading, i.e. more representative of the actual extreme bending moment. For static testing, the implementation of this test requirement is not very demanding; however, for fatigue testing, it is very complicated due to load introduction points and load excitation.

Currently, testing of large blades is performed by exciting its natural frequency and, depending on the test acceleration, localized damages at load introduction points may occur. Combined fatigue loading may, most likely, be achieved only by forced excitation. This may potentially introduce higher load levels at the load introduction points that could damage the blade. Force

excitation may be very expensive and may not be attractive for test centres. Further research is needed in the area of fatigue testing under combined loading.

In summary, the details of implementing the aforementioned approaches are being examined and assessed internally at DNV GL. As mentioned above, DNV GL is working on developing a DNV GL blade standard and the items presented above are on the agenda. The DNV GL blade standard is foreseen to be ready by end of 2015. EBR-II has produced research results that are relevant for the wind turbine blade industry.

3. Load envelope and load carrying capacity

Wind turbine blades are today normally tested in four directions as a part of the certification process. These four directions are typically the maximum and minimum flapwise and edgewise directions. In phase 1 of this project (Experimental Blade Research - phase 1) a discussion was started regarding if other load configurations could be more critical. Or in other words maybe the load carrying capacity in other load directions/configurations could be significant lower and more critical when the loading is considered.

To answer these questions a large number of numerical calculations were performed in this project in order to study the load carrying capacity of the SSP 34m blades and the loads that the blades could experience. Based on the outcome of these studies, the most critical load configuration would be then be tested utilizing the three SSP 34m blades available in this project.

In this section the two main objectives is to:

- a. Formulate/develop a 3D load envelope based on aeroelastic simulations
- b. Compute the load carrying capacity of SSP 34m blade in different load directions/configurations and determine the governing failure modes

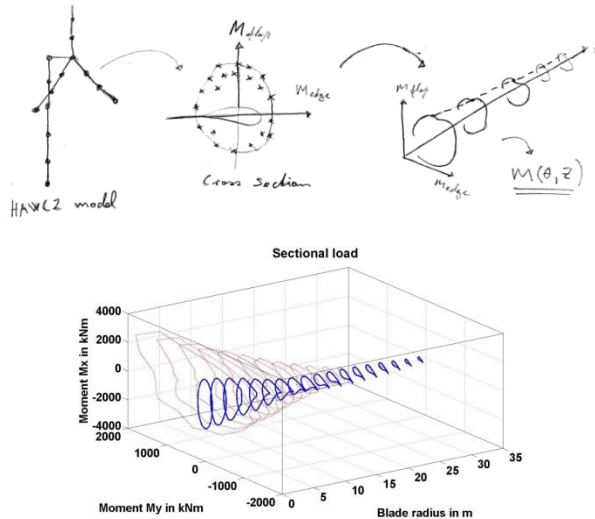
3.1 The 3D load envelope

Concerning determination of 3D load envelope/surface based on aeroelastic simulations, the following steps are completed in this project (see Figure 2 and Figure 3):

- A HAWC2 model is generated and tested. The aeroelastic input files for the SSP 34m blades to HAWC2 are generated - The blades are applied on an existing generic turbine and the controller is fine tuned to the blades.
- The relevant ultimate load cases suggested by IEC are performed except controller dependent load cases such as starts up, run-away condition, special fault condition etc. The performed load cases are applied to derive the extreme 3D load envelop.
- The program/script of generating the 3D load envelope is completed and tested on the data from the aeroelastic data. The outcome is the bending moment as a function of the radial position along the blade and the angle ($M(z, \text{angle})$).

- A method/script is generated which computes the cross sectional loads (Mx and My) from the 3D envelop and applies to the detailed numerical model for evaluating the strength in different loading directions.

Based on the development of the 3D envelop a journal paper is being written utilizing the results of this work.

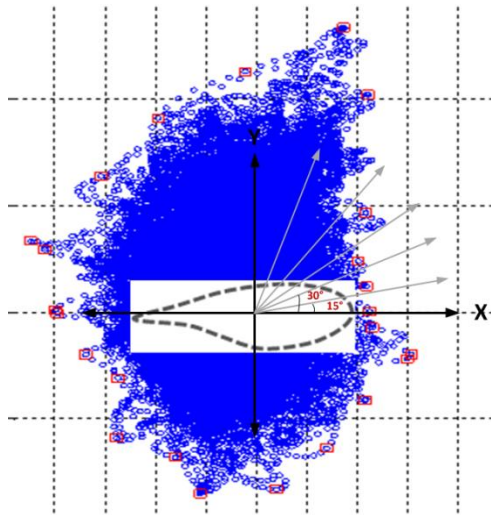


Design Load Case	Load description	Considered number of turbulence seed	Safety factor
DLC1.1	Normal power production with normal turbulence model (NTM)	6	1.35
DLC1.3	Normal power production with extreme turbulence model (ETM)	-	1.35
DLC1.5	Normal power production with extreme wind shear (EWS)	-	1.35
DLC2.1	Power production with fault, normal turbulence model (NTM)	6	1.35
DLC2.3	Power production with fault, extreme operating gust (EOG)	-	1.1
DLC4.2	Normal shut-down with EOG	-	1.35
DLC5.1	Emergency shut-down with NTM	-	1.35
DLC6.1	Parked condition with extreme wind speed model (EWM)	6	1.35
DLC6.2	Parked condition with EWM, grid fault without backup more than 6 hr. (all azimuth angles are considered. It means that wind comes from all direction in 30deg space)	6	1.1
DLC6.3	Parked condition with WEM, extreme way misalignment, +20deg.	6	1.35

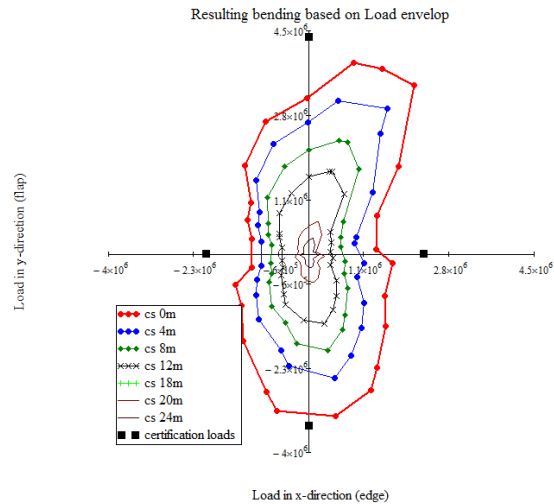
Sketch showing the methodology for generating the load envelop (top) and plot of the load envelop (bottom)

The aeroelastic load cases applied in this study

Figure 2 Sketch of method and list of load cases.



The method for selecting the largest resulting bending moments applied to generate the load envelop



The load envelope depict at a number of radial positions

Figure 3 3D load envelope/surface.

3.2 Load carrying capacity and failure modes

Concerning determination of the most critical load configuration based on the 3D load envelope the following has been done in this project.

The SSP blade is analyzed and the failure load for different load directions is estimated. The blade is modeled with 20-noded layered continuum elements. The model is densely meshed with a typical element size of 40x40mm and the entire model has approximately 83600 elements.

A moment and shear force distribution generated by four point loads (which can be applied at the test facility) at 13.2m, 18.6m, 24.9m and 28.75m from the root. This moment and shear force distribution is then rotated 360 degrees in steps of 15 degrees.

In order to simplify the evaluation of the results certain parts of the model is not considered, as the stress state in these parts are affected by singularities. One of these parts is the adhesive bonds. Methods to be able to evaluate critical loading of adhesive bonds are developed elsewhere in the project. The strength of the blade in different loading direction is compared with the loading in the different directions (load envelope) and it is found that the load direction used for the ultimate blade tests indeed may be the most critical load directions.

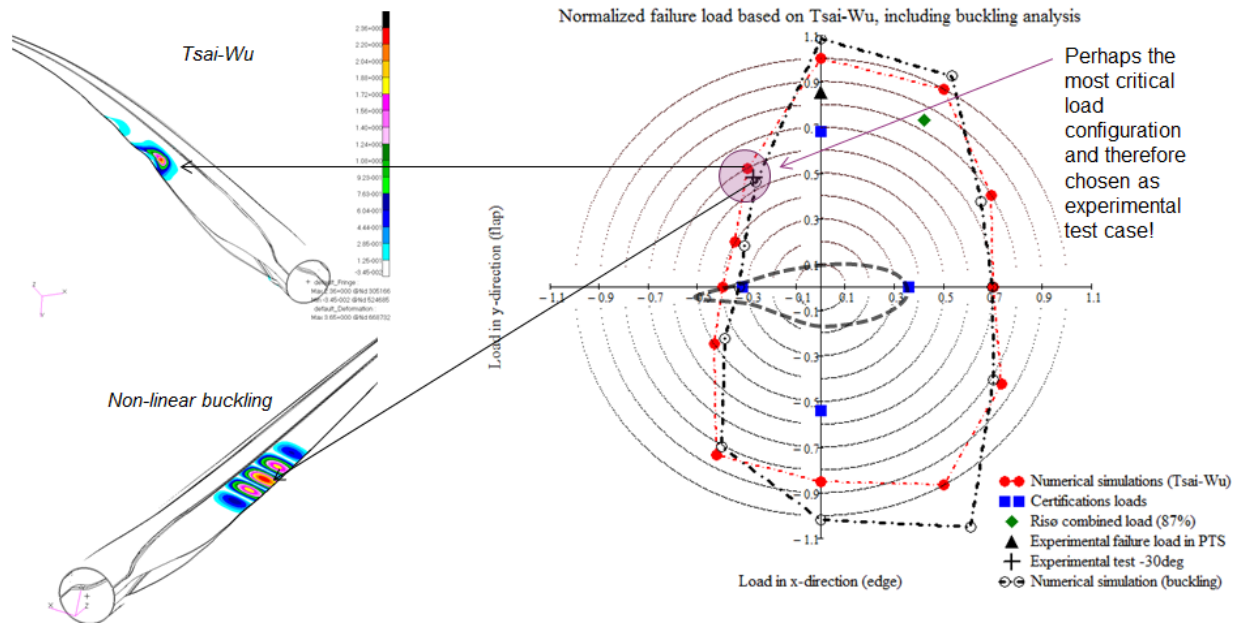


Figure 4 The load carrying capacity for different load directions.

To evaluate the different failure modes when the blade is subjected to different load configurations the following three methods have been applied:

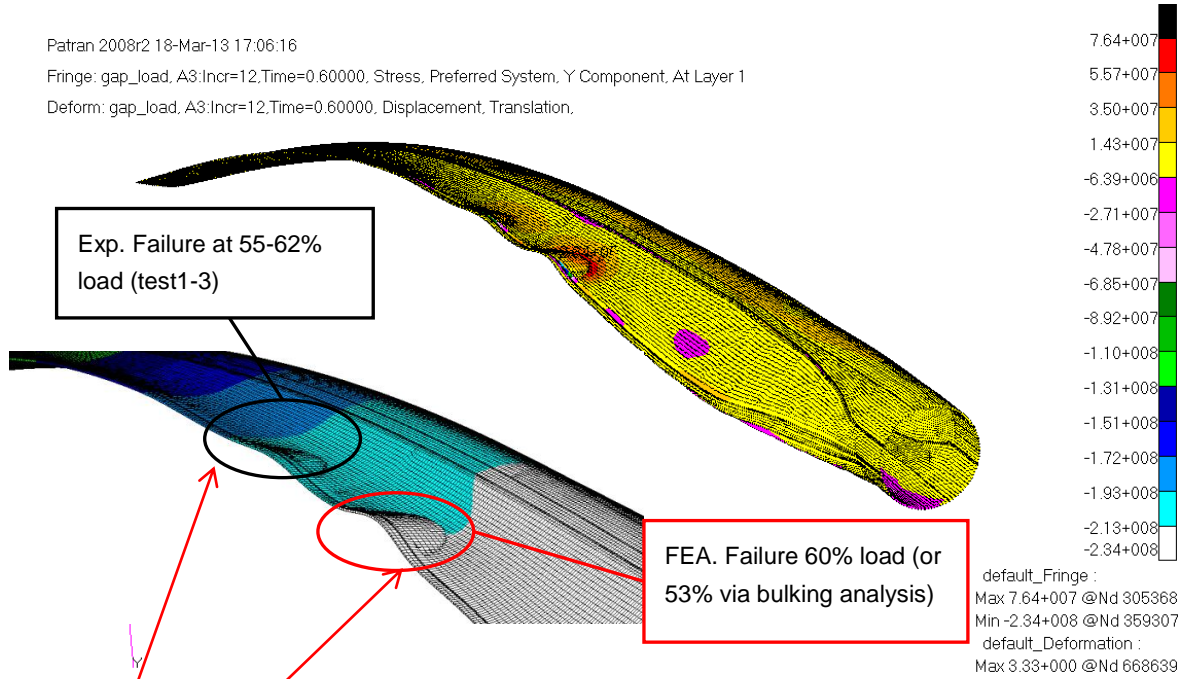
- Material failure criterion Tsai-Wu
- Nonlinear Eigenvalue buckling analysis
- Shear distortion failure (lateral buckling)

Nonlinear Eigenvalue buckling analysis is performed for all load configurations. In general a good agreement between the failure locations determined based on the material failure criterion Tsai-Wu and the buckling analysis are observed (see Figure 4). The ultimate load carrying capacity determined based on the two approaches deviates a bit more and the buckling analysis sometimes overestimates the ultimate strength. Shear distortion failure (lateral buckling) is evaluated for all load configurations. No indication of stability problems are found due to shear distortion.

Patran 2008r2 18-Mar-13 17:06:16

Fringe: gap_load, A3:Incr=12,Time=0.60000, Stress, Preferred System, Y Component, At Layer 1

Deform: gap_load, A3:Incr=12,Time=0.60000, Displacement, Translation.



At approximately 50% load, waves forming in the trailing edge (test 1)

At approximately 50% load, waves forming in the trailing edge (test 2)

At approximately 50% load, waves forming in the trailing edge (test 3)



At approximately 55% load, ultimate failure (test 1)

At approximately 62% load, Pre-failure (test 2)

At approximately 56% load, ultimate failure (test 3)

Figure 5 Comparison of ultimate blade tests with numerical predictions.

Concerning the comparison between experimental and numerical investigations the following have been performed in this project. The results from the ultimate blade tests are compared with the expected failure predicted by the numerical simulations (see Figure 5). The failure

modes observed in all three tests were very similar and was in very good agreement with the numerical predictions in this project.

The first ultimate blade test

At approximately 50% load in the ultimate test the blades trailing edge starts forming highly nonlinear waves (buckling). Two wave peaks can be seen at approximately 12.5m (red ellipse) and 14.5 meter (black ellipse) from the root. At approximately 55% load the blade failed in the trailing edge/panels at radial position 14.5m.

The second ultimate blade test

A very similar response of the blade was observed with waves forming in the trailing edge. At approximately 62% of the load a pre-failure in the trailing edge/panels at radial position 14.5m was observed. The blade was still capable of carrying additional load and therefore the blade was loaded further and the ultimate failure accorded at approximately 71% load at radial position 14.5m.

The third ultimate blade test

A very similar response as the two previous two blades was observed with waves forming in the trailing edge. At approximately 56% of the load ultimate failure occurred at the trailing edge/panels approximately at radial position 14.3m. Data from videos/pictures and DIC indicate that an earlier failure in the core material in sandwich panels could have occurred at approximately 45% load.

FEA predicts failure at 60% load at radial position 12.3m. Experimentally the blades applied in the three tests were subjected to significant material failure at approximately radial position 14.3-14.5m at approximately 55%, 56% and 62% load. The predicted failure load is very close to the failure loads observed in the tests and the buckling behavior of the trailing edge is just as expected.

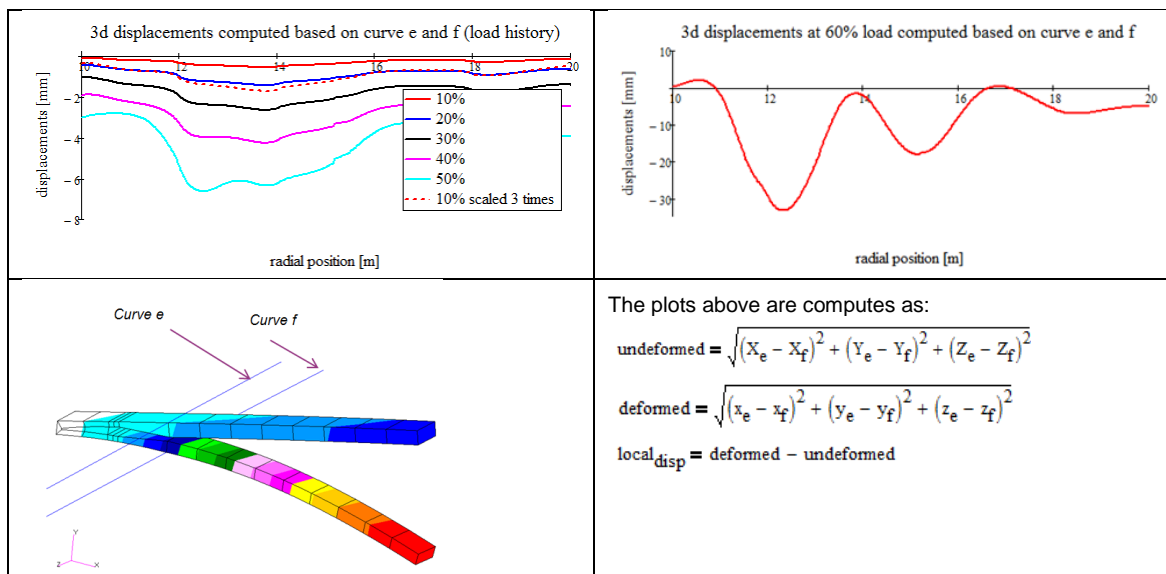


Figure 6 Numerical study of closing of the sandwich panels

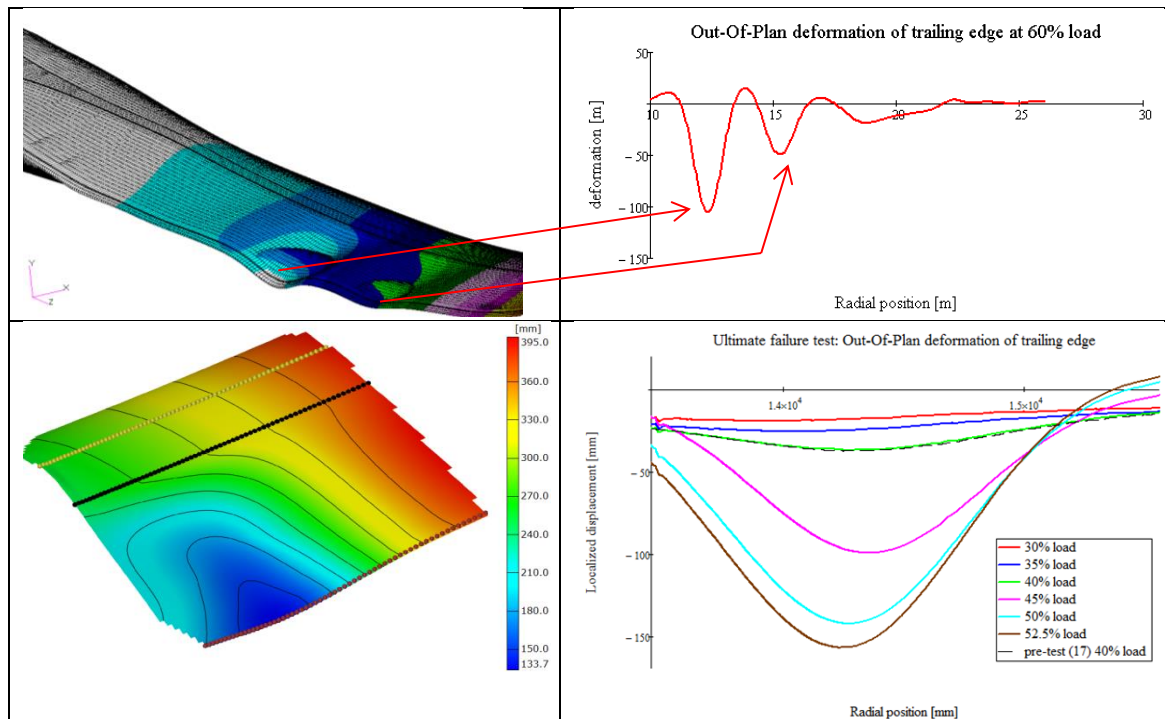


Figure 7 Numerical (top) and experimental via DIC (bottom) study of rigid-body deformation of the trailing edge.

The numerical studies performed in this project shows that sandwich panels move closer together and waves start forming in the trailing edge from very low load levels (see Figure 6). This response of the blades trailing edge/panels results eventually in buckling of the trailing edge/panels and in ultimate failure. Experimental strain and DIC measurements show a very similar response (see Figure 7).

4. Full-scale blade testing

Wind turbine rotor blades are glass fiber reinforced multicellular thin walled cantilever beams that can undergo considerable deformations up to 20% of their span. This large deformation made possible through adoption of fiber reinforced composite materials immediately suggests that geometric nonlinearity has a significant influence on the structural blade behaviour. Whilst looking into the integrity of blades empiricism tells us that the focus should lie on the performance of the adhesive joints in the blade. Blades are simply rather likely to fail in the joints rather than in the composite material itself where – in principle - it does not make a difference whether adhesives are present or not; every connection that involves abrupt non-smooth changes of geometry involving the creation of local stress singularities must be considered as a joint with all its issues.

By looking into the behaviour of adhesive joints in wind turbine rotor blades it turns out that their behaviour is inherently complex because of manifold reasons. Adhesive joints are affected by non-uniform cross sections struggling with each other caused by taper and twist, cross-sectional curvature of panels associated with ovalisation effects (i.e. in-plane cross-section deformations caused by geometric nonlinearity), local buckling effects, and material anisotropy associated with Poisson ratio effects. Furthermore, adhesive joints are affected by adhesive properties, bi-material interface properties (e.g. fiber bridging capabilities), local joint geometry (stiffness) all of which affected by different manufacturing techniques themselves affecting the presence of flaws and imperfections in the bond-lines. The complexity is even more increased by the fact that blades are subject to aero-elastic loads which depend on many factors bearing high levels of uncertainty (e.g. turbulence levels, yaw direction, controller performance, etc.). Although the reader might be well aware of it, it needs to be stressed that aero-elastic loads are a fully coupled problem in a sense that the stiffness of the blade (i.e. the blade design) affects the loads acting on it.

It is abundantly clear that the aforementioned factors are highly design specific which makes it difficult to infer a generic behaviour with general applicability. On the other hand this was one of the aims and challenges of this research programme. If the general structural blade behaviour can be associated with specific design parameters, design recommendations can be made which increase the life span of wind turbine blades.

In this report research emphasis was put on a specific adhesive joint namely the trailing edge joint. Proprietary maintenance reports are consistently showing that the trailing edge joint can de-bond over several meters decreasing the performance and operation time of the blade. The trailing edge joint was extensively studied not only experimentally but also numerically and analytically. At that time the project started little was known about the causes of trailing edge damage and literature is still quite tacit about it. This lack of information gave rise to start from the only available point available at that time which was to measure the prevailing relative fracture mode displacements in close vicinity of the internal flow front of the adhesive trailing edge joint. Later these displacements were corroborated by numerical analysis which stirred further research activities helping to explain the governing mechanisms.

In order to improve adhesive joints two different strategies can be pursued. The first strategy concerns the improvement of material properties such as fracture toughness, fibre bridging, reduction of residual stresses, fiber architecture, soft adhesives to name only a few. The second strategy concerns the improvement of utilisation capabilities of the aforementioned material properties such as composite material and adhesive. The best material is only as good as the utilisation of its properties. It is a well-known fact that geometry and global stiffness properties of the cross section sub-components has a significant influence on the forces that act on an adhesive joint. Mitigation of force levels or avoidance of specific detrimental force components by tuning certain design parameters can be used to improve the resistance of adhesive joints to fracture. Furthermore, the blade could be designed in such a way as to reduce or avoid the occurrence of bending moments in different directions by passive control systems such as bend twist coupling or by active controller techniques. All of which emphasises the importance of collaboration between material science and structural mechanics.

Experiments are an essential part of research as they provide realistic insights into the behaviour of entire blades or its sub-components. Furthermore, experimental results are needed for validation of numerical or analytical models as they will be presented later in this report. It is noteworthy to say that the experiments presented are somewhat models themselves as they still represent an approximation of the real conditions wind turbine rotor blades are subjected to. The experimental tests presented in this report are quasi-static which means that loads were applied at a rather low rate in such a way that inertia effects can be neglected. Still, time dependent behaviour such as creep and relaxation effects might affect the test results. Furthermore, inertia effects arising from a sudden loss of stability due to local buckling and-or unstable crack growth can have a significant influence on the behaviour. However, these effects are either considered insignificant or are affecting the post failure regime where the latter was beyond the scope of this research programme.

Although it is by now widely accepted by both the scientific community and by industry that fatigue situations are the main contributors to adhesive joint failure static tests can provide valuable insights that proved to be useful for fatigue considerations. That is to say that the adoption of strategies like the minimisation of energy release rates and mitigation of singularities under static loading conditions are very likely also mitigating the fatigue drivers.

4.1 Blade testing methodology

4.1.1 Loading methodology

The blade test involved a quasi-static multi-point loading of a 34m long SSP blade. The blade was truncated at 29m in order to accommodate it in the blade test facility. The blade was rigidly bolted to a steel rig at the root section. The blade was loaded at four points by pulley systems which pulled the blade towards the strong floor via displacement controlled winches (see Figure 10). The pulleys were attached to anchor plates made from carbon steel themselves adhesively connected to the cap of the blade in order to ensure sufficient structural integrity during load introduction. Additional blind bolts were used to reinforce the connection. The location of the load introduction points can be seen in Figure 8 and Figure 9.

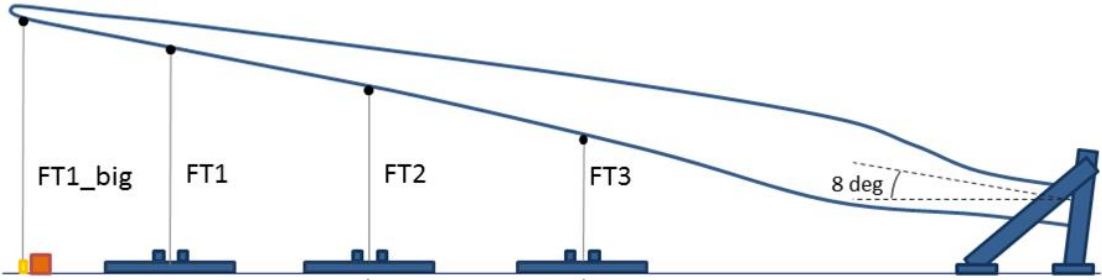


Figure 8 Test setup for four loading point blade testing with rigid steel rig and four winches. The blade has got a tilt angle of 8 degrees in order to increase the available space for tip displacement.

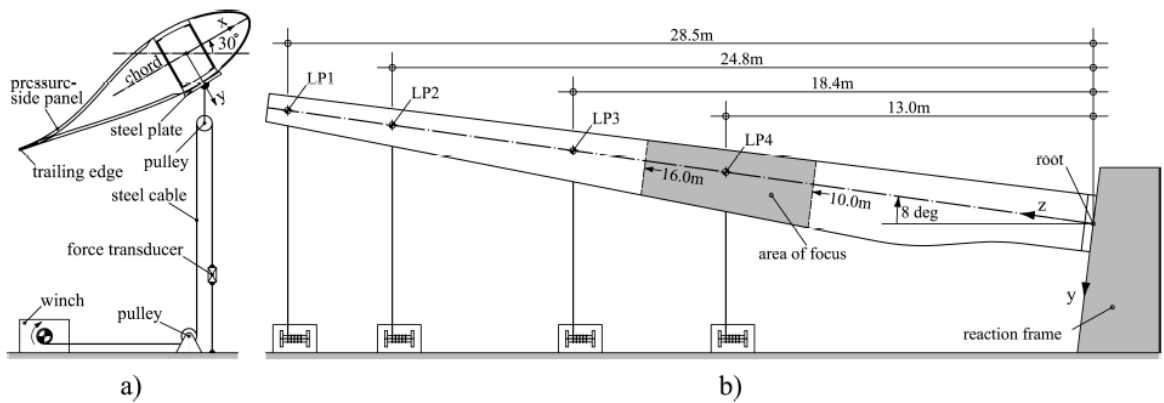


Figure 9 Side view and cross section with pulley setup for the -30degree testing configuration. Distances of different load introduction points measured horizontally from root section. (taken from Haselbach et al. (2015))

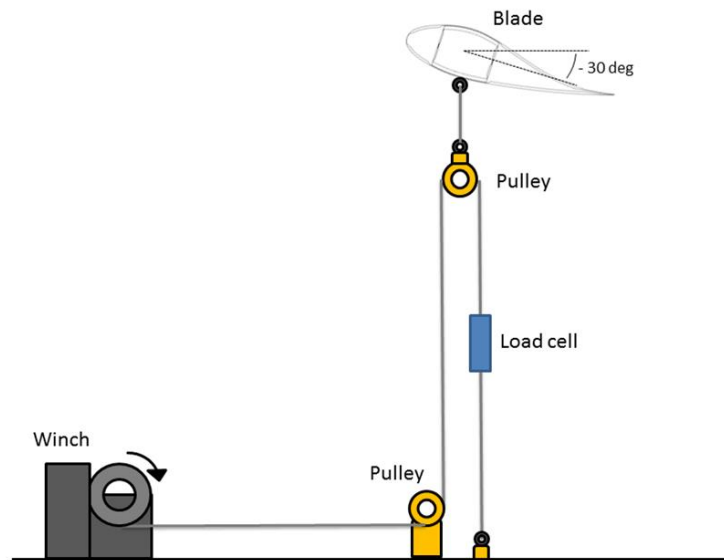


Figure 10 Detail of pulley system with winch and load introduction setup with interconnected load cell measuring half of the applied load.

Two loading conditions are presented in this report namely a combined +30 degree and a -30 degree test. Combined refers to the fact that the blade is subject to a combination of edge-wise and flap-wise (bi-axial) shear bending. The aforementioned angle refers to the direction of the applied tensile force which is measured clockwise positive from the y-axis of the wind turbine blade cross section (see Figure 9)

A multi load introduction scheme as the one used for the blade tests is a non-linear problem as a matter of structural coupling effects unloading inactive load introduction points. This poses a challenge in terms of meeting target load levels and in terms of repeatability of load cases. For this purpose usually controllers are used to actuate the winches in such a way that a smooth

and monotone load increase is achieved in every load introduction point by simultaneously maintaining accuracy. Such a controller system was not available at the time of testing and therefore, a simplified iterative based loading scheme was used. In this scheme loads are applied only in one load introduction point at the time until the specified target load was reached within a specified threshold. The threshold was defined as the relative error between the target load and the actually applied load. Subsequently the adjacent loading point was actuated until the specified target load was reached. This procedure was repeated several times in loops where one loop refers to a complete set four subsequent loadings. Usually up to 20 iterations were necessary to reach one target load step which shows that the convergence of this scheme was slow. Moreover, the load history of the single load introduction points was not monotone and showed fluctuations. However, the adopted iterative loading scheme proved to enable accurate load application and repeatability of load steps.

The blade was loaded in seven discrete load steps starting from 10% every 5% up to failure. Loads have been maintained constant for a minute in order to allow vibrations to decay which would have had a detrimental effect on measurements otherwise.

4.1.2 Measurement methodology

Forces were measured with force transducers that were interconnected between the steel cables as shown in Figure 10.

Total displacement magnitudes were measured by means of draw wire transducers (ASMs) that were mounted on the strong floor. The wire heads were attached to the cap of the blade at several locations.

Cracks in a structure only feel local relative displacements (LRDs) as they will be referred to in this report. LRDs are basically the warping deformations of a cross section which can be obtained by subtracting the Euler-Bernoulli deformations from the total displacements. In order to measure the prevailing Mode-I,II,III fracture modes between two points located on the opposite sides of the suction side panel and the pressure side panel a novel measurement device was devised. This DTU-owned small displacement measurement system (SDMS) is stereo photogrammetry based and capable of measuring with an accuracy of +/-15 micro meters. A detailed documentation of the measurement principle can be found in Tesauro et al [3] The SDMS consists of an Aluminium frame that was rigidly connected to one side of the blade. Two digital cameras were mounted on the frame and electronically modified in such a way that a set of pictures could be taken simultaneously. A so called calibration grid which featured a laser engraved checkerboard pattern was also mounted on the frame for camera calibration purposes (see Figure 16). A target was mounted on the other side of the trailing edge with the purpose of transporting information from one side to the other. By taking a set of pictures of the target before and after deformation the 3D relative motion vector of the target with respect to the cameras could be measured (see Figure 13). In a first step camera calibration was performed where the known real world coordinates of the calibration grid were used to obtain the extrinsic and intrinsic camera parameters such as focal length, aspect ratio and the Euler angles of the optical camera axis. In a second step these parameters can be used to triangulate the real world coordinates of the target using the known pixel coordinates of the same point in two images according to the pinhole camera principle. Using rigid body kinematics and 3D transformation procedures it was possible to analytically calculate the full 3D

LRD displacement vector between two points as described before. The components of this vector represent the fracture mode displacements and can be used to infer to prevailing mode mixities. In addition these measurements can be used to corroborate finite element analysis as will be shown later.

Figure 11 shows a close-up of the trailing edge joint and the fracture modes that should be measured between the two panels shown close to the flow front of the adhesive.

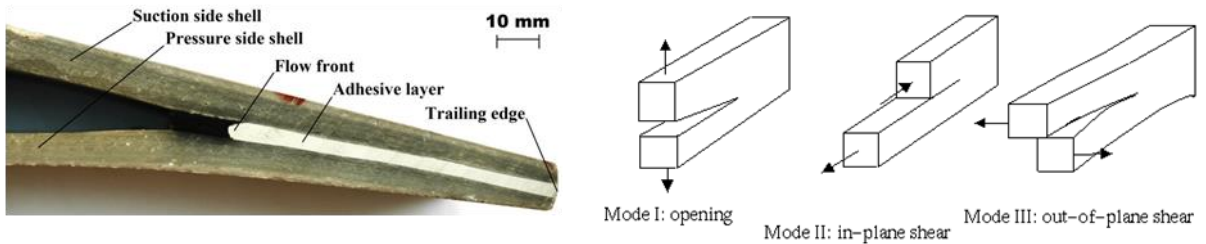


Figure 11 (left) Detail of trailing edge joint of the SSP34 blade; (right) Three different fracture modes and their associated displacements as a function of the loading direction

Figure 12 shows the measurement principle as described above. The LRD refers to the relative displacement between points P1 and P2 which could be achieved by the SDMS following the rigid body motions of the cross section.

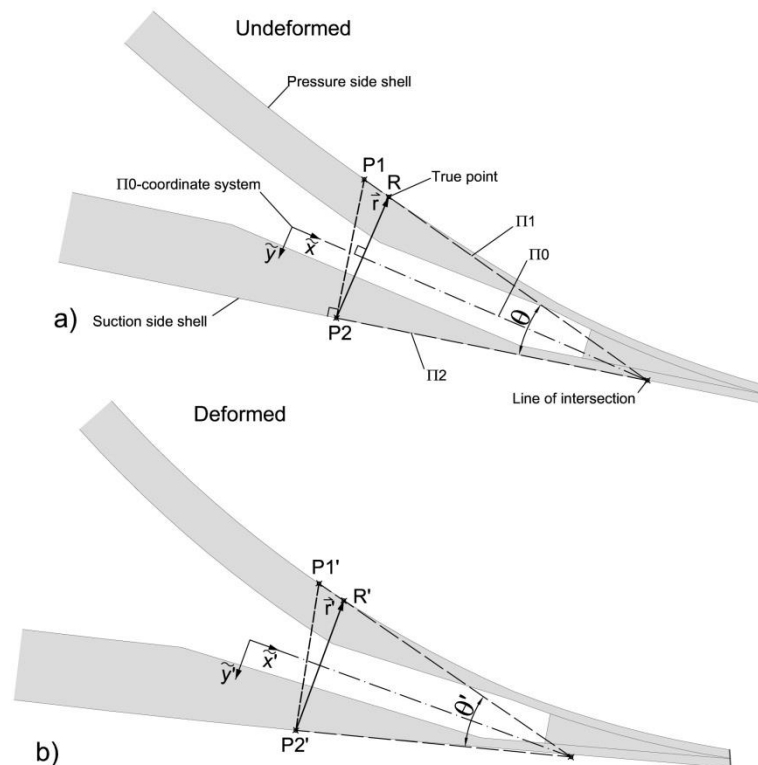


Figure 12 Measurement aim showing local relative displacement between two points P1 and P2 with bisector transformation between two tangential planes in points P1 and P2. The primed entities are referring to the deformed configuration. (taken from Tesauro et al. (2014))

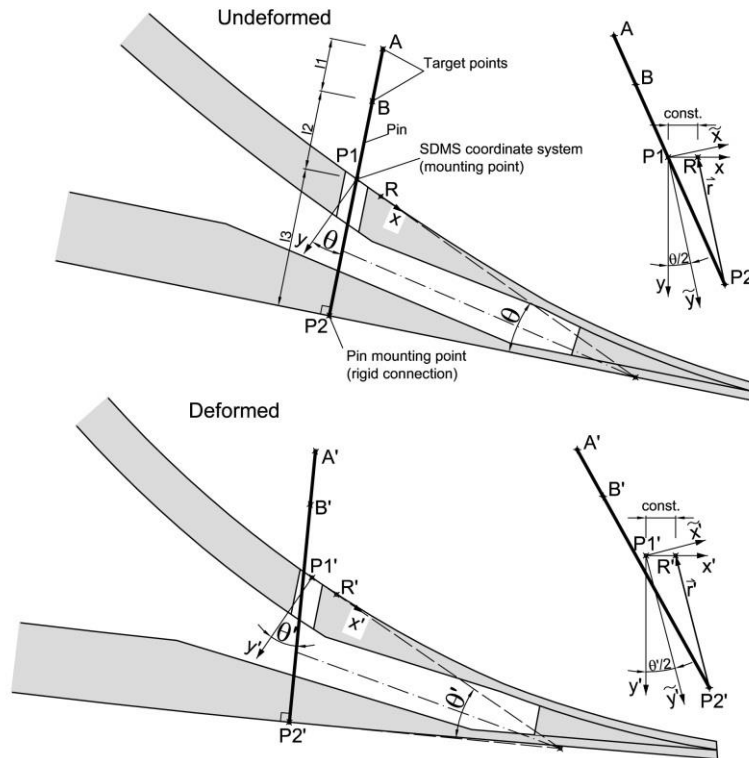


Figure 13 Measurement principle of the first generation. A tungsten rod is mounted in point P2 and extends through a borehole to the other side. A target with two target points – A and B - is mounted on the other end of the rod. Measurement of relative displacements of target points leads to the desired local relative displacement as depicted above. (taken from Tesauro et al. (2014))

Figure 14 shows the non-intrusive extension of the intrusive measurement method as reported in Shmueli et al. (2015). A lightweight frame was used to transfer the information from the suction side panel around the trailing edge to the other side. This of course works only in case of the trailing edge joint. Otherwise the same measurement principle was applied to obtain the LRD components.

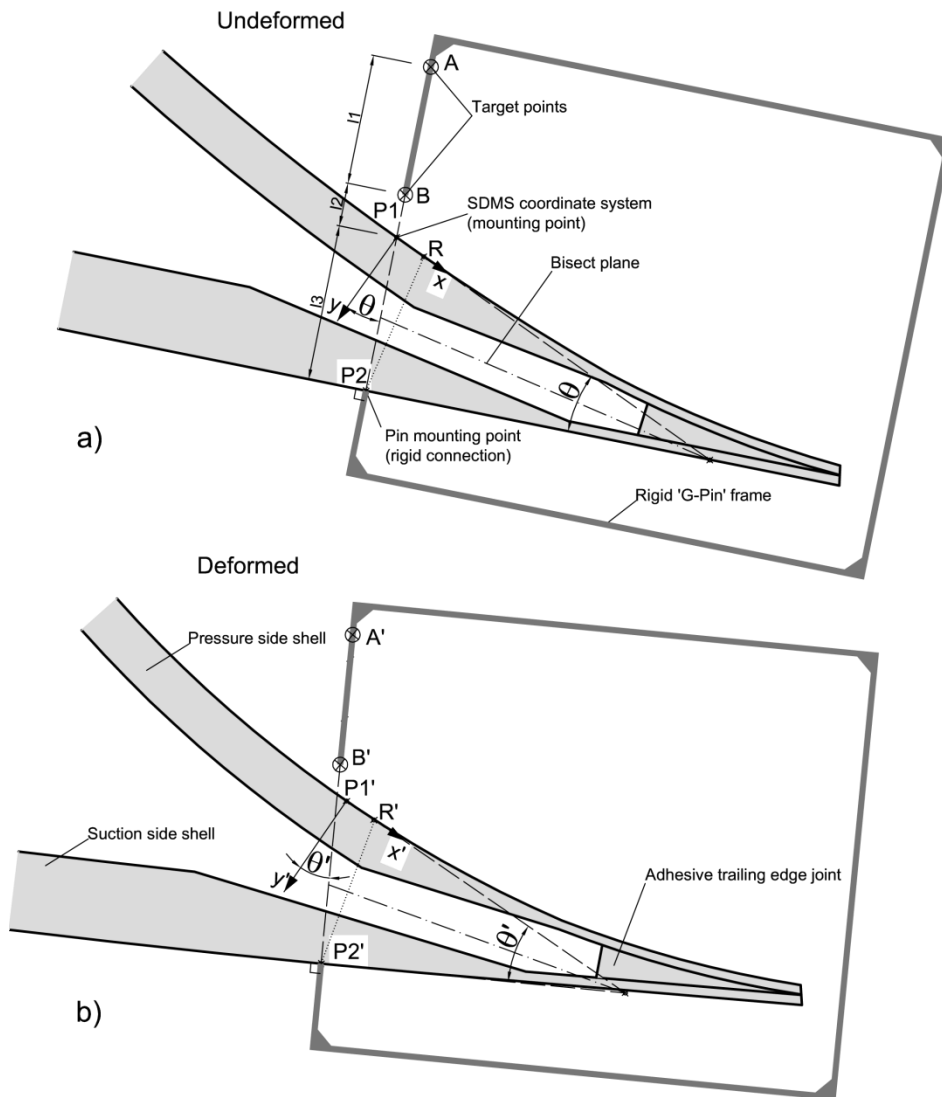


Figure 14 Measurement principle of the second generation (non-intrusive) with a light weight rigid frame going around the trailing edge. Otherwise same measurement principle as the one used for the first generation approach. (taken from Shmueli et al. (2015))

Figure 15 shows two mounting stages of the SDMS on the blade. The rotation of the SDMS was done in order to get a second set of measurements for the repeated load. In this way the out of plane measurements could be discarded and the accuracy of the measurements could be increased significantly. The drawback was that the test needed to be repeated twice for the same load.

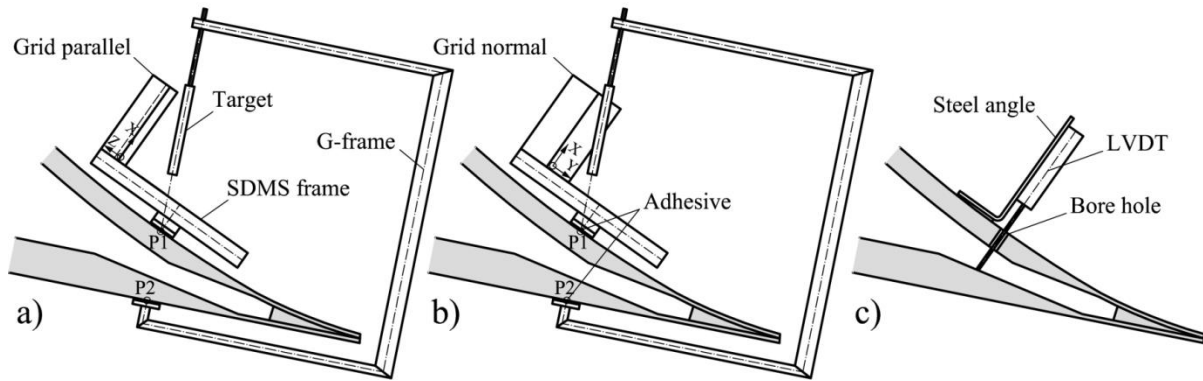


Figure 15 (left) Mounting principle of the SDMS for the second generation measurement principle. The rotation of the SDMS increased the accuracy of the measurements by discarding out-of-plane measurements; (right) complimentary measurement system in form of an LVDT. This setup was used to measure the Mode-I opening component and compare it with the SDMS results. (taken from Shmueli et al. (2015))

Figure 16 shows the SDMS mounted on the blade with its components with the target passing through the blade and the second generation where the target is built around the trailing edge. Swivels on the frame enabled rotation of the cameras in order to improve the focus and the contrast. The challenge was to optimise the focus on both the calibration grid and the target simultaneously.

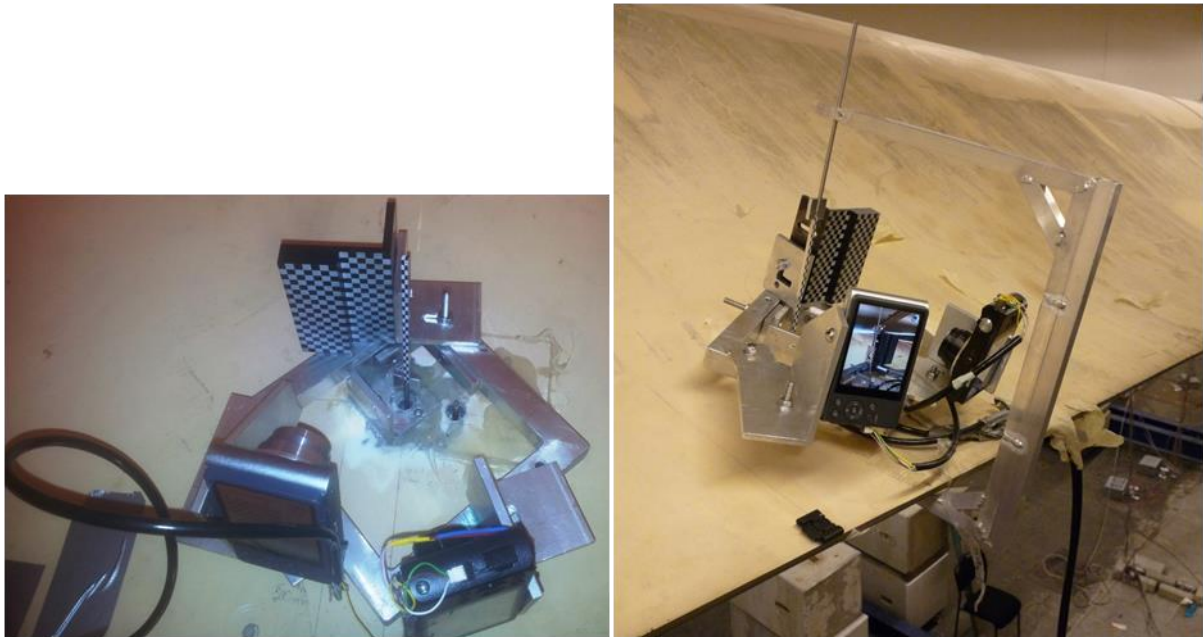


Figure 16 (left) SDMS as mounted on the blade in the first generation setup showing the rigid frame, the calibration grid, two SAMSUNG digital cameras and the target equipped with a checkerboard pattern for automatic recognition (DIC) of the AIPS; (right) SDMS as mounted on the blade in the second generation with C-shaped Aluminium frame. (taken from Tesauro et al. (2014) and Shmueli et al. (2015))

Figure 17 shows the 3 measurement locations of the SDMS in the longitudinal direction and in the transverse direction.

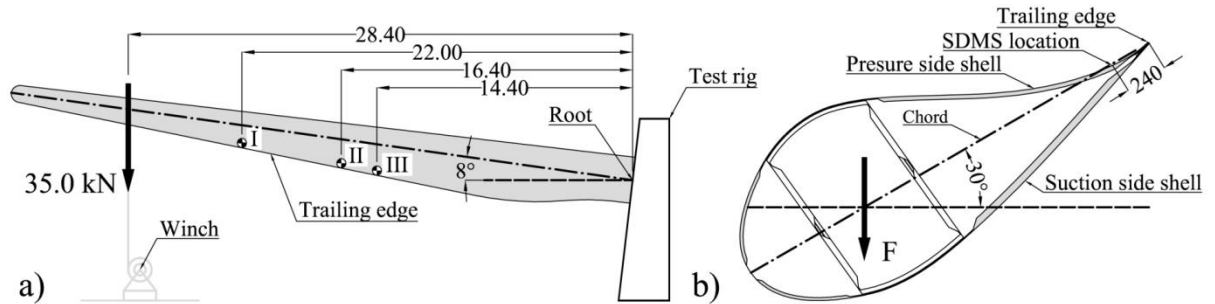


Figure 17 (left) Measurement locations at 3 different points along the trailing edge indicated by dimension lines. (right) cross section with location of the SDMS in the transverse direction being mounted 240mm away of the trailing edge. (taken from Shmueli et al. (2015))

Figure 18 shows the complimentary applied LVDT used to validate the Mode-I component of the LRD vector.

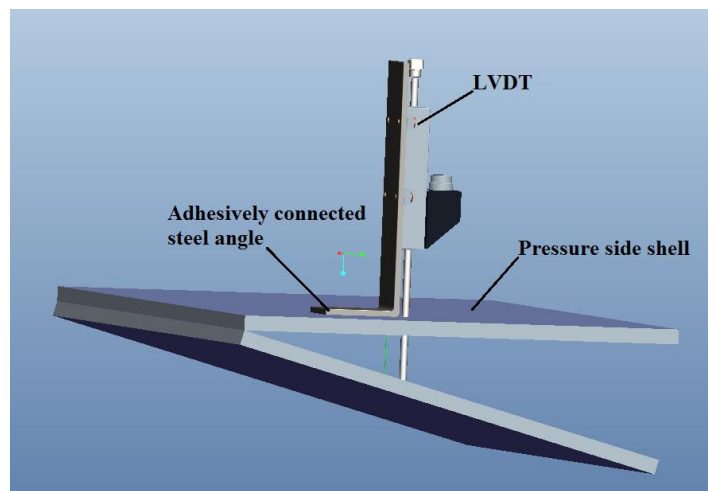


Figure 18 Detailed representation of the LVDT being used for verification of the SDMS Mode-I component. The LVDT was mounted on a steel angle itself adhesively connected to the pressure side shell of the blade. The sensor head was resting on the internal surface of the suction side shell. (taken from Tesaura et al. (2014))

In a second stage a DTU-owned fully automatic image processing software (AIPS) was developed with the capability to automatically process a large number of images avoiding the introduction of human error. For a detailed documentation the reader is referred to Shmueli et al (2015) The AIPS automatically performs the camera calibration procedure in order to obtain the extrinsic and intrinsic camera parameters. Subsequently the software can automatically track the target points as they move relative to the cameras and calculate the LRD vectors as a function of the load increment. The seven single steps involved in obtaining the LRD components are shown in Figure 19.

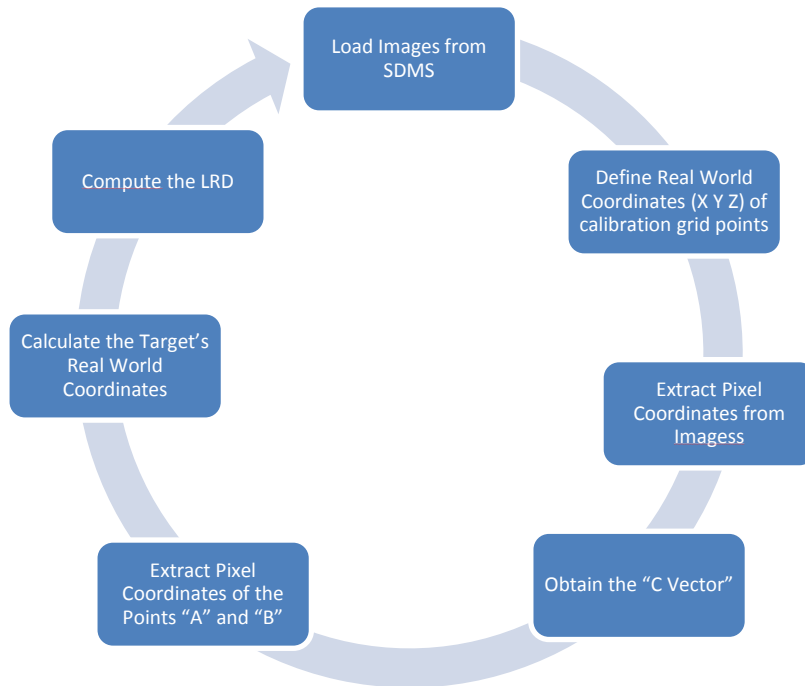


Figure 19 Simplified procedure of the AIPS with the steps involved to obtain the relative displacement components.

During previously conducted blade tests the occurrence of a local buckling wave along the trailing edge was observed for a loading direction of -30 degrees. These waves occurred at load levels well below the ultimate capacity and were considered as potential root cause for trailing edge failure. In order to scrutinise this effect and in order to identify the load level at which it occurs the measurement focus was put on the designated failure area between 10m and 16m blade length.

The same stereo photogrammetry based procedure previously described was used along with the AIPS on a larger scale to measure the global deformations i.e. buckling wave of the trailing edge. For this purpose the same cameras used for the SDMS were placed at an elevated position on the wall of the testing facility facing the trailing edge. The cameras were placed in such a way that two images of the same measurement volume could be taken. A large scale calibration grid that consisted of two staggered wooden boards was placed underneath the trailing edge. Figure 20 shows the arrangement of the cameras and the position of the calibration grid.

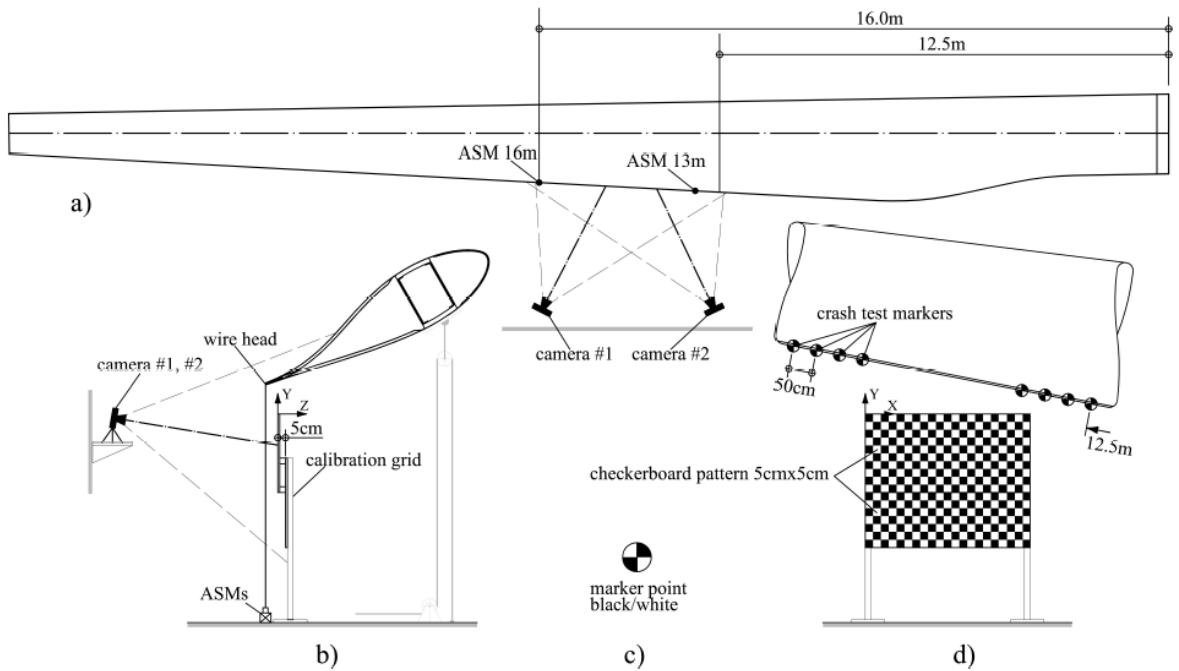


Figure 20 Camera system setup as used to obtain trailing edge deformation measurements. (taken from Haselbach et al. (2015))



Figure 21 Two cameras on tripods sitting on a shelf at an elevated height facing the trailing edge. The wires seen are part of the electronic shutter system enabling simultaneous triggering of digital cameras. Laser level (red) used to adjust the calibration grid alignment.

Crash test marker points were attached at a spacing of 0.25m along the trailing edge between a radial position of 10m and 16m of the blade as shown in Figure 22.

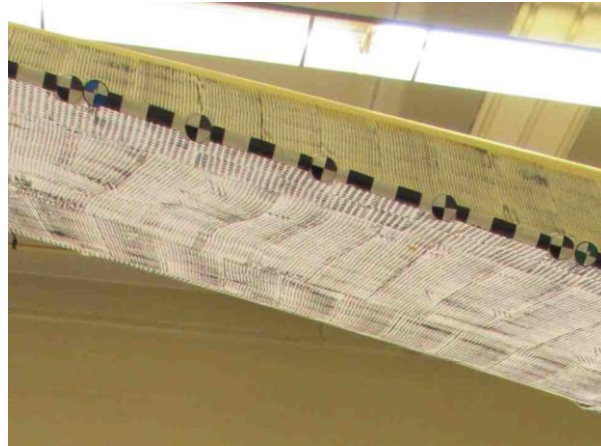


Figure 22 Detailed photograph of trailing edge with speckle pattern and crash test markers used for the corner extraction procedure of the AIPS.

The AIPS was used to calculate the global displacements of the marker points with respect to a coordinate system defined by the upper surface of the calibration grid. Additional ASMS were placed below the trailing edge at 13m and 16m for validation purposes of the optical measurements. Furthermore, the commercially available digital image correlation based measurement equipment ARAMIS was used to measure the 3D displacement field of the pressure side panel close to the trailing edge within the same area. For this purpose a black and white speckle pattern with an optimised speckle size was manually applied by means of modified rollers onto the surface of the pressure side panel between 10m and 16m radial position.

Fiber optical strain gauges were used to measure both longitudinal and transversal surface strains along the trailing edge of the blade. The measurement methodology was tailor made to pick up the occurrence of the buckling wave at an early loading stage. Two measurement lines with different sensor spacing were used. A coarse resolution line with a spacing of 0.4m was used to measure strains between 10m and 23m. A fine resolution line with a spacing of 0.15m was used to measure strains in the designated failure area between 10m and 16m. Transverse strains were also measured on the pressure side and suction side shell adjacent to the longitudinal sensors at a spacing of 0.15m. The sensors were adhesively attached to the top laminate after the gel-coat was removed by grinding. Figure 32 to Figure 34 show the general setup of the fiber sensors as applied on the blade for the -30 degree test.

4.2 Blade test results

Figure 23 shows a comparison between the Mode-I LRD component obtained by the LVDT and by the SDMS. The fit of the LVDT measurements would actually agree better with the SDMS if a more suitable fitting algorithm would have been adopted. It can be seen that the fit is artificially attracted by the last point on the diagram.

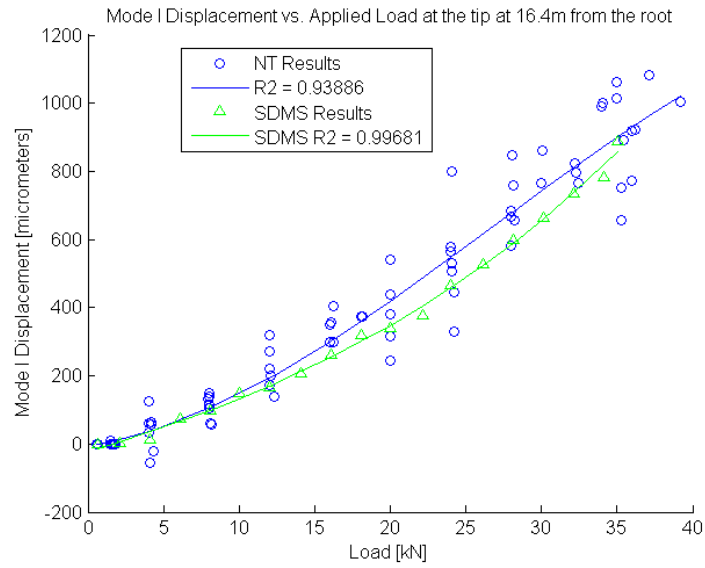


Figure 23 Comparison of LVDT and Mode-I SDMS LRD component showing good agreement. The scatter in the results were caused by noise as a matter of the LVDT being operated close to its accuracy range.

Figure 24 and Figure 25 are showing the measured SDMS LRD vector components (or fracture mode displacements) for a -30 degree test and a +30 degree test respectively. The solid lines represent numerical results obtained by coordinate transformation that follows the rigid body motion of the blade.

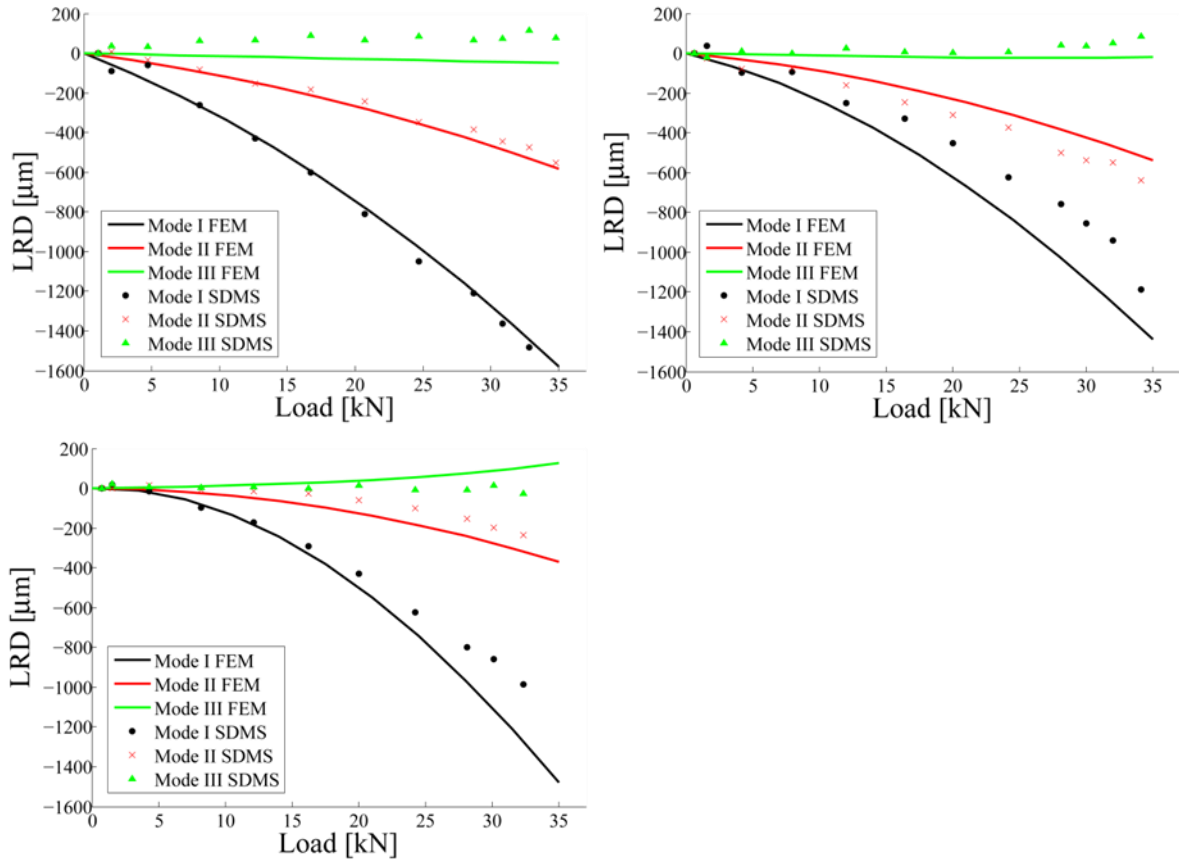


Figure 24 LRD measurement at 3 different locations 22.0m (left top), 16.4m (right top) and 14.4m (bottom) from the blade root for a -30 degree test under single tip loading

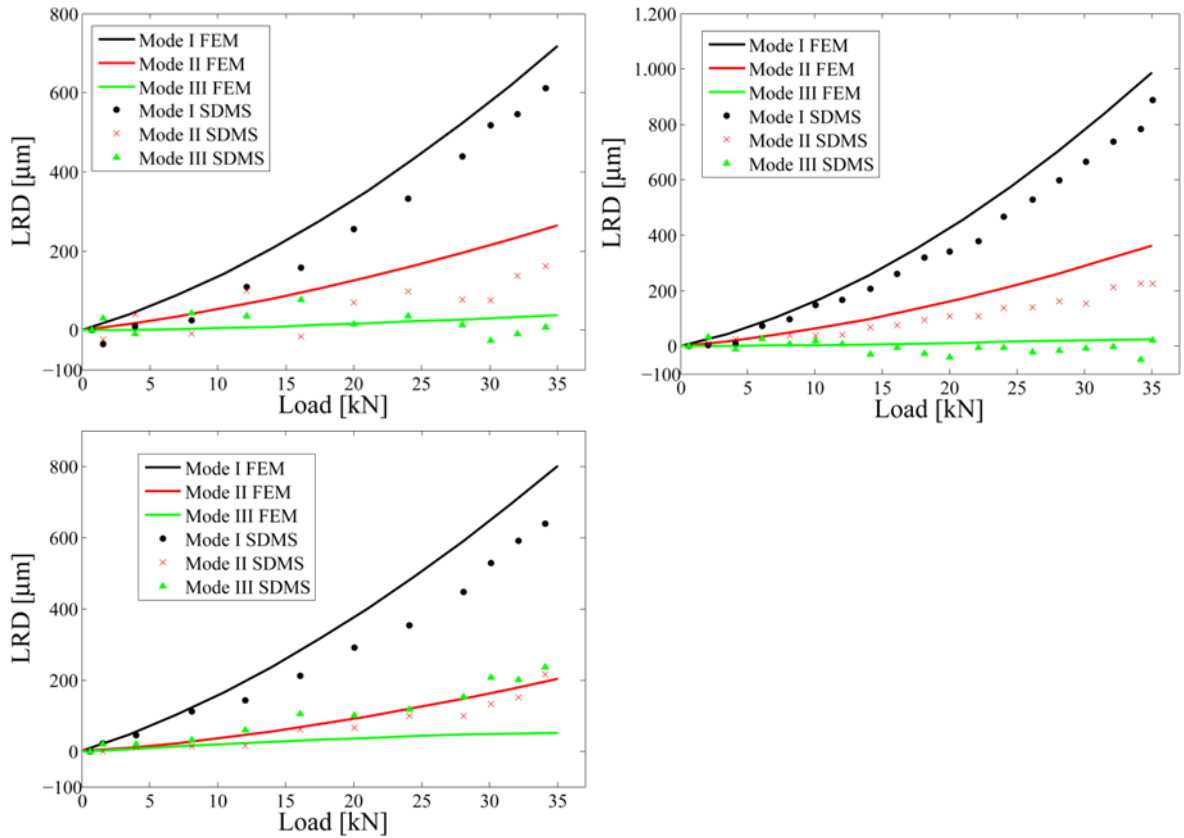


Figure 25 LRD measurement at 3 different locations 22.0m (left top), 16.4m (right top) and 14.4m (bottom) from the blade root for a +30 degree test under single tip loading

Figure 26 shows the load steps applied during the SDMS measurement sessions. Adoption of a single tip load by a hydraulic winch enabled accurate repetition of the load steps required for SDMS measurements.

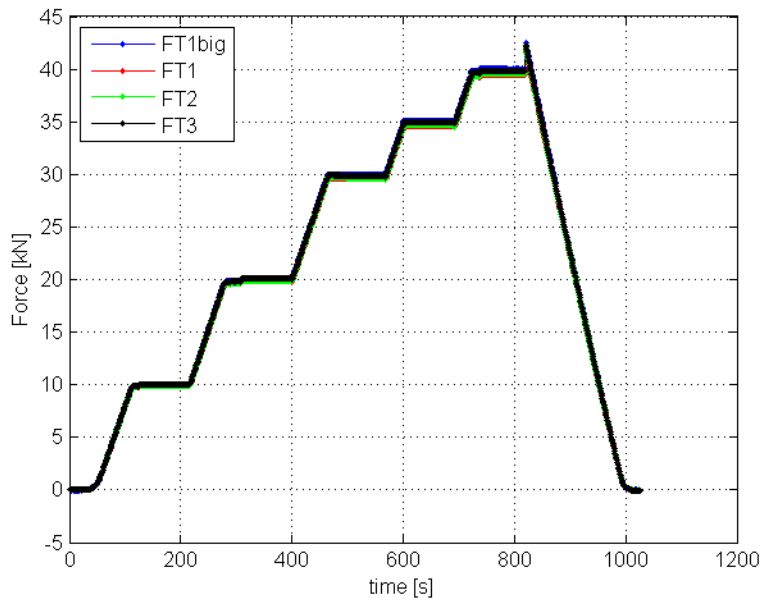


Figure 26 Load steps for the single tip load applied for SDMS measurements. FT1 big refers to the tip load cell whereas, FT1, FT2 and FT3 are the remaining load cells connected in series in this test for load cell calibration purposes.

Figure 27 and Figure 28 shows the difference between the conventional and the novel loading approach. Figure 28 shows that the novel loading approach smoothly converged to the designated load step.

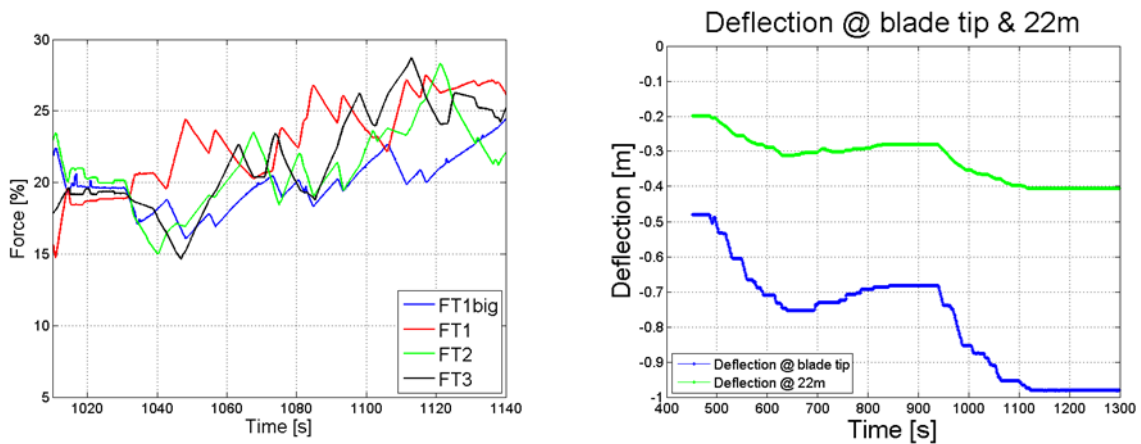


Figure 27 (left) Load history in load application points as measured during a previous blade test using the conventional loading approach; (right) displacement history of blade tip (blue) and at 22m (green).

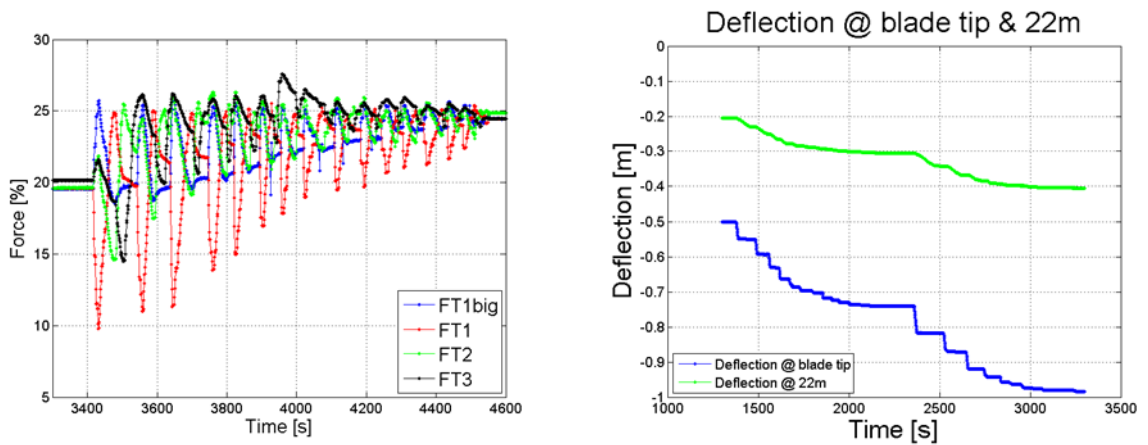


Figure 28 (left) Load history in load application points as measured during a previous blade test using the novel iterative loading approach; (right) displacement history of blade tip (blue) and at 22m (green).

Figure 29 shows a screen shot of the AIPS corner extraction step (step number 3). The red points are located at the corners of the checkerboard pattern obtained by corner extraction.

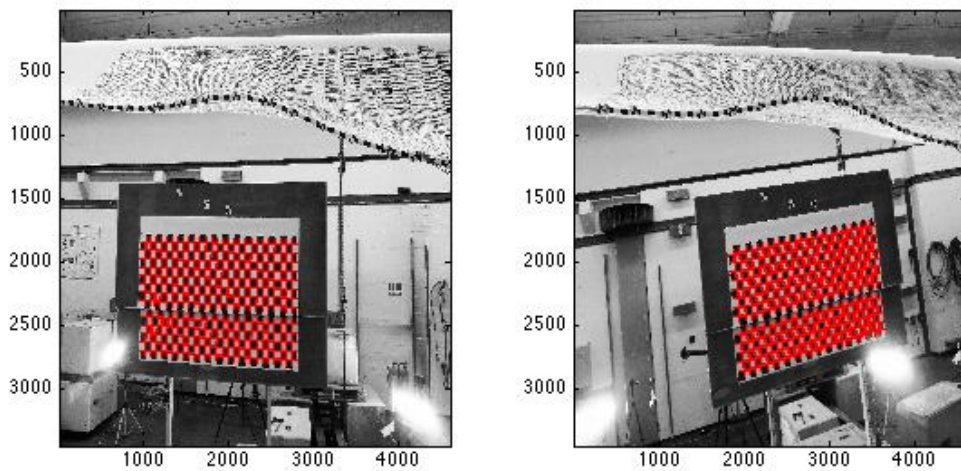


Figure 29 Corner extraction images of the AIPS used for camera calibration. The red crosses are automatically detected corners of the calibration grid below the blade.

Figure 30 shows the trailing edge buckling wave developing during loading until failure where the trailing edge joint debonded and opened up along a long distance.

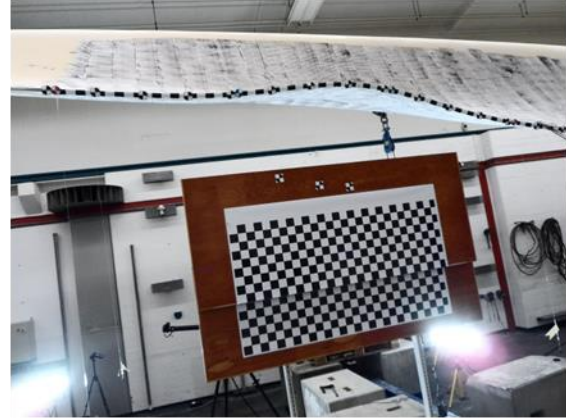
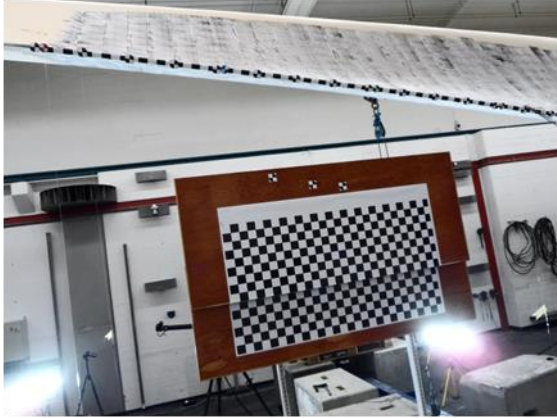


Figure 30 Trailing edge deformation at different load level for the multi-point loading test. (top left) prior to loading, (top right) 40% of load and (bottom) ultimate failure due to local buckling induced debonding of the trailing edge joint. (partially taken from Haselbach et al. (2015))

Figure 31 shows the trailing edge deformation at different load levels from 30%, 35% up to 40%. Solid line is a curve fit that consists of a polynomial and a sine function. The polynomial represents the rigid body motion whereas the sine function represents the contribution of the buckling wave.

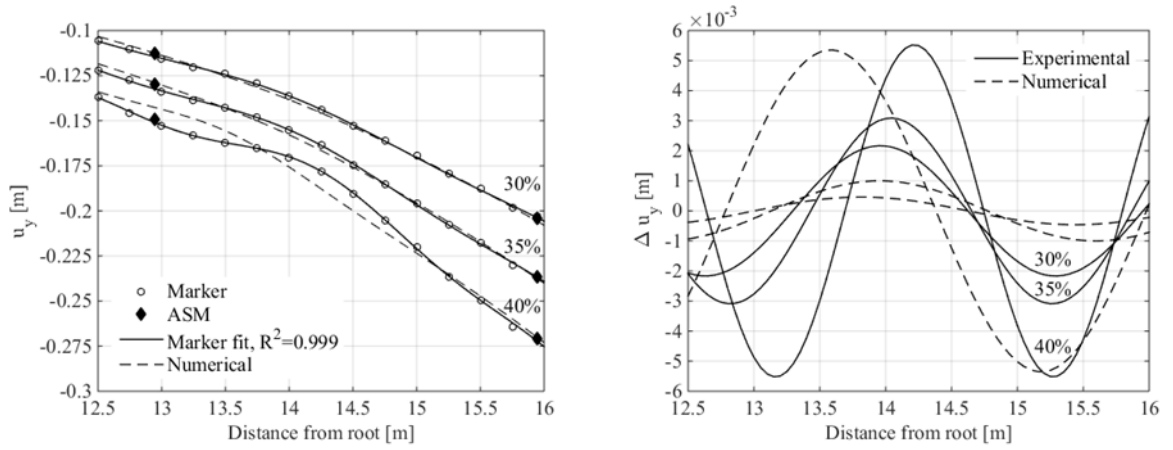


Figure 31 (left) measured global deformation u_y -component of trailing edge at different load steps. Circular markers are SDMS measurements and diamonds are ASM readings. Dashed lines are global deformations of numerical model; (right) Extracted wave by subtracting assumed polynomial fit from total deformations. (taken from Haselbach et al. (2015))

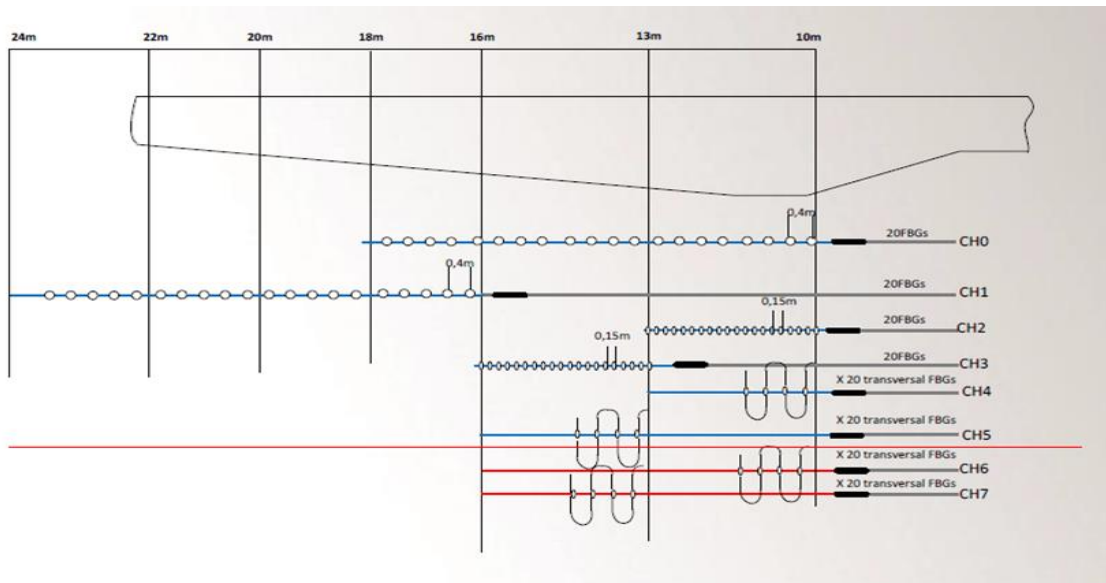


Figure 32 Array of fiber sensors along trailing edge split in different channels. Channel 0 to 1 longitudinal strain coarse resolution line, channels 2 to 3 longitudinal strain fine resolution line, channels 4 to 5 transverse strains pressure side and channels 6 to 7 transverse strains suction side.

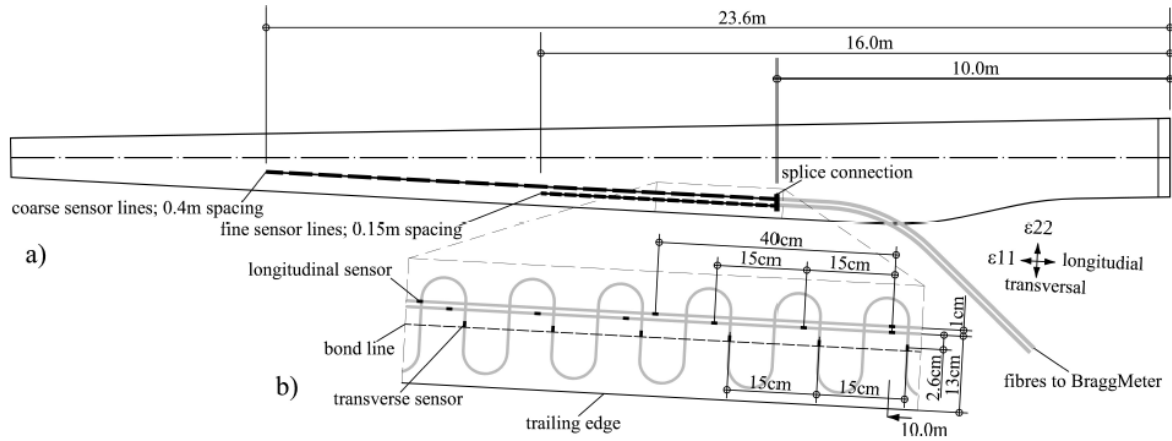


Figure 33 General location of coarse and fine resolution lines with a detail of the sensor array in the designated failure area between 10m and 16m. (taken from Haselbach et al. (2015))

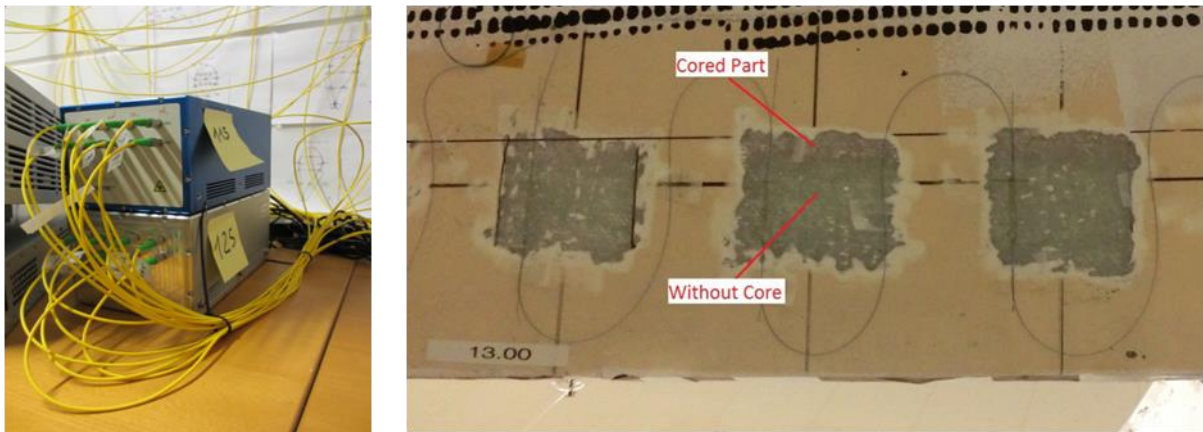


Figure 34 (left) Bragg meters (laser spectrometers) as used within the data acquisition system. Each Bragg meter accommodates 8 channels with 10 sensors. (right) close up of transverse sensors as mounted on the trailing edge.

Figure 35 shows the measurement bandwidth showing the issue of intersecting peaks. This means that the number of sensors limits the strain bandwidth.

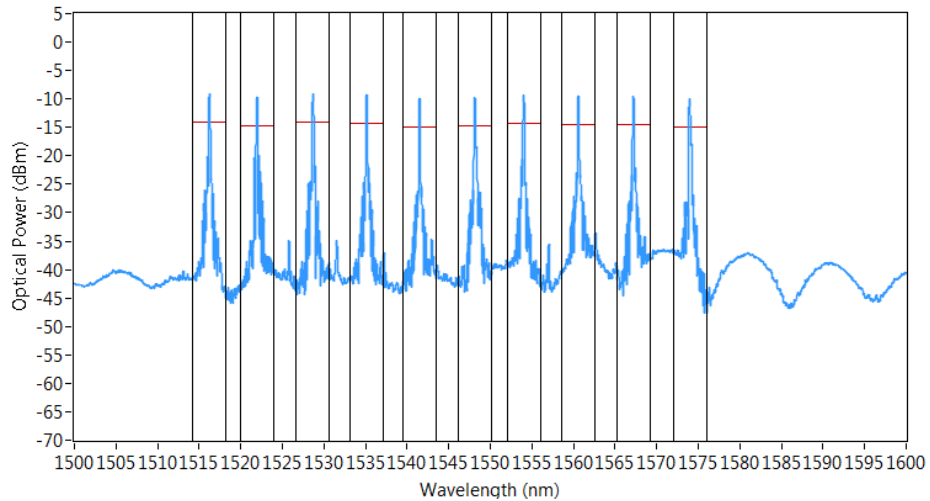


Figure 35 Power output [dB] versus wavelength signal plot of a typical channel. Every peak represents a sensor whereas the black vertical lines are representing the measurement bandwidth.



Figure 36 Detail of trailing edge joint showing the bonded area with laminate and the panels with sandwich core material where sensors in the sandwich core area gave a noisier signal when compared to sensors placed within the pure laminate.

Figure 37 shows that the fine resolution measurement lines are quite noisy depending on the location of the sensor on the blade. Fine and coarse resolution line are quite consistent between 13m and 16m where the occurrence of the buckling wave can clearly be seen from 30%.

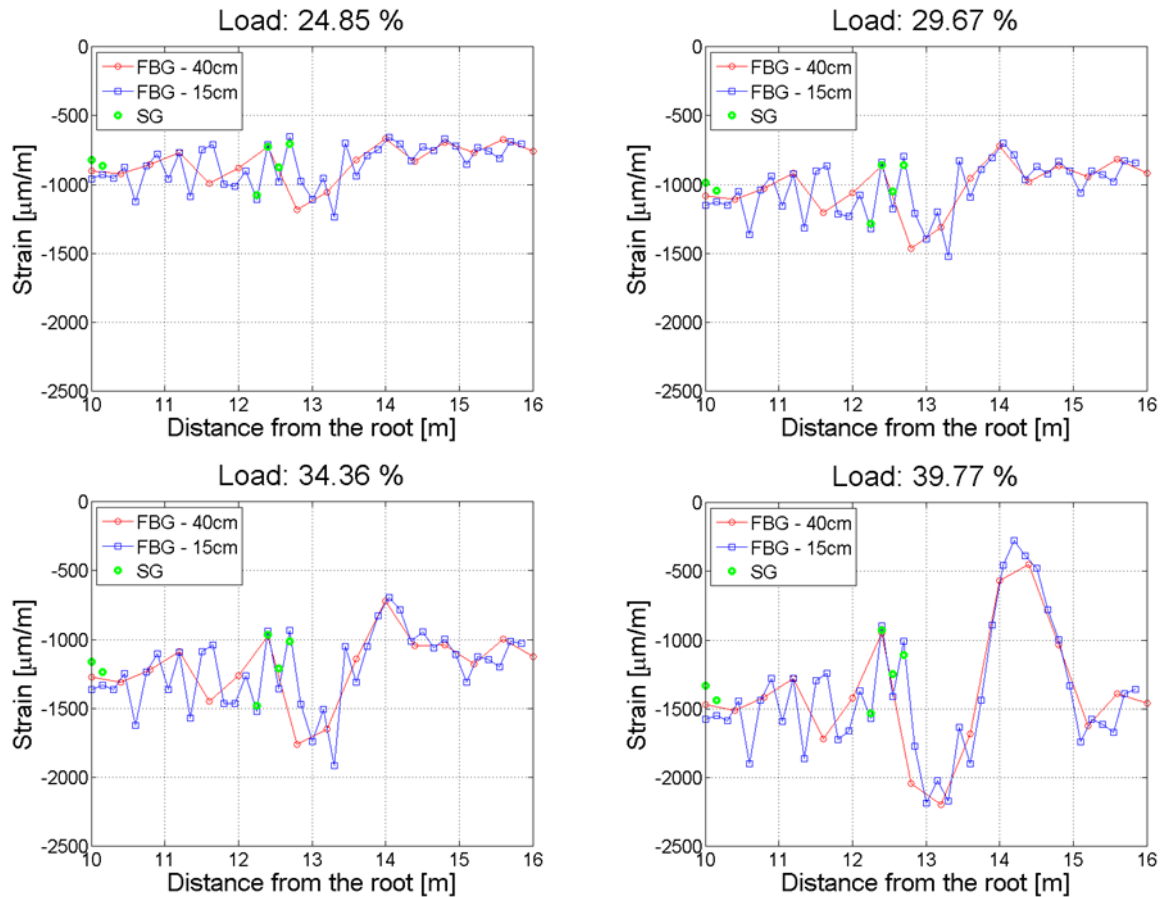


Figure 37 Longitudinal strain measurements of the coarse measurement line (red) and the refined measurement line (blue) and the conventional electrical resistance strain gauges (green) for different load levels along the refined measurement area.

A detailed discussion about buckling waves and their effect on ERRs in the SSP 34m blade can be found in Haselbach et al. (2015).

5. Numerical analysis methods

The computational capacity to date on the DTU cluster limits the size of finite element models to say about 5.0×10^5 elements if results are expected within a reasonable amount computation time. The aforementioned computational efficiency threshold and the size of a typical full scale wind turbine rotor blades leads to mesh discretisation levels which are generally not sufficient for fracture analysis. In other words the mesh resolution is not high enough as to realistically model connection details and not high enough as to predict the near crack tip stress fields. There exist several work-arounds for this dilemma. One possibility is the adoption of numerical sub-component modelling techniques where a sub-component with high level of modelling detail and mesh resolution is connected to a coarse low mesh resolution blade model. The mesh density of the sub-model can be made high enough as to use e.g. cohesive-zone element modelling

techniques. Cohesive zone element modelling can be considered as state of the art in composite material fracture mechanics with the capability to simulate crack initiation as well as crack propagation including fiber bridging (i.e. bridging of crack faces due to glass fibers behind the crack tip). The basis for this technique are traction separation laws that are considered a material property and which can be experimentally obtained such as for instance by DCB fracture tests.

The sub-modelling approach has the disadvantage that the area of failure is arbitrarily imposed by the choice of the location of the subcomponent within the model. Subcomponent modelling approaches might lead to an over estimation of the structural capacity if the wrong sub-model is considered. Moreover, coupling constraints are necessary to connect the coarse model (e.g. shell elements) with the sub-model (e.g. solid elements) which causes boundary effects that can distort the results.

Another option is the adoption of the Virtual Crack Closure Technique (VCCT). The advantage of the VCCT are twofold: First, the VCCT is a computationally inexpensive method and provides the Mode-I,II,III energy release rates separately which proves to be rather useful. Secondly, acceptable levels of accuracy for engineering practise can be achieved with rather coarse mesh resolutions. One disadvantage is that VCCT is based on linear elastic fracture mechanics which means that finite lengths of fracture process zones and fiber bridging cannot be taken into account. Moreover, crack initiation cannot be modelled since the presence of a fully established crack is mandatory. Another drawback concerns the element size dependency of the mode-mixity in bi-material interface problems due to oscillating near crack tip stress fields. A solution to the element size dependency of the VCCT in bi-material interface problems as they can be typically encountered in adhesive joints can be found in literature.

However, the advantages of the VCCT in fracture analysis are so striking that the authors of this report resorted to it as a useful indicator of energy release rates and mode-mixities. The cracks in the analysis presented were put in the adhesive layer for two reasons: First, to avoid bi-material interface situations and secondly to comply with linear elastic fracture mechanics avoiding fiber bridging. Additionally crack propagation was avoided by assigning high values of critical fracture energy values to the model. This is clearly a simplification of a much more complex situation but within the framework of this project the VCCT was used to study how some specific parameters such as cross-section geometry, load types and load directions are causing which fracture mode. The VCCT therefore was an essential tool to study and understand the global structural blade behaviour and its effect on fracture in adhesive joints in general and on the trailing edge in particular. The intention of this initial study was not to conduct advanced fracture analysis in terms of crack initiation and crack propagation.

5.1 3D-modelling methodology

Two full 3D blade models are presented in this section. Figure 38 shows a blade section taken from the light rotor blade where taper and twist was ignored. The model was fully fixed on one end and subject to pure bending on the other beam end. The analysis was displacement controlled for numerical stability purposes. The load was applied via rigid coupling constraints.

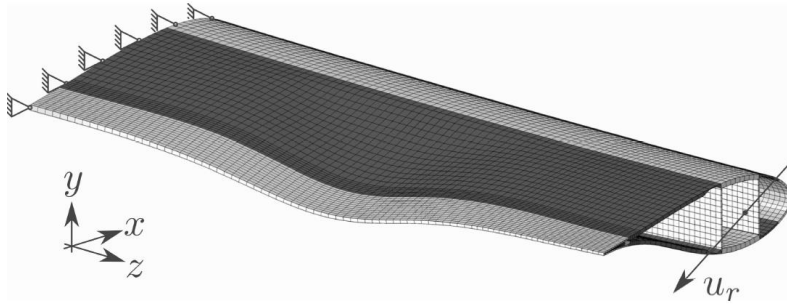


Figure 38 Deformation plot of the 3D model with buckling wave. Boundary conditions left and load (rotation in x-y plane) on the right hand side. (taken from Eder et al. (2014))

Figure 39 shows a super imposed plot of the undeformed configuration and the deformed mesh with Tsai Wu contours. The buckling wave can clearly be seen close to the location observed during the test.

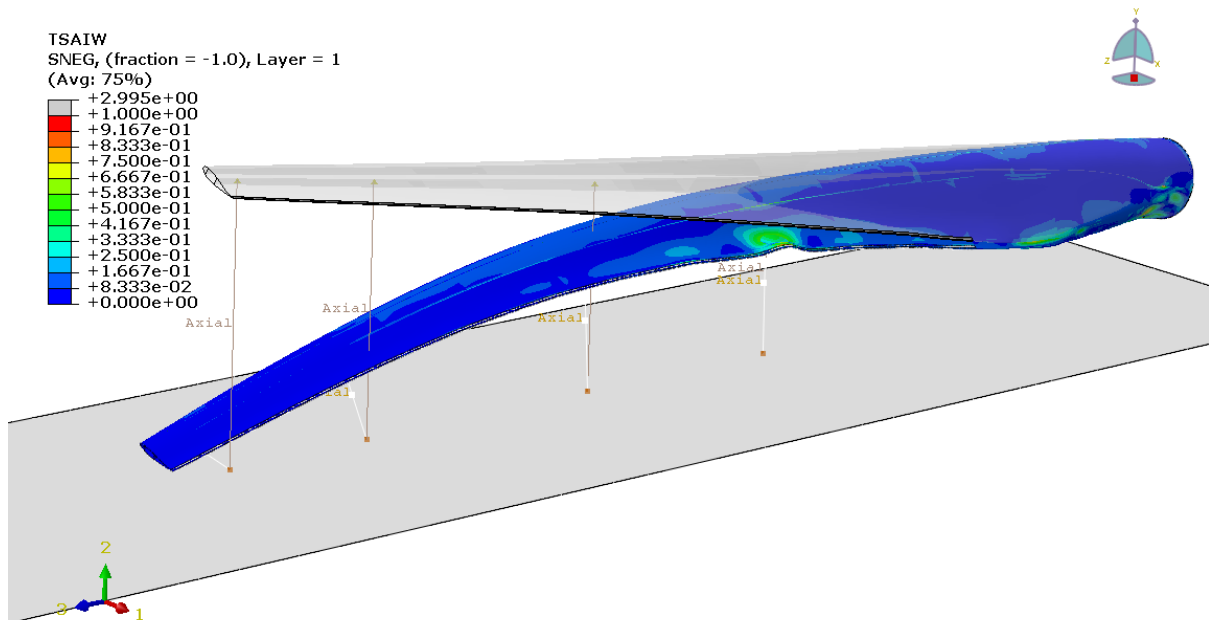


Figure 39 3D shell model of SSP34 blade simulating -30 deg. blade test. The model is fully fixed with kinematic coupling constraints in the root section (right hand side) and loaded through connector elements that can decrease their length in the axial direction (shrinking). This modelling strategy closely reflects the loading configuration during the blade tests. (taken from Haselbach et al. (2015))

5.2 3D-modelling results

Figure 40 and Figure 41 show that local buckling can induce high ERR peaks on the flanks and in the peak area of the local buckling wave. Longer cracks are generally increasing the ERR values which explains the unstable crack propagation.

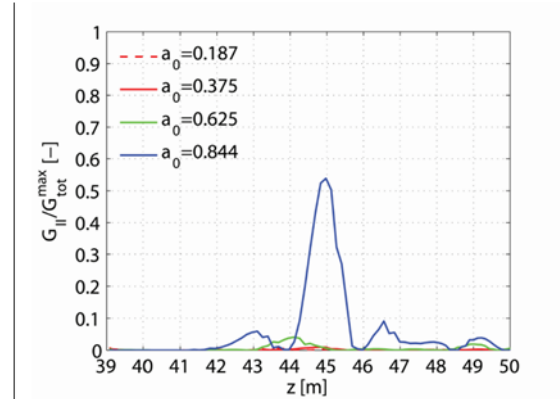
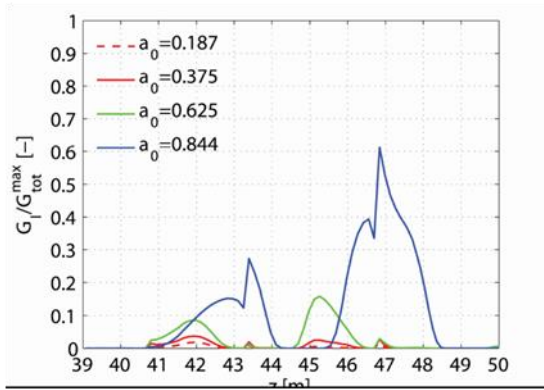


Figure 40 (left) normalised Mode-I energy release rates along crack front for different crack lengths; (right) normalised Mode-II energy release rates along crack front. (taken from Eder et al. (2014))

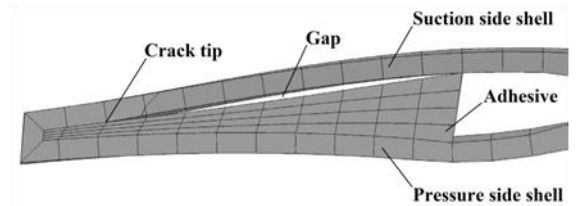
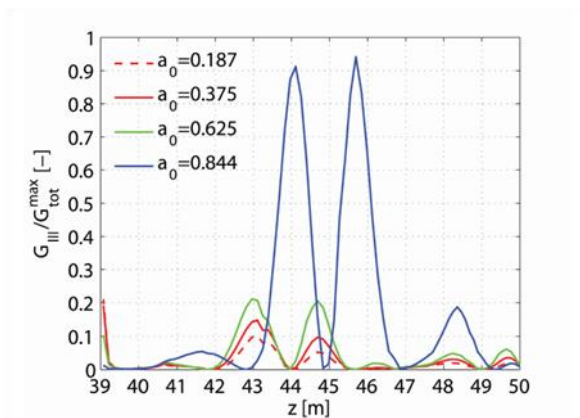


Figure 41 (left) normalised Mode-III energy release rates along crack front for different crack lengths; (right) invert scissors effect for long cracks in bondline leading to Mode-I ERRs in a panel closing situation (taken from Eder et al. (2014))

Figure 42 shows that the sandwich core of the pressure side panel was already damaged prior to trailing edge debonding caused by steep curvatures in the transverse direction at the radial position of the buckling wave peak.

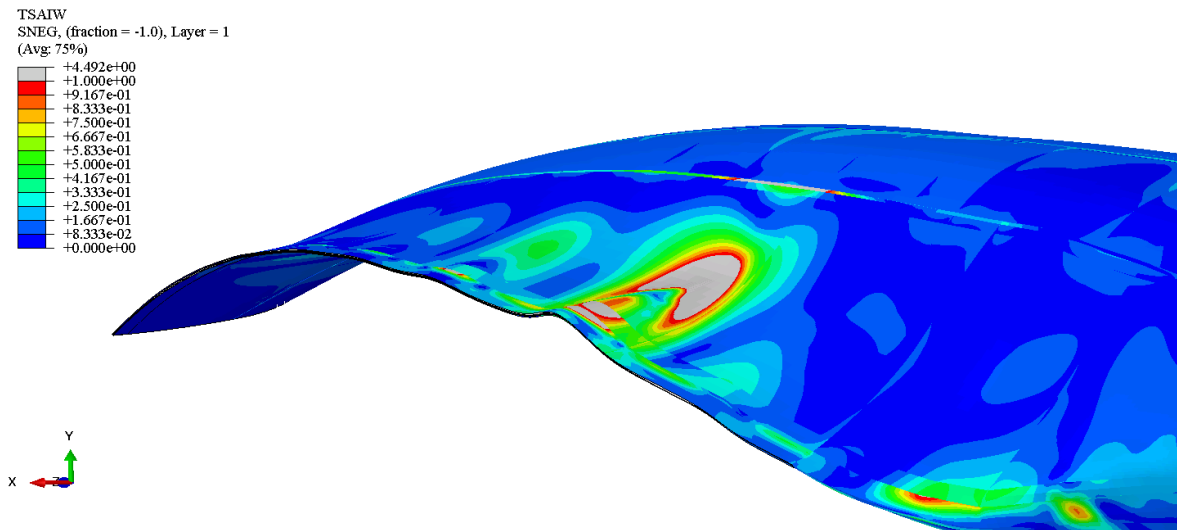


Figure 42 Local buckling wave in the trailing edge of the SSP34 model with Tsai Wu failure criterion contour plots indicating pressure side panel failure. (with courtesy of Philipp Haselbach)

Figure 43 and Figure 44 show contour plots of the ERRs in a crack that was introduced in the adhesive of the trailing edge of the model depicted in Figure 39. The crack length was kept short and could represent a flaw that is already present which runs along the trailing edge. ERRs were computed by means of the VCCT. Figure 44 also shows a G_{tot}/G_{equ} plot where G_{tot} is the sum of all ERR contributions and G_{equ} is the equivalent fracture toughness according to the well-known interaction law proposed by Benzegagh and Kenane. It can be seen that the highest levels occurred for bending moment directions in the second quadrant.

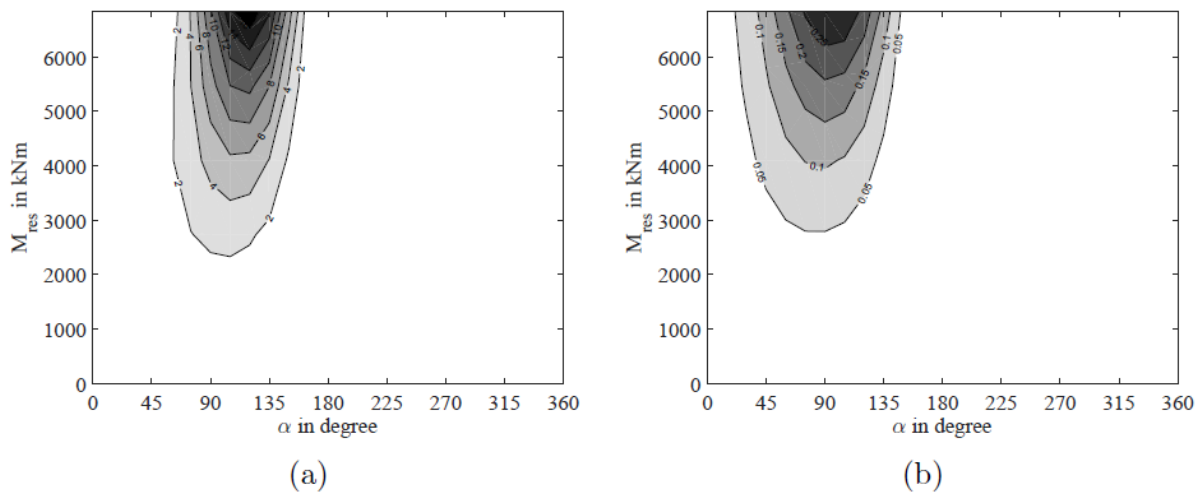


Figure 43 (left) Mode-I ERR contour plots in the crack tip located in the peak of the buckling wave as a function of bending moment magnitude (ordinate) and angle of bending moment vector (abscissa); (right) Mode-II contour plots in the crack tip located in the peak of the buckling wave as a function of bending moment magnitude (ordinate) and angle of bending moment vector (abscissa) (taken from Haselbach et al. (2015))

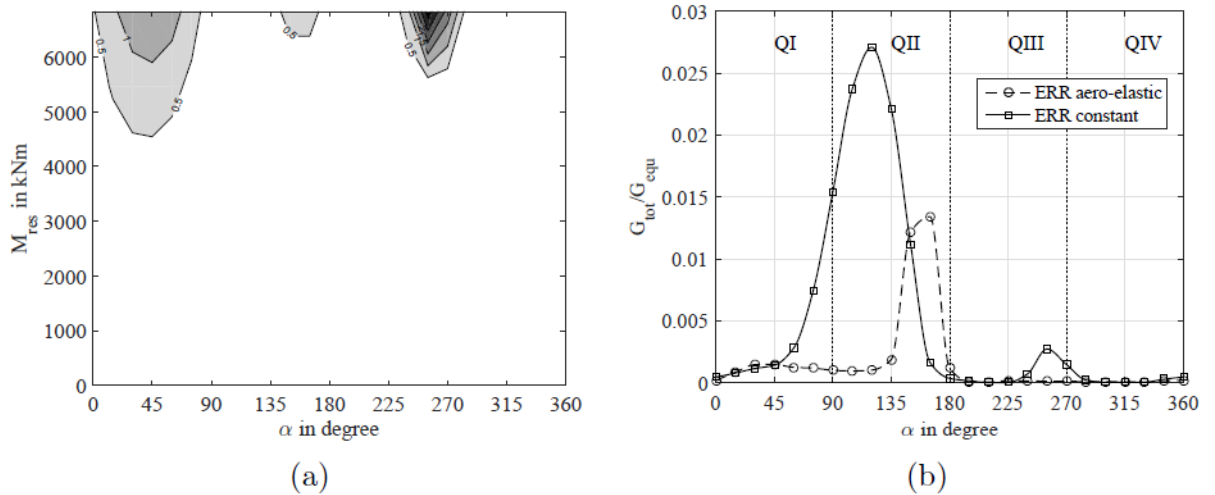


Figure 44 (left) Mode-III ERR contour plots in the crack tip located in the peak of the buckling wave as a function of bending moment magnitude (ordinate) and angle of bending moment vector (abscissa); (right) Normalised ERRs versus bending moment angle for constant bending moment and aero elastic loads (dashed line). (taken from Haselbach et al. (2015))

Figure 45 shows the phase angles in-plane and out-of-plane as a function of the angular direction of the bending moment vector.

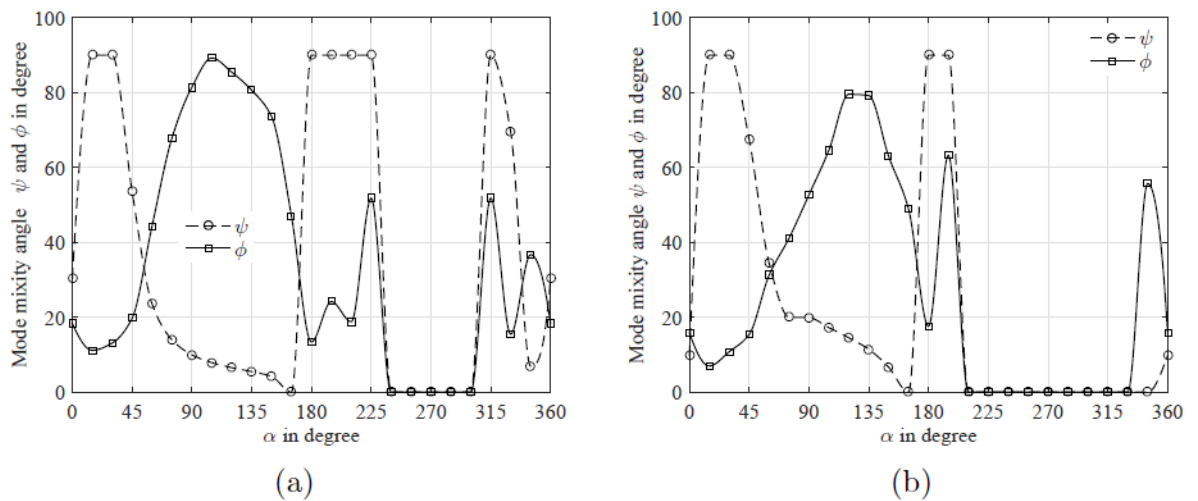


Figure 45 (left) In and out-of-plane mode mixity angles for constant bending moment; (right) the same for aero-elastic loads as a function of the bending moment vector angle. (taken from Haselbach et al. (2015))

5.3 Slice model methodology

The slice model approach is based on the theoretical work done by Brazier (1927), which was later further extended for application at wind turbine cross sections. In the slice model approach only a cross sectional slice of the wind turbine blade is modelled. The motivation for this approach is to study the effects of in-plane cross sectional deformations (i.e. ovalisation) on

adhesive joints on a numerical model that allows a high mesh discretisation level by simultaneously maintaining its computational efficiency. Figure 46 illustrates the Brazier pressure which causes the in-plane cross-section deformation commonly also referred to as ovalisation.

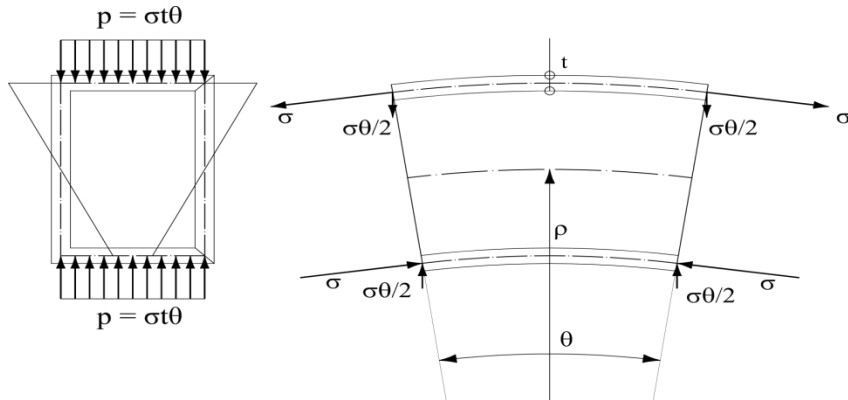


Figure 46 The source of the Brazier pressure depicted on a rectangular hollow section. Second order considerations lead to vertical components of the bending stress vector which leads to cross-section ovalisation.

Figure 47 shows the location of the six main joints as they occur in wind turbine rotor blades. The classic design consists of a main carrying box girder comprising two caps and two webs. The lift generating surfaces also called panels are adhesively connected to the main spar. The joint details shown in Figure 48 are only one possibility and design specific. It can be seen from Figure 48 that the connections of the panels offer a low rotational stiffness which affects the force transfer to the joints.

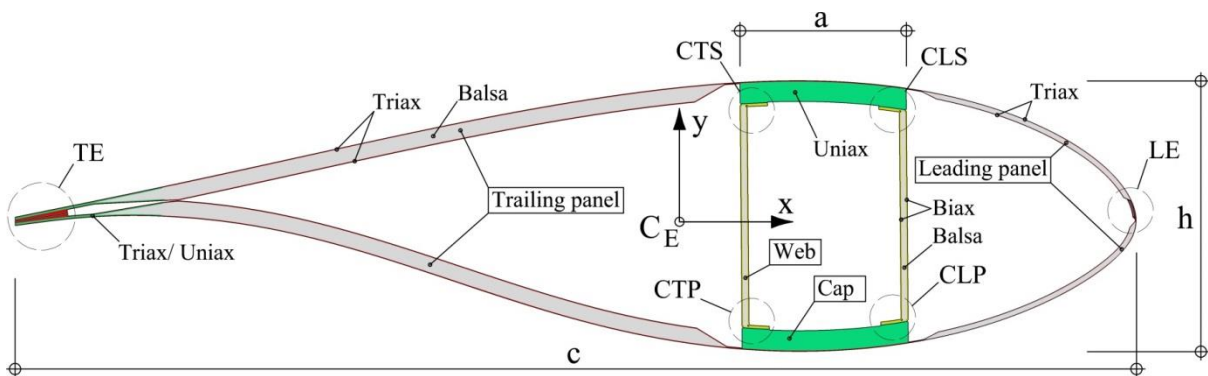


Figure 47 10MW Light rotor blade cross section at 70m with different materials and 6 main joints in the cross-section. (taken from Bitsche et al. (2015))

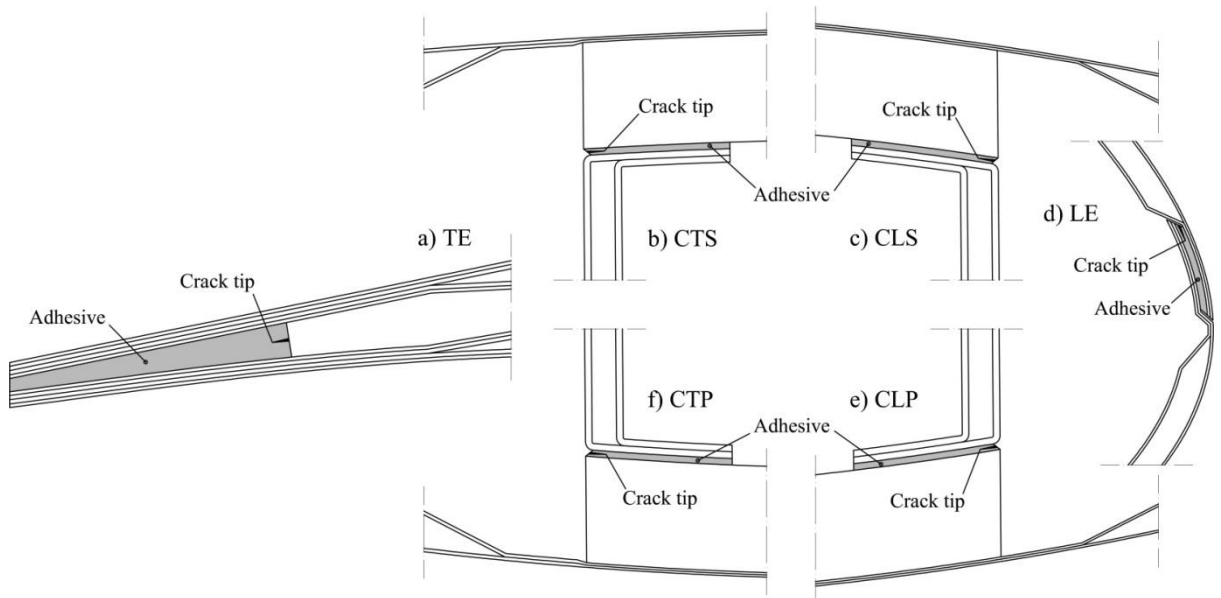


Figure 48 Details of 6 adhesive joints with crack locations and crack lengths. (taken from Bitsche et al. (2015))

Figure 49 shows the slice modelling approach as discussed in the last section of this report. The boundary conditions of the slice allowed in-plane deformations but no out-of plane warping deformations as a necessity of pure bending situations. Loads were applied via a kinematic coupling constraint on the front surface.

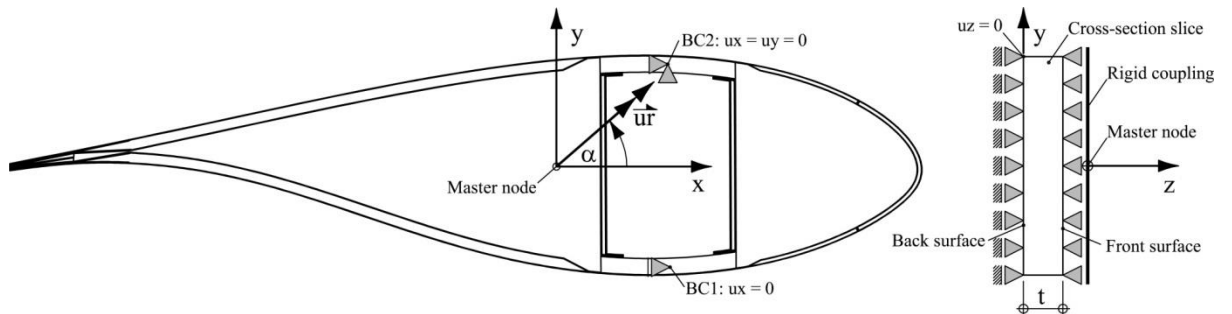


Figure 49 (left) cross section with coordinate system, rotation vector (load) and the angle of the rotation vector; (right) cross-section slice with boundary conditions and kinematic coupling constraint assigned to the front surface. (taken from Bitsche et al. (2015))

Figure 50 shows how the three main joint types were discretised in the model. It can be seen that the slice approach allows a detailed representation of the joint geometry at a level which cannot be achieved in a full 3D model without increasing the computation time tremendously.

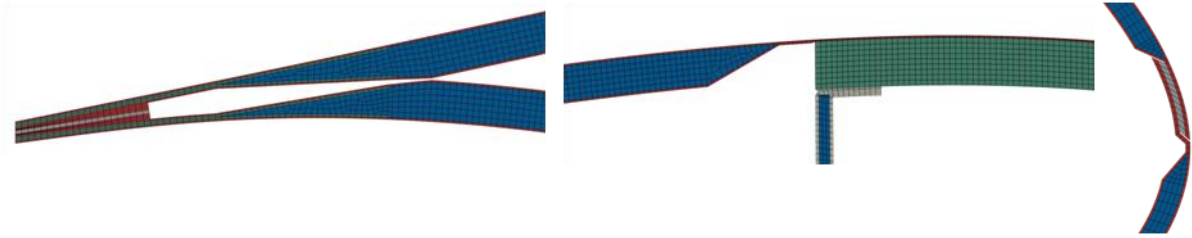


Figure 50 Mesh details of three typical joints namely the trailing edge joint (left), cap joint (centre) and leading edge joint with different materials. (taken from Bitsche et al. (2015))

5.4 Slice modelling results

Figure 51 and Figure 52 show Mode-I and Mode-II ERRs in the trailing edge and the leading edge crack respectively. It can be seen that in every joint critical loading directions exist. Especially the trailing edge behaves in a similar way like the analytical model.

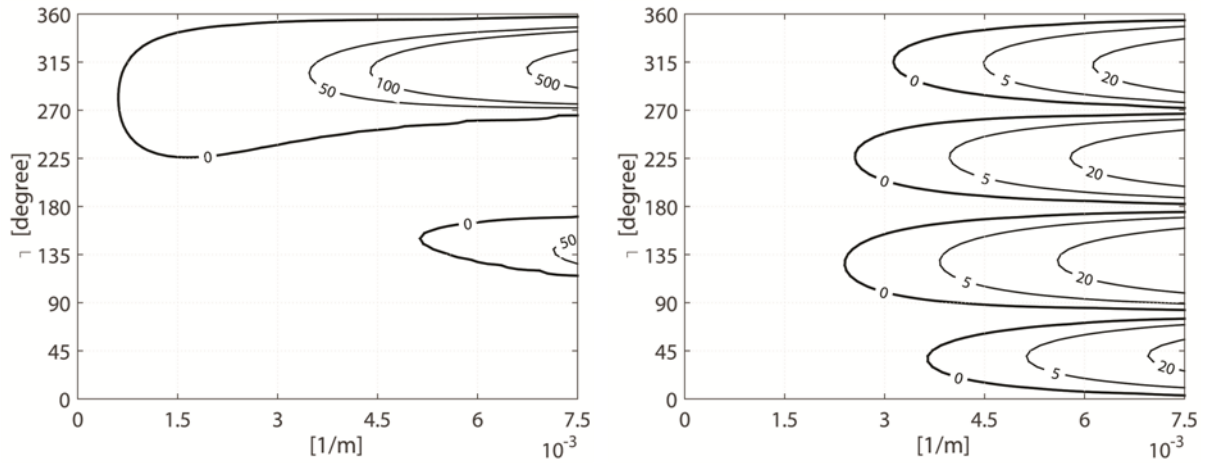


Figure 51 (left) Mode-I ERR contour plots for angle of bending axis and curvature for trailing edge joint; (right) Mode-II ERR contour plots for angle of bending axis and curvature for trailing edge joint. (taken from Bitsche et al. (2015))

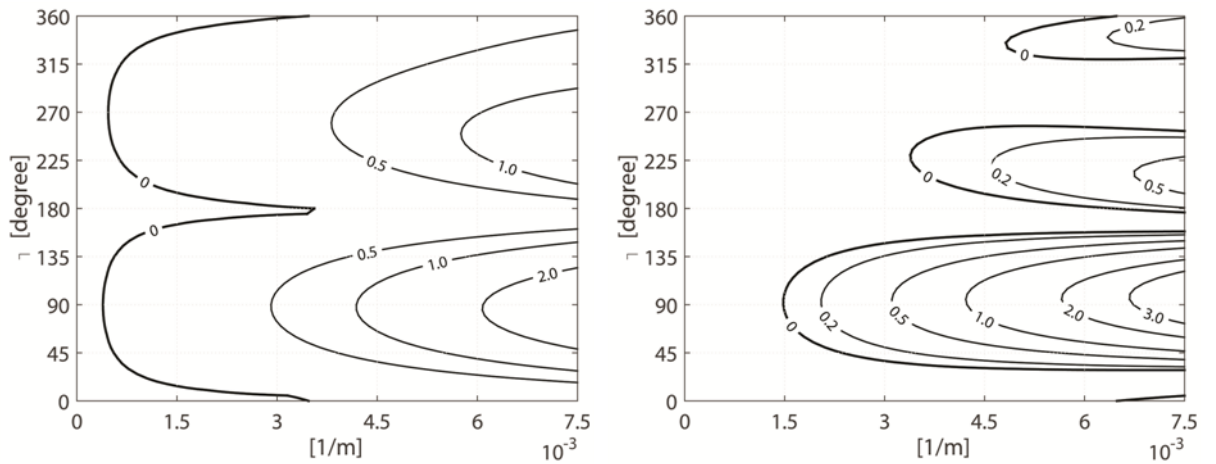


Figure 52 (left) Mode-I ERR contour plots for angle of bending axis and curvature for leading edge joint; (right) Mode-II ERR contour plots for angle of bending axis and curvature for leading edge joint. (taken from Bitsche et al. (2015))

Figure 53 shows a G_{tot}/G_{eq} plot of the trailing edge joint as a function of the bending moment direction and the beam curvature. with a clear peak at 315 degrees which clearly identifies the critical loading direction for the trailing edge in this specific blade.

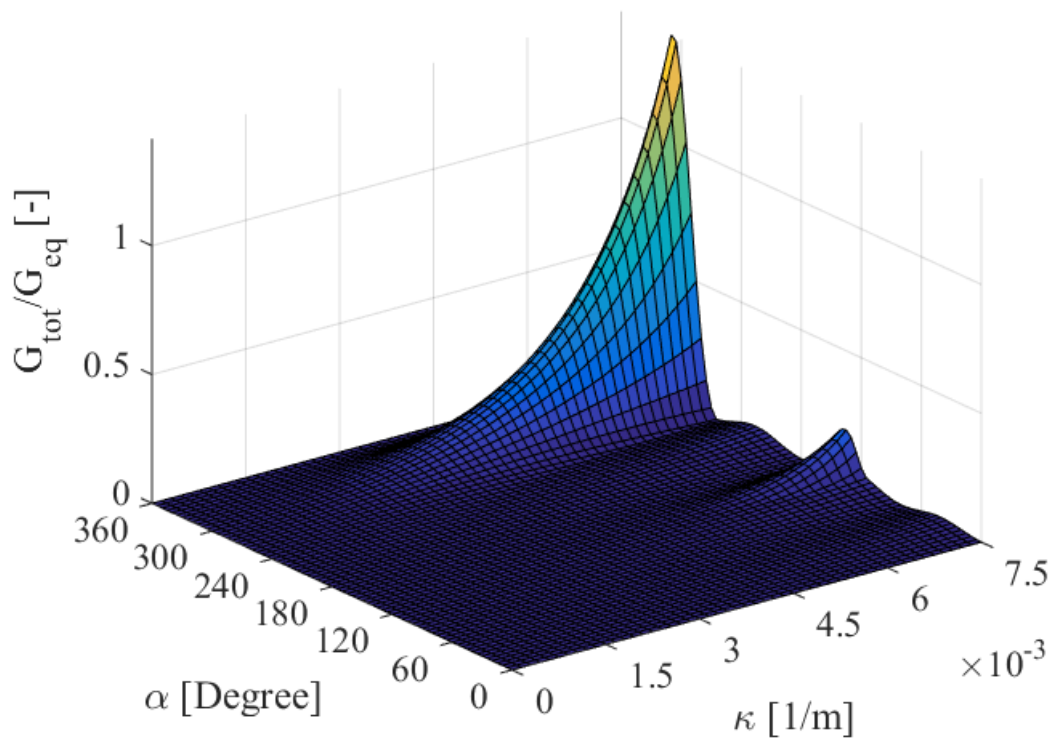


Figure 53 Normalised ERRs as a function of curvature and angle of bending axis.

Figure 54 shows the axial forces in the suction side and the pressure side panel in the analytical model and the numerical slice model. In both cases the axial forces follow an oscillating function of the angular direction of the bending moment direction. It can be seen that opening of the trailing edge is associated with tension in the pressure side panel and compression in the suction side panel.

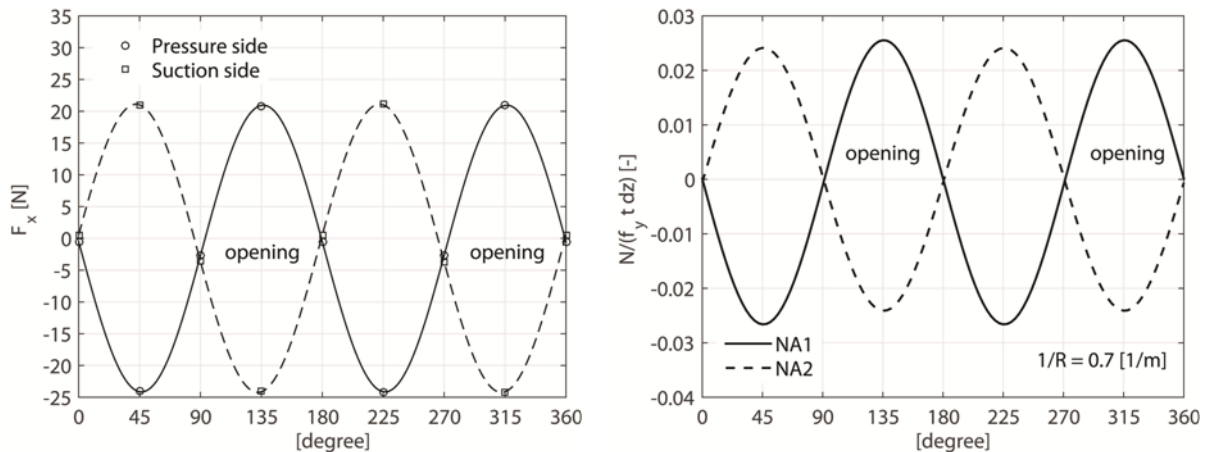


Figure 54 (left) axial force close to the flow front of the adhesive joint in the pressure side panel and the suction side panel; (right) axial forces of the upper and lower cross section beam adjacent to point A. (taken from Eder & Bitsche (2015) and Bitsche et al. (2015))

A detailed investigation of fracture behaviour of adhesive joints in the 70m section of the 10MW light rotor blade with comprehensive results can be found in Bitsche et al. (2015).

6. Analytical method

Analytical methods are an important means to gain deep insight into the governing equations from which generic structural behaviour can be inferred. It is well known that analytical solutions – if available - can provide more answers than numerical solutions. However, the complexity of the structural behaviour of wind turbine blades owing to material anisotropy and varying geometry makes analytical solutions unavailable most of the time and numerical solutions are the only resort. The motivation of the analytical solution presented in the subsequent section was to corroborate a conjecture. The conjecture shared with many blade designers was that airfoils with a higher cross sectional curvature of the trailing edge panels are more likely to have problems in the trailing edge joint. Although this effect could already be seen in numerical models it was rather difficult to trace the cause of this effect. It was relatively straight forward to identify this effect being attributed to geometric nonlinearity by running the same model with and without geometric nonlinearity effects. It appeared that the Mode-I in-plane trailing edge deformations were negligibly small in linear analysis when compared to geometrical nonlinear analysis.

It was obvious that the observed effect was caused by the Brazier effect especially as literature already pointed in a similar direction. The astonishing thing was that the Brazier pressure

usually tends to squeeze sections together which would explain the closing but not the counter intuitive opening effects which have clearly been measured and seen in numerical models. This gave rise to embark on an analytical cross section that resembled the geometry of the trailing edge. In other words a thin walled, asymmetrically curved cross section where two edges are joining at an acute angle forming a re-entrant corner. For the sake of simplicity the material was assumed to be linear elastic and isotropic. The beam was assumed to be straight i.e. without taper and twist and subject to pure bending i.e. shear forces were neglected. The solution should incorporate parameters such as panel curvature, aspect ratio, wall thickness and arbitrary bending direction. If the model can predict the behaviour correctly then the identification of the root cause should be possible by looking at the equations.

6.1 Analytical methodology

The analytical approach is an extension of the Brazier solution for asymmetrically curved cross sections. It is based on second order deformation theory where the bending stresses in a cross section are causing deviatoric stresses which are pointing perpendicularly towards the axis of bending (see Figure 55). These stresses are commonly referred to as Brazier pressure but noteworthy to point out that the pressure as such is only a thought model and must not be confused with an externally applied pressure but merely as an internal cross-sectional stress component. A description of the theoretical background with a discussion of its implications on fracture analysis of wind turbine blades can be found in Eder & Bitsche (2015).

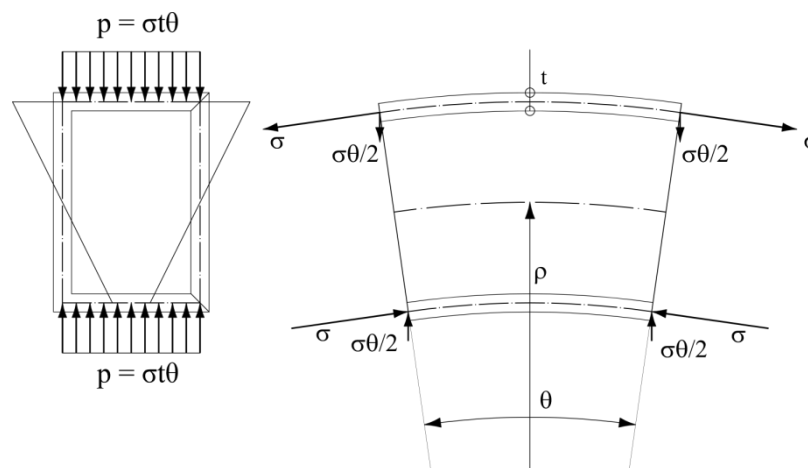


Figure 55 Source of the Brazier effect explained on a rectangular cross section and an infinitesimally long beam element subject to pure bending.

The beauty of the Brazier approach is that in an initially straight beam that is subject to pure bending situations symmetry is preserved which means that every cross section deforms in exactly the same way as its neighbouring cross sections. This means that the initially 3D problem can be condensed down to a 2D problem which can be solved on a cross section level. However, if the Brazier effect is applied to an asymmetrically curved thin walled hollow section, symmetry is no longer preserved and it turns out that a so called Brazier torsion is induced into the cross-section (see Figure 56). This torsional moment per unit length induces rigid body rotations which make the solution dependent on the boundary conditions assigned to that

section. The source of the torsional moment can be seen in Figure 56 where the infinitesimal Brazier pressure dp causes a torsional moment contribution regarding the elastic centre.

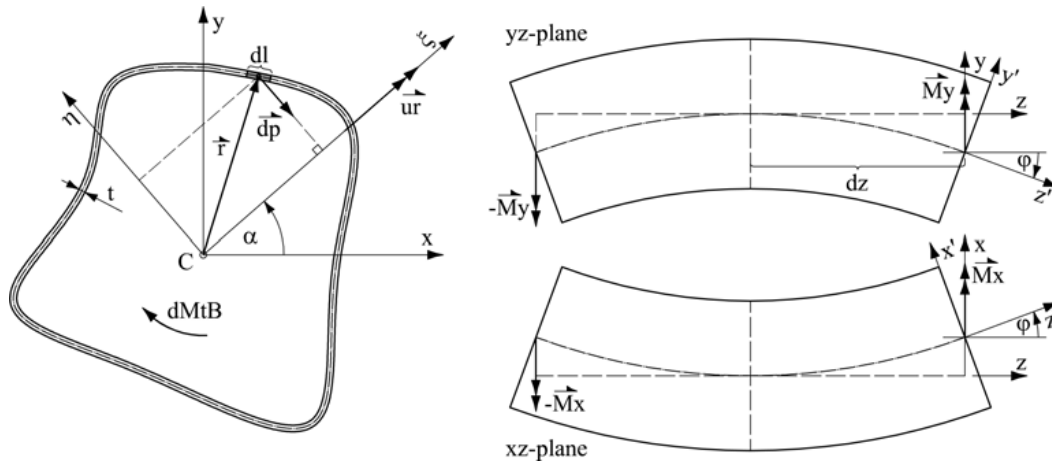


Figure 56 (left) arbitrary cross section with coordinate system and displacement based loading convention used to derive the Brazier torsion; (right) infinitesimal beam element with moment based loading used to derive Brazier pressure from different point of view. (taken from Eder & Bitsche (2015))

In order to let the reaction forces of the boundary constraints vanish a compensation shear stress was applied in the opposite direction. Figure 57 shows the cross section with a uniform thickness. The analytical approach followed the idea of considering the walls of the cross section as beams themselves which can be solved in 2D using classical beam theory.

The points A, B and C are located on an isosceles triangle where points A-B and A-C were connected by circular arcs joining in point A at a shallow angle (see Figure 57).

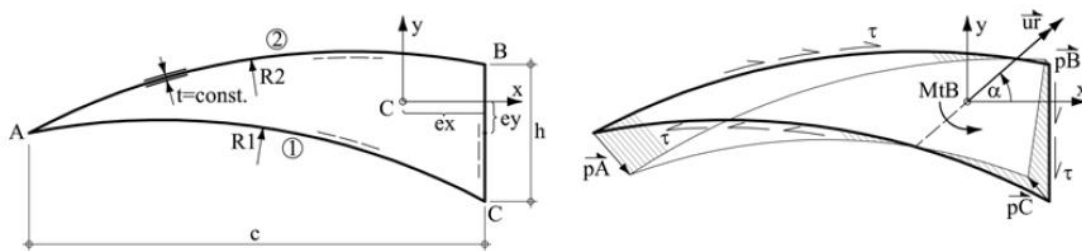


Figure 57 (left) wind turbine blade inspired mono-cellular cross-section used for analytical investigation; (right) Brazier pressure with compensation shear stress and Brazier torsion. (taken from Eder & Bitsche (2015))

The problem at hand is statically in-determined linear elastic and the solutions were obtained by the principle of virtual work. The model was subject to a rotation vector that was rotated by 360 degrees. The rotation can be transformed into a beam curvature which causes a bending moment that produces out-of-plane bending stresses.

6.2 Analytical results

Figure 58 shows the in-plane bending moment in point A as a function of the angular direction of the rotation vector and the panel curvature. It can be seen that the panel curvature has a significant influence on the in-plane-deformation behaviour. To be more precise, an increase of curvature increases the bending moment M_A for the same out-of-plane bending moment magnitude.

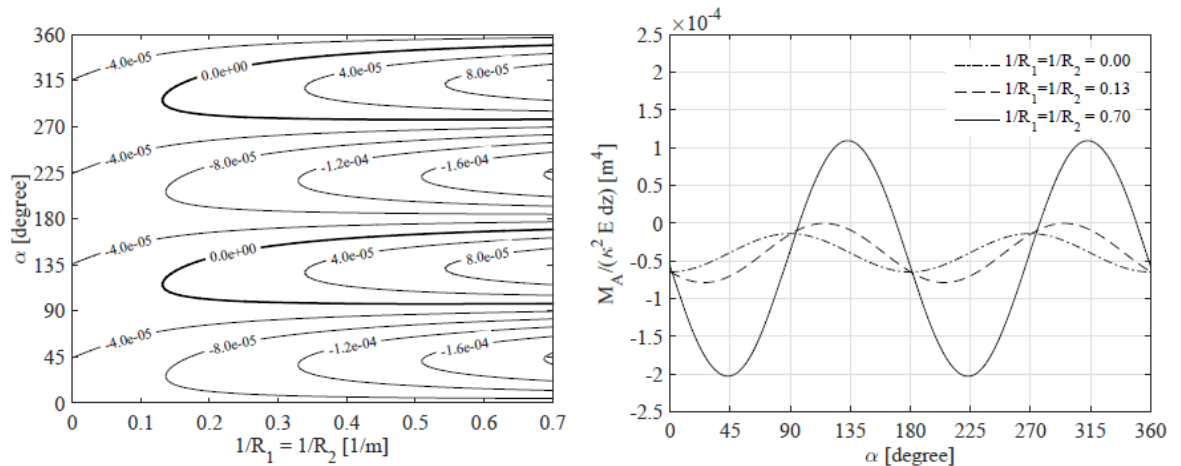


Figure 58 (left) in-plane corner point bending moment M_A contour plots as function of the angle of bending axis and cross-section panel curvature; (right) bending moment M_A as function of the bending axis angle for three different cross-section panel curvatures. (taken from Eder & Bitsche (2015))

Figure 59 shows the KI values obtained by the analytical solution for a UBM-DCB specimen. It shows that Mode-I stress intensity factors occur at two bending moment directions and that these can exceed the fatigue threshold in the example presented.

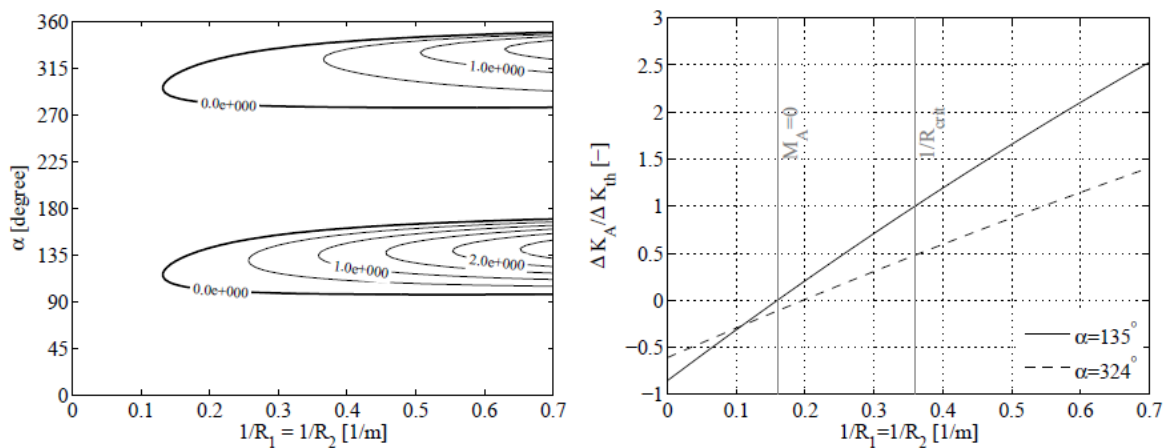


Figure 59 (left) Normalised $K-I$ stress intensity factor contour plots; (right) normalised $K-I$ values at two distinct angles of bending axis versus cross-section panel curvature. (taken from Eder & Bitsche (2015))

The analytical results were validated against a 3D shell model as shown in Figure 60 that for the 135 degree loading direction.



Figure 60 (left) 3D shell model of main beam with superimposed deformation plot; (right) cross-section beam slice taken from mid span with superimposed cross-section deformation. Deformation scale factor 10. (taken from Eder & Bitsche (2015))

Good agreement between the analytical solution and the numerical results was found which can be seen in Figure 61.

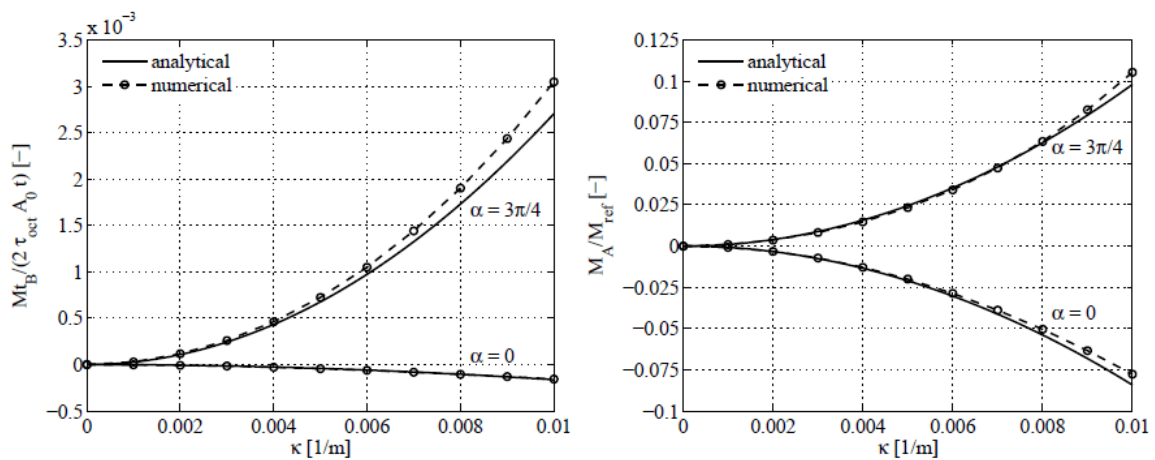


Figure 61 (left) Comparison of numerically obtained Brazier torsion (dashed) with analytical solution for two different angles of bending; (right) comparison of numerically obtained in plane bending moment M_A (dashed) with analytical solution for the same angles. (taken from Eder & Bitsche (2015))

Figure 62 shows good agreement between in-plane deformations of the cross-section shown in Figure 57 for two different loading angles. It can be seen how the corner in point A closes and opens for depending on the direction of bending. The opening of corner point is associated with Mode-I stress intensity factors which are deemed as being a main contributor to fatigue damage.

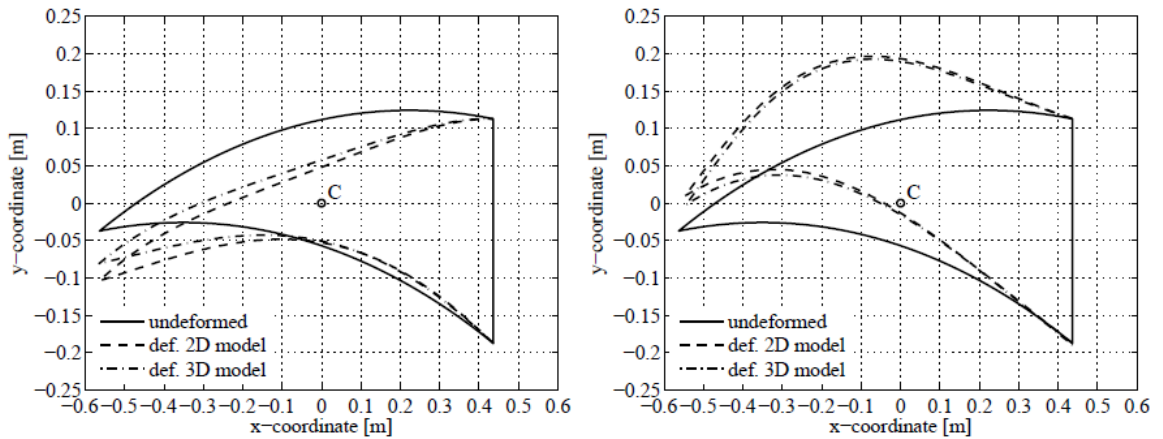


Figure 62 (left) comparison of numerically obtained cross section deformation (dashed) with analytical solution for $\alpha=0$ degrees (dash-dot); (right) comparison of numerically obtained cross section deformation (dashed) with analytical solution for $\alpha=135$ degrees (dash-dot). (taken from Eder & Bitsche (2015))

7. Sub-component test

7.1 Sub-component testing methodology

Sub-component tests play a significant role in experimental research. Sub-components are parts of a larger structure and the idea of testing sub-components is mainly driven by time and cost savings when compared to the costs of full scale tests. Especially in the realm of fracture mechanics down scaling of full scale structures in order to work around the issue inevitably leads to size effects. The implication of the size effect is that conversely to material plasticity the failure loads – caused by fracture - do not scale proportionally to the size of the structure. Even worse, the fracture location and governing fracture mode between different scales might differ significantly. As a general rule of thumb the capacity of a structure is inversely proportional to its size. In the literature different reasons for the size effect can be found. One explanation is that the likelihood of the presence of flaws increases when the size increases which statistically lowers the capacity according to the Weibull distribution. Another explanation is that the fracture process zone at the crack tip does not scale with the size of the structure but is merely a material constant which can be expressed by the Young's modulus and the critical fracture energy. One possibility to overcome size effects in structural testing is scaling laws which proved to be to-date unavailable for complex structures especially for composite materials. This means in order to have a realistic representation of the real structural behaviour, the sub-component needs to have a similar size like the ones applied at full scale.

Sub-component testing has originally been developed by the automotive industry but also finds applications in civil- and aeronautical engineering practise to name only a few. Sub-components can also be used in the framework of pseudo dynamic testing where sub-component tests are combined with numerical models where the entire structure is cost efficiently discretized by finite elements. In such a scheme the displacements measured during the tests are transferred to a finite element model which uses these displacements to calculate the stiffness and the forces

acting on the subcomponent. Subsequently these forces are applied to the sub-component in a feed-back loop. In this way dynamic processes and their effect on the full scale structure can be simulated where material strength and stiffness degradation processes owing to plasticity or fracture can be taken into account. Since the numerical computation of the solution of the governing differential equations takes usually longer than the dynamic process in real time these tests are conducted in pseudo time. Pseudo time means that certain effects like strain rate effects as they typically occur in a dynamic loading situation cannot be taken into account.

However, the principle and simultaneously the challenge of sub-component tests is to replicate both force- and displacement boundary conditions along the free body cut of the sub-component. In other words to satisfy the von Neuman and Dirichlet boundary conditions along the edges and/or points the subcomponent has virtually been 'cut out' and removed from the bigger structure. Although this is relatively straight forward for some mechanical parts e.g. like dampers or the like with well-defined boundary conditions such as rotational hinges it becomes less straight forward in the case of wind turbine blades.

A trailing edge sub-component typically consists of a part of the suction side and pressure side panel which includes the adhesively bonded area. The edges of the panels – following the free body cut principle - are subjected to complex 3D stress conditions that vary nonlinearly along its edges. The reasons are that on this level of structural detail the panels are shells that undergo out-of-plane and in-plane deformations involving all six components of the local shell section forces along the free body cuts. In fact these boundary conditions are rather difficult to realise in a testing condition which would involve the control of multiple actuators with the ability to follow the deformation of the sub-component. One issue involves boundary effects as they appear along the load introduction points which need to be reinforced in such a way that failure is prevented in the boundaries. Reinforcement of the load introduction points however, alters the stiffness of the sub-component. Moreover, boundary effects can travel a long distance into the specimen potentially changing the real stress and strain state in the fracture process zone. Moving the boundaries further away according to St. Venant's principle increases the sub-component size and compromises the advantages of sub-component tests.

In order to overcome these shortcomings it makes sense to find a compromise by identifying the prevailing damage mode and by simplification of the sub-component testing methodology. That is to say that the sub-component and the testing methodology are specifically designed for the specific failure mode under investigation.

This was done in this research project by means of uniform bending double cantilever beam (UBM-DCM) sub components. The research interest was to investigate the fracture behaviour of an adhesively bonded trailing edge joint subject to in-plane cross-section forces (also referred to as prying forces). Prying forces in wind turbine blades are caused by Poisson's ratio effects and geometrically nonlinear effects as explained in the next section. The basic assumption of these sub-components is that transversely oriented cracks are already present in the bond line and that these prying force driven cracks would propagate in the transverse direction. This on one hand represents a simplification of the real situation where such a sub-component would also be subject to out-of-plane forces. Moreover, such a crack would almost certainly change its propagation direction and continue to propagate in the longitudinal blade direction. On the other hand, considering that prying forces are causing Mode-I energy release rates in the flow front of

the adhesive which are more severe than those caused by Mode-III out-of-plane forces the present sub-component represents a good approximation for a fracture initiation situation. Thickness and layup as well as the stacking sequence of the UBM-DCB sub-components (specimens) were made in close agreement with the layup architecture of the trailing edge of the SSP34 blade. The beams were adhesively connected by an epoxy based bonding paste. All specimens were manufactured under controlled conditions in the DTU-KOM fiber lab. The motivation was to study how different flow front geometries could be used to increase the fracture initiation in order to delay crack growth e.g. under fatigue loading situations. Additionally, critical fracture energies for steady state crack growth could be obtained. It is noteworthy to say that the energy release rate in UBM-DCM tests are not depending on the crack length as no shear forces are present in the beams. This generally enables steady state crack growth and the development of fiber bridging which eases the experimental determination of critical energy release rates.

Three different flow front geometries were used to investigate the fracture initiation levels as shown in Figure 63. Five specimens were tested at DTU-KOM under nominal Mode-I and under mixed mode conditions for every detail giving a total number of 30 specimens.

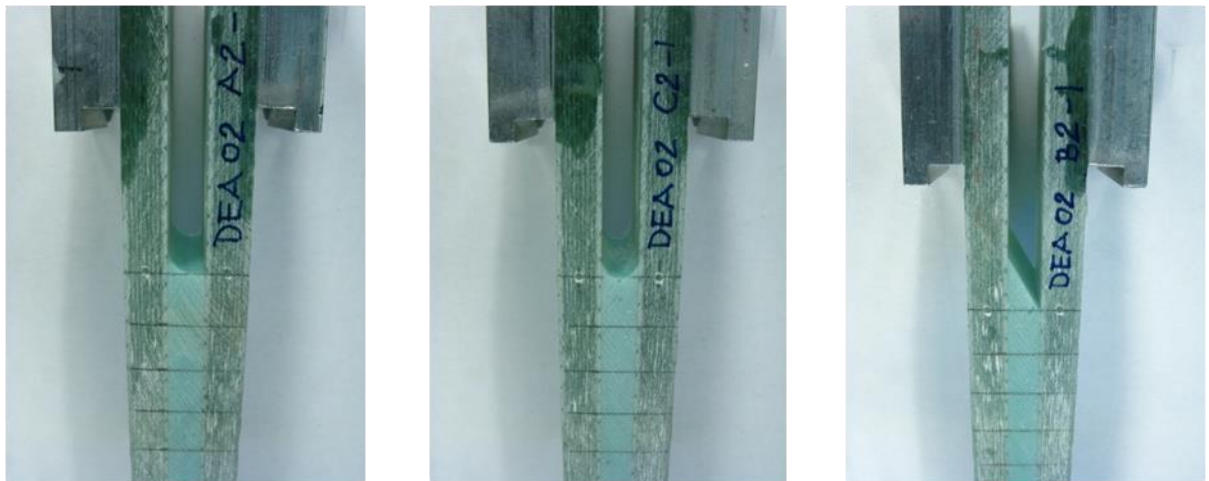


Figure 63 Close-ups of three different flow front details of UBM-DCB specimens. (left) Type-B with 90 degree singularity, (centre) Type-C semi circular 150 degree singularity and (right) Type-A 30 degree singularity. (taken from Eder et al. (2014))

7.1.1 Sub-component test results

Figure 64 and Figure 65 are showing the Mode-I and the mixed mode ERRs of three different details. It can be seen that the initiation energy is higher in the Type-C detail but the fracture toughness decreases significantly as a matter of unstable crack propagation in the adhesive.

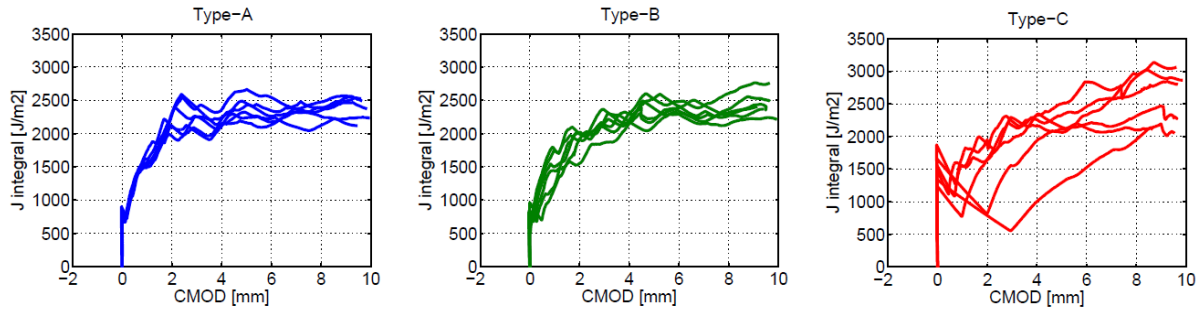


Figure 64 Energy release rates as function of crack mouth opening displacements for nominal Mode-I tests for three different types as indicated in the headers of the figure. (taken from Eder et al. (2014))

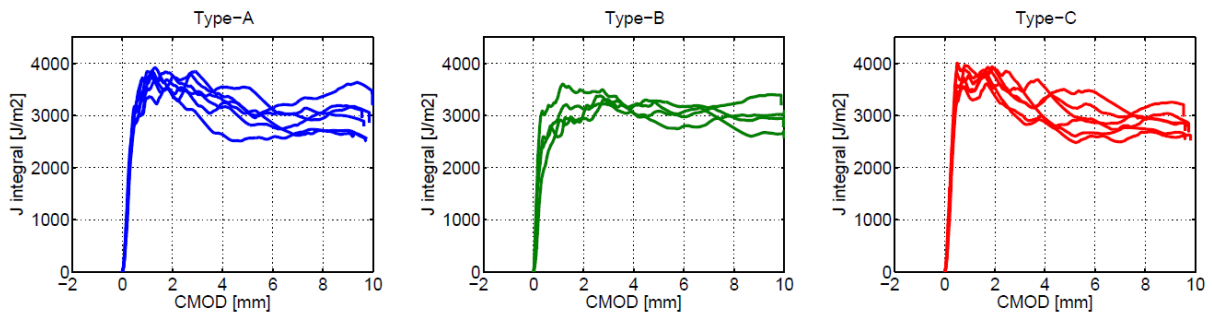


Figure 65 Energy release rates as function of crack mouth opening displacements for mixed mode tests for three different types as indicated in the headers of the figure. (taken from Eder et al. (2014))

Figure 66 shows the mode mixity dependence of the VCCT in bi-material interface problems following a logarithmic distribution. The out of plane mode mixity (blue square) is not affected by the element size.

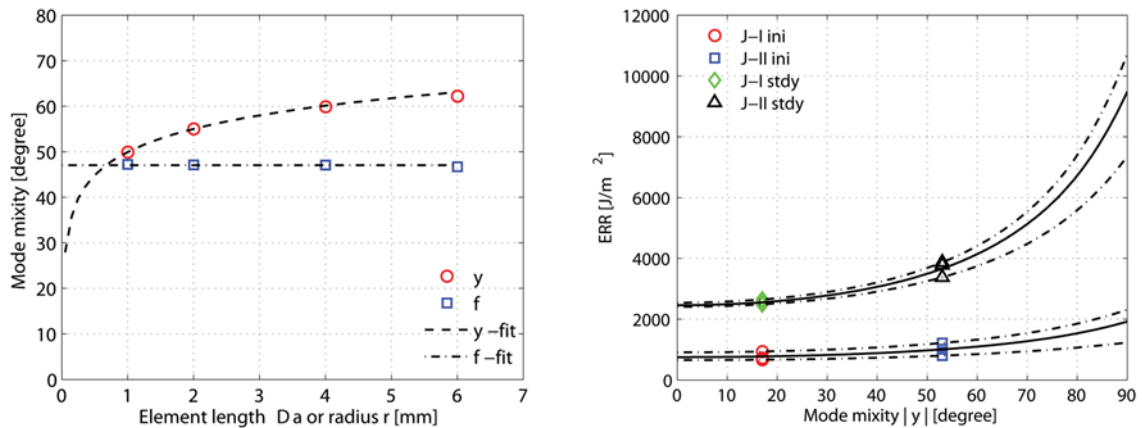


Figure 66 (left) phase angle or mode mixity between Mode-I and Mode-II as a function of the element length computed by VCCT; (right) averaged Initiation and steady state ERRs for Type-A detail. (taken from Eder et al. (2014))

Figure 67 shows the specimen in the testing machine with fixtures for the LVDTs used for measurement of crack mouth displacements. Acoustic emission sensors were applied by

clamps on both sides of the specimen in order to detect crack initiation. Crack initiation and propagation in the adhesive led to decreased ERRs.

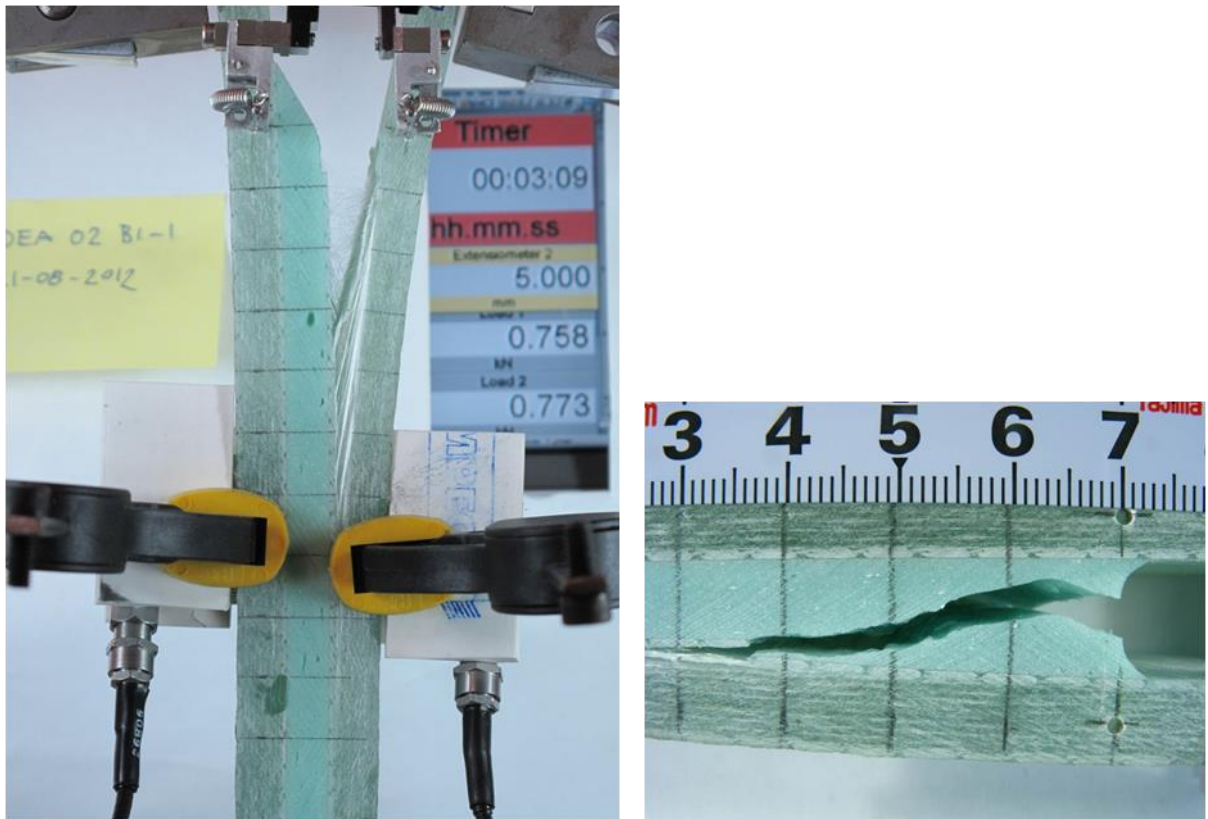


Figure 67 (left) mixed mode test close up in the testing machine. Fully developed steady state crack propagation with fiber bridging propagating in the biax layers adjacent to the interface; (right) close-up of nominal Mode-I test with crack initiating in the centre of the adhesive and propagating in the adhesive. Crack eventually kinks to one interface and continues to grow in the biax material.

The application of measured critical ERRs of adhesive joint sin numerical fracture analysis of wind turbine blades can be found in Eder & Bitsche (2014) and Eder et al. (2014).

7.2 Development of a framework for reliability analysis of wind turbine blades

During design of wind turbine blades tests on several scales are normally performed in order to estimate the material properties and to verify the computational design models used to estimate the load bearing capacity, see Figure 68.

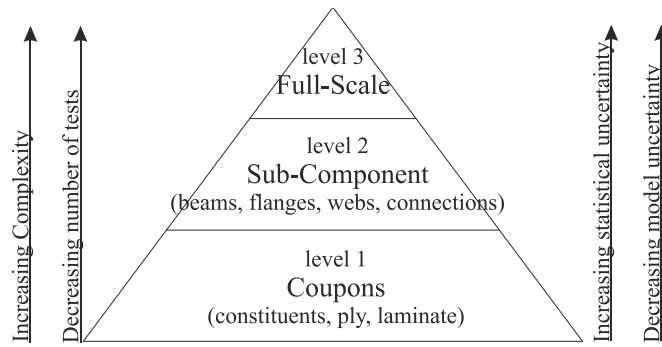


Figure 68 Illustration of tests performed for assessment of load bearing capacity of wind turbine blades.

At coupon level small tests specimens with the basic material are tested in order to determine the material properties and their statistical characteristics in both ultimate and fatigue limit states. The test specimens at coupon level are normally relative inexpensive to produce and test by which many repetitions can be performed if beneficial.

At sub-component level parts of a wind turbine blade are tested in order to determine selected parts load bearing capacity and verify computational models for potential critical details. Sub-component tests are in general more expensive and complicated to test than coupons for which reason only a few tests are performed with each sub-component.

At full-scale level prototypes of the blade are tested both dynamic and static following the requirements in the IEC 61400-23 standard on full-scale testing. Since the cost of a blade itself is high and the time needed for the dynamic test can be several months for large blades also costs due to waiting time for market introduction are significantly.

Additionally, down-scaled blades, components or details can be tested in order to obtain additional information. However, for these tests scale-effects should be carefully addressed. Numerical models based on the finite-element model are normally used to estimate the load bearing capacity of full-scale wind turbine blades or sub-components. By investigating different finite-element models with e.g. different load application methods, boundary conditions or element-types these estimates can also to a certain extend be considered as test results. The theoretical and physical background for finite-element modelling should never be compromised in order to obtain additional information.

The purpose of work package 5 has among others been to develop the basis for using coupon, sub-component, full-scale and partly numerical tests as part of the design process. In the development of the theoretical basis probabilistic models has been adopted in order to take the number of tests and the natural variation in test results into account. Additionally, these models allow for a quantification of the structural reliability and partial safety factors. The results of the work package have been reported in the two reports "Milestone 6: Recommendations for future sub component tests" and "Modelling of uncertainties and framework for reliability analysis of wind turbine blades". Additionally, the results have been published in the conference paper "Modelling of uncertainties for wind turbine blade design" and the journal paper "Uncertainty

modelling and code calibration for composite materials”, see publication list. In the following a short summary and a numerical example based on the full-scale tests are given.

Parameters like material properties, geometrical properties and load properties are subjected to uncertainty and assumed to be modelled by stochastic variables. The uncertainties related to structural design can in general be divided into the following four groups:

- Physical uncertainty also denoted inherent uncertainty is related to the natural randomness of a quantity (e.g. the material tension strength) for example due to variability in the production processes. Another example is the annual maximum wind speed.
- Measurement uncertainty is related to imperfect measurements of e.g. geometrical quantities and applied forces.
- Statistical uncertainty is due to limited sample sizes of observed quantities. Data of observations are in many cases scarce and limited for which reason the parameters of the random variables cannot be determined exactly. If additional observations are provided the statistical uncertainty may be reduced.
- Model uncertainty is the uncertainty related to imperfect knowledge or idealizations of the mathematical models used. Also uncertainty related to the choice of probability distribution types for the stochastic variables contains model uncertainty.

Another ‘type’ of uncertainty which is not covered by these methods is gross errors or human errors. These types of errors can be defined as deviation of an event or process from acceptable engineering practice and is generally handled by quality control.

The uncertainty related to the basic material properties \mathbf{X} can be determined at coupon level, where distribution functions can be fitted based on the available test samples. The basic material properties and geometrical parameters will normally follow a Lognormal, Normal or Weibull distribution function. Statistical uncertainty related to the fitted distribution parameters can be determined using the Maximum Likelihood Method, Bayesian statistics or Bootstrapping as described in the report “Modelling of uncertainties and framework for reliability analysis of wind turbine blades”.

Sub-component and full-scale tests are often used to assess the model uncertainty incl. bias related to the numerical models used to assess the load bearing capacity. The model uncertainty can be assessed if a mathematical model $h(\cdot)$ is introduced to describe / approximate the resistance for a given failure mode. The mathematical model is assumed to be a function of a number of physical uncertainties (e.g. strength parameters and/or stiffness parameters) modelled by stochastic variables \mathbf{X} with realizations denoted \mathbf{x} . Further, the model is assumed to be a function of a number of regression parameters denoted R_1, \dots, R_m . The regression parameters are determined by statistical methods, and are therefore subject to statistical uncertainty. The model uncertainty incl. bias is introduced by a multiplicative stochastic variable R_0 . The model can thus be written:

$$Y = f(\mathbf{X}) \cong R_0 \cdot h(\mathbf{X}, R_1, \dots, R_m) \quad (1)$$

It is assumed that N independent sub-component or full-scale tests of the resistance Y is performed leading to the information in Table 2 and Figure 69.

Table 2 Test results for estimating model uncertainty.

Test	Physical parameters	Resistance
1	\mathbf{x}_1	y_1
2	\mathbf{x}_2	y_2
...
N	\mathbf{x}_N	y_N

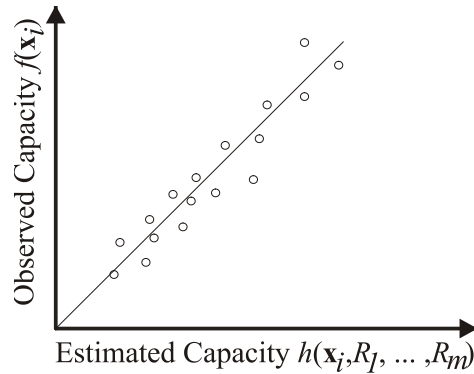


Figure 69 Observed capacity in experiments versus estimated capacity from mathematical models.

The model uncertainty incl. bias can be estimated by different statistical methods. In annex D to EN 1990 (Eurocode 0: Basis of structural design) a general approach is presented based on linear least square regression and a lognormal distribution for the model uncertainty. The model uncertainty can also be assessed using Bayesian statistics or Classical statistics.

In Bayesian statistics subjective information and can be combined with objective information from sub-components or full-scale blade tests. The subjective information can e.g. be based on previous tests with “similar” sub-components or full-scale blade designs or simply by engineering judgement. By taking the subjective information into account it is often possible to reduce the number of tests. However, care should be taken that the subjective information is well justified. A typical approach in Bayesian statistics is to assume that the bias is statistically unknown, whereas the model uncertainty is statistical known using a conservative coefficient of variation.

In classical statistics the model uncertainty incl. bias can be determined using e.g. the Maximum Likelihood Method. The benefits from this approach are that information from proof-loading of the subcomponents can be taken into account and the statistical uncertainty can be easily assessed. However, the investigations in the present project has shown that the proof-loading should be performed with a high loading in order to have a significant influence on the reliability. The physical, model, statistical and measurement uncertainties can based on the approaches described above be estimated based on the coupon, sub-component and full-scale tests. These uncertainties can be introduced in the developed probabilistic framework in order to determine the reliability of the wind turbine blade. Alternatively, partial safety factors for use in traditional code based design can be derived.

The partial safety factors given in wind turbine blade standards are in principle calibrated based on a general set of physical, model, statistical and measurement uncertainties. By using the probabilistic framework, it will therefore be possible for wind turbine manufactures which are able to document lower uncertainties, to reduce the partial safety factors.

The reliability of a wind turbine blade can in general be determined based on a limit state function which is solved using structural reliability methods. The limit state function involves both the load bearing capacity and the applied loading along with their respective uncertainties which complicates the assessment of the reliability. A simpler but also less accurate approach focusing on assessment of the partial safety factor is the design value format approach. Here, a certain proportion of the uncertainty is assumed to be related to the load bearing capacity. Thereby, it is possible to derive the characteristic load bearing capacity Y_C and design load bearing capacity Y_d based on different quantiles in the resulting statistical distribution. The partial safety factor for the resistance can then be estimated by:

$$\gamma_{Rd} = \frac{Y_c}{Y_d} \quad (2)$$

In the following the probabilistic framework is demonstrated based on the three full-scale tests conducted within this project. The available data are given in Table 3 and in Figure 70. It is noted that the failure load for the numerical model is subjected to uncertainty related to the load increments applied in the finite-element model.

Table 3 Estimated and observed capacity for full-scale blade tests.

Data	Failure load [%]
Numerical model	60%
Full-scale test – Blade 3	55%
Full-scale test – Blade 4	62%
Full-scale test – Blade 5	56%

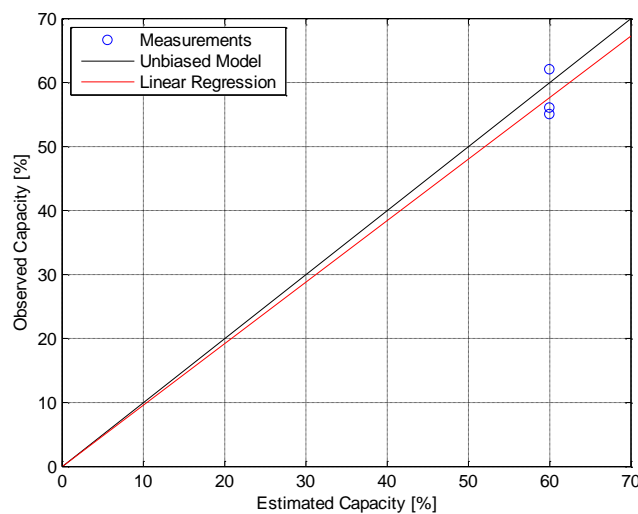


Figure 70 Observed capacity versus estimated capacity for full-scale blade tests.

The bias is based on the three full-scale tests estimated to $b=0.96$, corresponding to that the average load bearing capacity of the blades was 96% of the prediction by the numerical model. The associated model uncertainty is estimated to $V_{\Delta}=0.065$, corresponding to a coefficient of variation on 6.5%.

The uncertainty in the load bearing capacity due to physical uncertainty in the material and geometrical properties (V_h) is assumed to be 10% and the measurement uncertainty (V_{ϵ}) is assumed to be 5%. Based on these assumptions the characteristic and design load bearing capacities are assessed in Table 4 along with the partial safety factor which is determined using the 'design value format' method.

Three cases have been considered in Table 4. The first case is based fully on the test results available in the present project. However, only three full-scale tests to estimate the model uncertainty V_{Δ} introduce a significant statistical uncertainty leading to a very large partial safety factor. In the second case it has been assumed that five full-scale tests were available leading to the same bias and model uncertainty. This reduces the statistical uncertainty and thereby the partial safety factor and thus illustrates the benefit by doing more tests. In the third approach subjective information have been introduced through a Bayesian approach by assuming a conservative but statistically known model uncertainty on $V_{\Delta}=0.10$. This also reduces the statistical uncertainty and thus the partial safety factor.

Table 4 Assessment of partial safety factor for load bearing capacity.

Data	Full-scale tests	Full-scale tests (5 test)	Full-scale tests (known V_{Δ})
Load bearing capacity (Numerical model)	0.60	0.60	0.60
Number of tests	3	5	3
Bias b	0.96	0.96	0.96
Model uncertainty V_{Δ}	0.065	0.065	0.100 (known)
Physical uncertainty V_h (assumed)	0.10	0.10	0.10
Measurement uncertainty V_{ϵ}	0.05	0.05	0.05
Characteristic load bearing capacity (5% quantile)	0.437	0.458	0.438
Design load bearing capacity ($\beta^t = 3.3$)	0.294	0.394	0.373
Partial safety factor	1.49	1.16	1.17

Based on the probabilistic framework developed within the project it is possible for wind turbine manufacturers to quantify the information obtained from coupon, sub-component and full-scale testing, and in some cases to combine the information obtained using a Bayesian approach. This information can be used for reliability assessment and calibration of partial safety factors, and for decision making on which types of tests to perform and how many tests. However, more research is needed on how to quantify existing and subjective information, and how to plan using a probabilistic approach tests with different load directions in order to maximize the value of the information obtained.

7.3 Sub-component tests focusing on failure of trailing edge bonds

In the project three 34m SSP Technology blades were tested to failure by loading the blades in a 30° angle to the flapwise direction. For all three blades pronounced buckling waves in the trailing edge region occurred before failure as shown in Figure 71 and described in section 4.2.

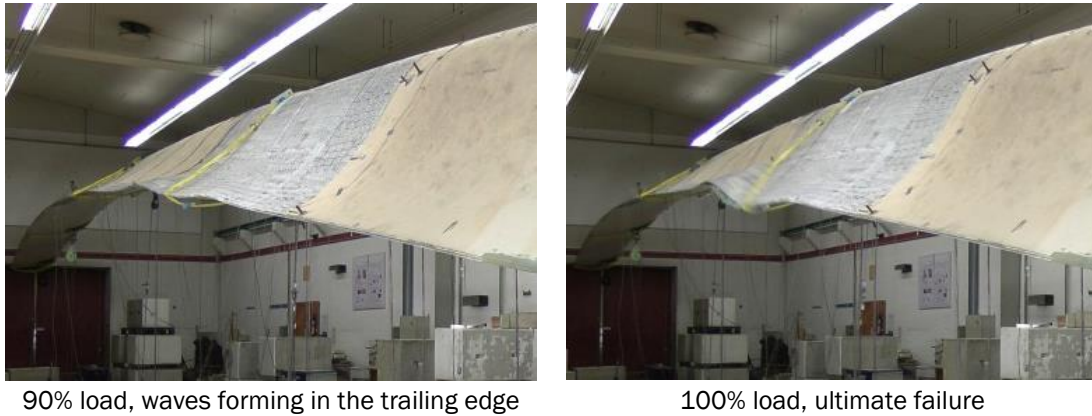


Figure 71 34m SSP Technology blade tested to failure by loading 30° to the flapwise direction.

A test rig for subcomponent testing of trailing edge panels and adhesive bonds has been developed and constructed at DTU and a subcomponent test has been made. The test setup (see Figure 72) is designed for testing cut-outs of the same blades tested in full-scale. The cut-outs consist of the trailing edge panels, the shear web closest to the trailing edge and part of the caps. The specimen is loaded by means of a spindle in which the top of the two vertical frames are forced towards each other forcing a linear varying compressive displacement on the specimen. The forced compressive displacement is then zero at the hinges approximately in the centre of the cap and maximum at the trailing edge. This will then mimic an edgewise bending moment on the section. The load history can be monitored via load cell designed for this setup.

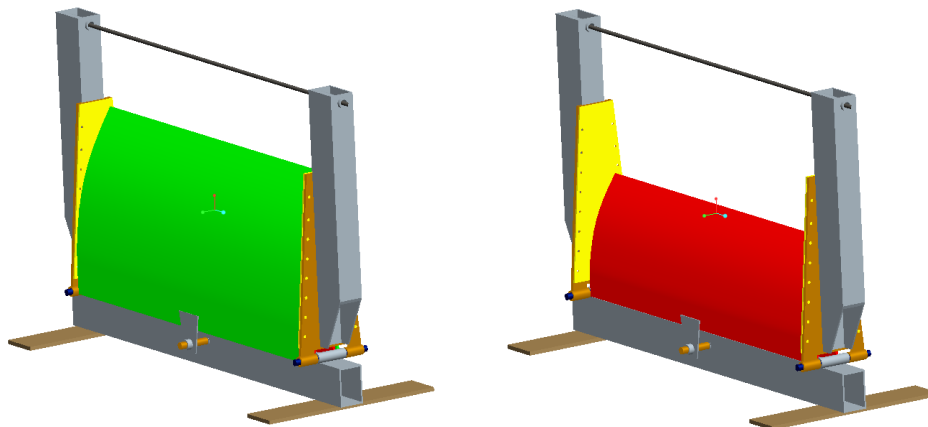


Figure 72 Test rig for subcomponent testing of trailing edge panels and adhesive bonds. Two subcomponent specimens from different lengthwise position are shown.

The idea with the subcomponent tests is to mimic the compressive loading of the trailing edge panels and bondline, which this region is subjected to under predominantly edgewise loading in

full-scale tests. Furthermore a minor bending moment generated by asymmetric loading is assumed to trigger the buckling waves in the trailing edge region as observed in numerical analyses and full-scale tests.

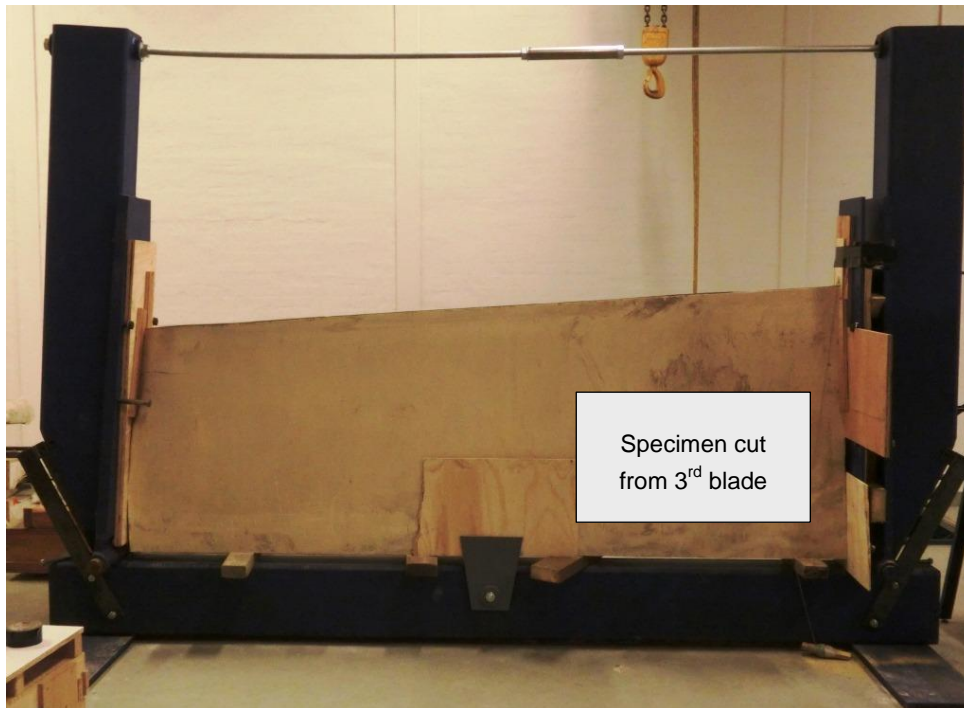


Figure 73 Trailing edge panel cut from SSP 34m blade from approximately 26m to 29m from blade root inserted in test rig.

7.3.1 Performed subcomponent test

In order to test if the subcomponent test setup will work as planned, an initial test was done. It is clear from this test that further analysis and work is needed before this subcomponent test method will be fully successful and useful for the industry.

The test was done using a specimen cut from SSP 34m blade approximately 26m to 29m from blade root and inserted into the test rig (see Figure 73). The displacement at the spindle was measured and the corresponding compressive displacement at the trailing edge can then be calculated.

The first damage sound, most likely from the adhesive bond, was heard at a compressive displacement of the trailing edge of approximately 0.02m. A pronounced buckle along the trailing edge then started to appear at approximately 28.5m from root. As the displacement increased further and the buckle grew in size progressive damage started to happen at a displacement of the trailing edge of approximately 0.045m. The progressive damage both happened at the 29m from root boundary as folding on the suction side and just below the trailing edge adhesive bond on the pressure side as a crack growing along the trailing edge (see Figure 74). The test was stopped at a displacement of the trailing edge of approximately 0.085m with the deformation and damage as seen in Figure 74.

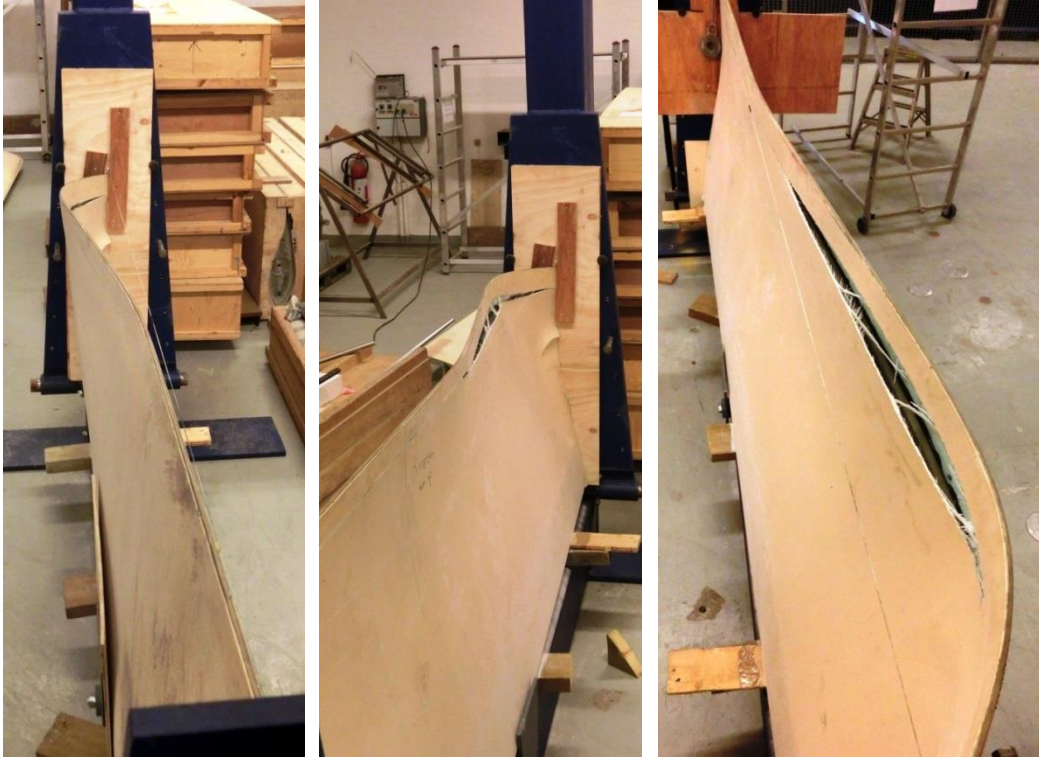


Figure 74 Buckling and failure of trailing edge panel on pressure side at approximately 27.5m to 29m from blade root. Failure is initiated close to the boundary condition at 29m from root.

7.3.2 Lessons learned

The test showed that the principle of the subcomponent test works. A buckle similarly to those seen in the full-scale tests was observed along the trailing edge. However, the boundary conditions at the 29m boundary clearly influenced the progressive failure. Therefore, further analysis and work is needed in order to find solutions to move the buckling further towards the middle part of the subcomponent specimen. Also further specimens can be modified to force failure in the middle part of the specimen. This can be done by introducing crack in the adhesive bond and/or strengthening the boundary region.

The purpose of this subcomponent test setup is to check the compressive strength of the trailing edge region under a simplified loading. Another method is to test larger subcomponents with much more complicated and realistic loading along their boundaries. This can in principle be done by applying intelligent boundary conditions to the subcomponents. With the use of a detailed numerical model of the full blade the behaviour of the subcomponent boundaries can be calculated and then applied during testing so that the subcomponent behaves as it was part of the full blade. Methods for obtaining and applying intelligent boundary conditions on larger subcomponent specimens are currently studied by different research groups, but we do not believe the technology is matured enough to be used for practical testing. The method to test subcomponents under a somewhat simplified loading with a specific failure mechanism in mind is more realistic for practical testing at the present state.

7.4 Trailing edge strength

In order to ensure blade integrity, LM Wind Power performs full scale, components, and coupon tests. The full scale test blade is a production line blade whereas coupon tests are performed with specimens made in the laboratory, with special care taken in the geometry, surface preparation, glue application, curing time and other parameters which could influence the strength.

At component level, the specimen can however be made in the laboratory especially for that purpose, or cut out from a produced blade (scrapped or tested blade). Both have pros and cons. A component, for example a trailing edge adhesive joint, made in the laboratory can somewhat differ from the way it looks in the real blade. Tolerances are more accurate, and less production variance is present in specimens made specifically for testing purpose. This will often lead to a lower scatter in the results, and a specific “wanted” failure mode can be simulated by the test. Accurate geometry will allow the engineer to benchmark the analytical model against test. On the other hand, some of the failure modes may be missed out, and the low scatter in the data could lead to non-conservative results.

Using cut out components from a production blade will allow testing a representative strength of the joint, but may lead to high data scatter, lowering the characteristic strength. Having different failure modes could also limit the possibilities of the use of analytical models, which are essential to avoid too costly test campaign of the full blade design space.

It is worth noticing that the level of scatter greatly depends on how sensitive the components are to production variance. In some areas of TE, LM uses some reinforcement elements, but this section only concerns the trailing edge common to most of the blade manufacturers, and therefore interesting to share in this project, see Figure 75.

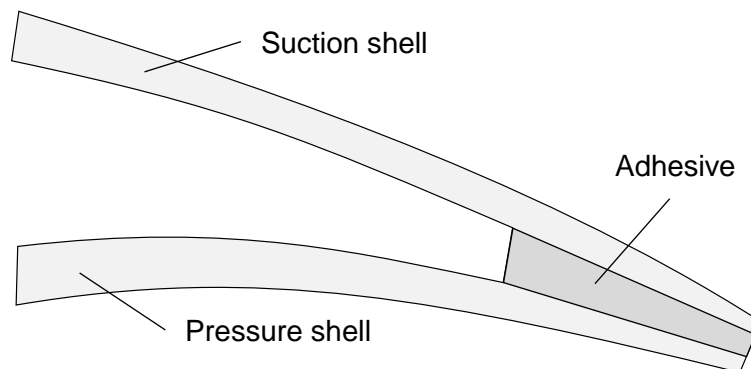


Figure 75 Trailing edge (TE).

The bending strength of the TE joint has been examined by manufacturing specimens in the laboratory. These specimens were meant to represent the trailing edge geometry of LM 73.5 P.

7.4.1 Trailing edge component tests

The tests involve 3 test series, in which 3 different configurations of laminate thickness, angle and adhesive thickness are tested. Table 5 and Figure 76 give an overview of the geometry configuration of each test series. α is the angle formed by the two laminate plates, and varies from 10° to 15° . t denotes the thickness of the adhesive before the tapering starts. Since the

angle formed by the tapering and laminate lines does not equal $\alpha/2$, the adhesive thickness will change throughout the bond. This is representative of the blade trailing edge. The laminate thickness h changes from 10 to 20 mm. The distances l_1 and l_2 remain the same for the 3 test series and equal 150 and 100 mm respectively.

Table 5 DoE of the trailing edge tests

Geometry	Test series	No of tested specimens
$\alpha = 10^\circ, t = 10\text{mm}, h = 10\text{mm}$	h1/t1	7 tension tests
$\alpha = 15^\circ, t = 15\text{mm}, h = 10\text{mm}$	h1/t2	7 tension tests
$\alpha = 15^\circ, t = 15\text{mm}, h = 20\text{mm}$	h2/t2	7 tension tests

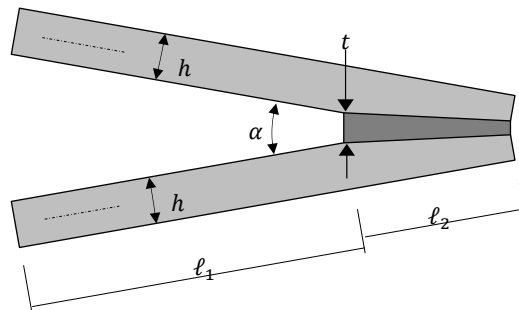


Figure 76 Illustration of DoE parameters

The manufacturing process is described in Appendix A.

One of the specimens for each of the 3 tested configurations is shown in Figure 77, Figure 78 and Figure 79.



Figure 77: Specimen of the series $h1/t1$, $\alpha = 10^\circ$, $t = 10\text{mm}$, $h = 10\text{mm}$



Figure 78: Specimen of the series $h1/t2$, $\alpha = 15^\circ$, $t = 15\text{mm}$, $h = 10\text{mm}$



Figure 79: Specimen of the series $h2/t2$, $\alpha = 15^\circ$, $t = 15\text{mm}$, $h = 20\text{mm}$

7.4.2 Testing methodology and test results

The test setup is illustrated in the following Figure 80. Hinges are screwed onto one extremity specimen, and a transducer that will measure the horizontal movement of the TE during test is placed at the other end of it. When the load is applied, the specimen deforms and the new moment arm can be measured, and the moment arm to failure can be calculated. Details on how the critical prying moment is calculated are given in Appendix B. Only positive prying moment is tested as it is seen as the most critical one. Indeed, it will open and propagate a crack between the adhesive and the laminate.

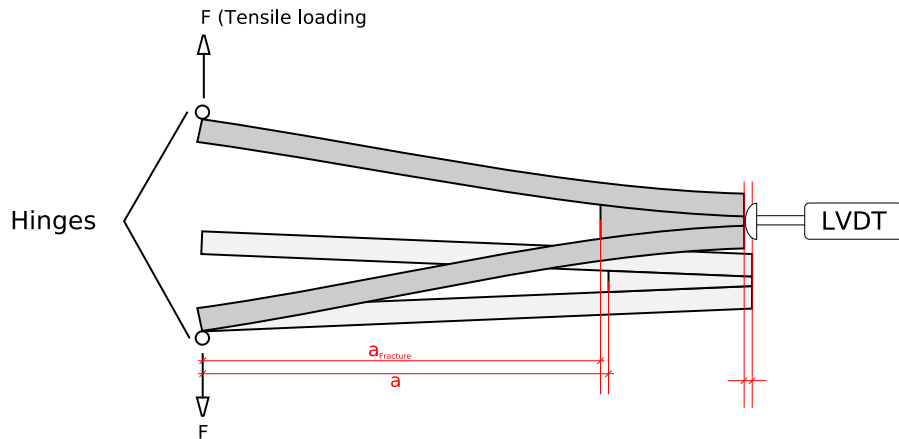


Figure 80 Test setup and measurement of the moment arm to failure.

Table 6 gives a summary of each test series in terms of mean value, standard deviation and characteristic value. The moment to failure is expressed per unit width [N.mm/mm], such that there is no dependency on the specimen width.

The weaker series is with the geometric configuration h1/t1 where the laminate thickness and adhesive thickness are both 10 mm, with a critical prying moment mean value of 850 N.mm/mm. The characteristic value is just below 600 N.mm/mm. Increasing the adhesive thickness to 15 mm instead of 10 mm gives slightly higher strength, see test series h1/t2 in Table 6. The test series h2/t2 with an adhesive thickness of 15 mm at crack front and a laminate of 20 mm shows a much higher mean value of strength, but the characteristic value is only slightly increased due to scatter in the results.

Table 6. Static test results for all 3 test series, with mean value, standard deviation and characteristic value.

Test series	Mean value [N. mm/mm]	Std. dev	Char. val [N. mm/mm]
h1/t1	850	110.2	599.8
h1/t2	927	100.8	693.7
h2/t2	1702	389.7	818.9

The failure modes within each test series of the specimens are very consistent, failing in the same way. Representative failure mode of the test series are shown in Figure 81. Failure occurs at the interface between the laminate and the adhesive. It is worth noticing that since tension is applied on both laminates and both laminate have the same stiffness, almost pure mode I fracture is achieved at the crack tip. 100% mode I would require the crack to propagate in the very centre of the adhesive layer.

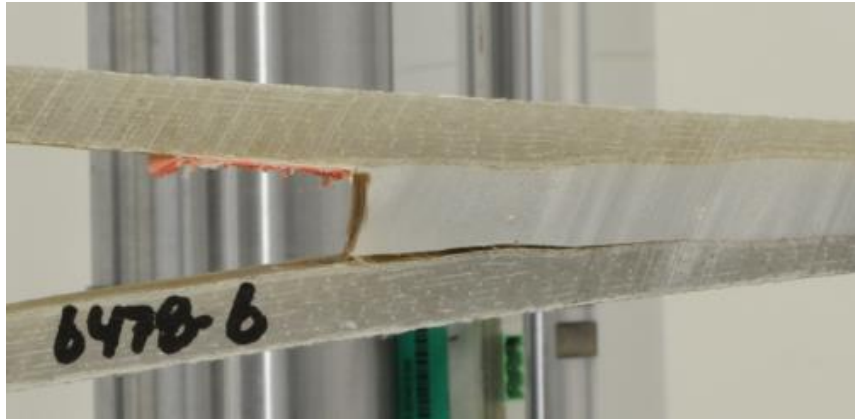


Figure 81 Typical failure mode of TE specimens (Test no. 6477 – 6479).

The variations within all the test results, except h2_t2 are within acceptable limits (<15%), indicating that both the specimen manufacturing and test procedures are in control. The variation for h2_t2 is 23%.

$$\text{Variation} = \frac{\text{Standard Deviation}}{\text{Mean value}} \times 100$$

Details about the strength of each tested specimen are given in Appendix C. There is fibre pull out on all specimens but it is observed that more fibre pull out is present on series h1/t1&h1/t2 – both of these series are trailing edge specimens with thin laminate.

Cohesion between an adhesive and its support may occur either by mechanical means in which the adhesive will enter into small cavities of both surfaces, or by chemical mechanism. The reason why interface strength is impacted by laminate thickness has to do with the second mechanism – the chemical reactivity. The laminate thickness governs the curing peak temperature. A thicker laminate means higher peak temperature because the laminate thermally isolates itself. This high peak temperature will result in a high degree of cure and thereby a low level of residual styrene, which means less styrene to interact with adhesive. There will therefore be a reduction in the chemical adhesion between laminate and glue.

7.4.3 Mode I fracture toughness tests

In order to confirm that the interface strength between the adhesive and the laminate varies with the laminate thickness, fracture toughness tests at coupon level have been performed.

The experimental set-up is shown in Figure 82. This type of set-up is called a “giraffe”, and is suitable for DCB testing at various mode mixities. As shown, the specimen is fixed at the triangular support on the lower beam and attached to the two grips on its sides.

The specimen is loaded when the upper beam is displaced, slowly, upwards (shown by the yellow arrow in Figure 82). This causes tension in the wires (red arrows). The magnitude of the force couple acting on each laminate part is set by adjusting the horizontal distance between the up and down going wires (green arrows). Likewise, the direction of the force couples (clockwise or counter clockwise) depends on the arrangement of the wire system.

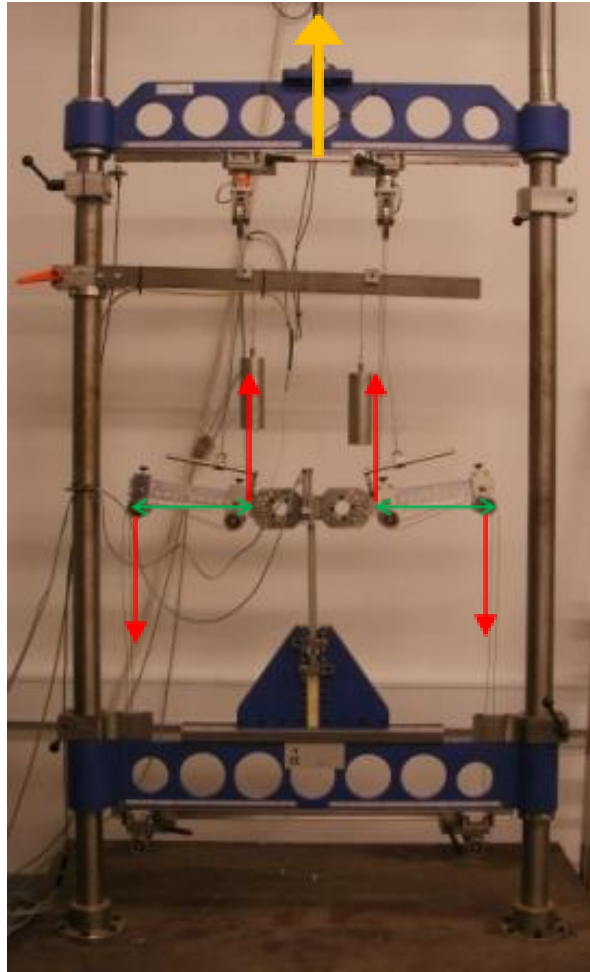


Figure 82 Experimental set-up. The shown equipment, called a "giraffe", is suitable for DCB tests at various mode mixities.

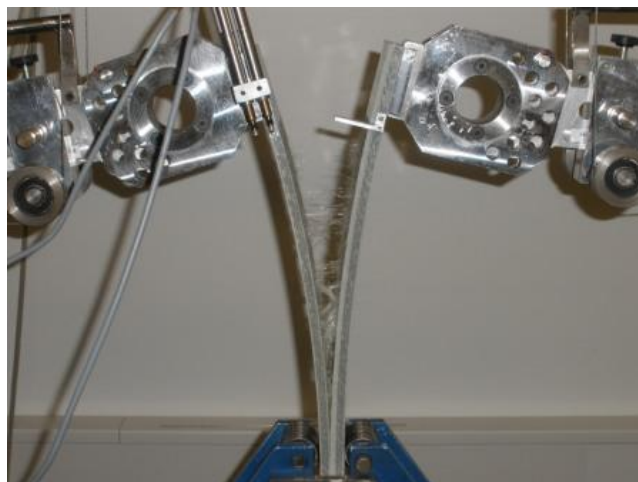


Figure 83 Specimen subjected to a peel load.

In the present case, the DCB specimen is subjected to two equal but opposite force couples, corresponding to a peel load (Mode I), see Figure 83.

The tested specimen is shown in Figure 84. It consists in a top and bottom plate, put together with 3 mm of the adhesive used at LM for blade bond lines. In all specimens, the top and bottom plates have the same layup and thickness such that pure mode I is achieved.

Two variants of the shell laminates – a thin and a thick shell laminate – are tested. In both cases, the final geometry to be tested is the same, but during the glass layup, extra layers resulting in a 10 mm thickness of the bottom plate are added to the basis configuration. Between these extra layers of glass and the plates, a release film is placed. Once it is cured, the extra layers added for the purpose of achieving a thickness of 10 mm are removed.

For manufacturing the thick shell laminate, the same is repeated with a sequence of glass resulting in a 23 mm thickness.

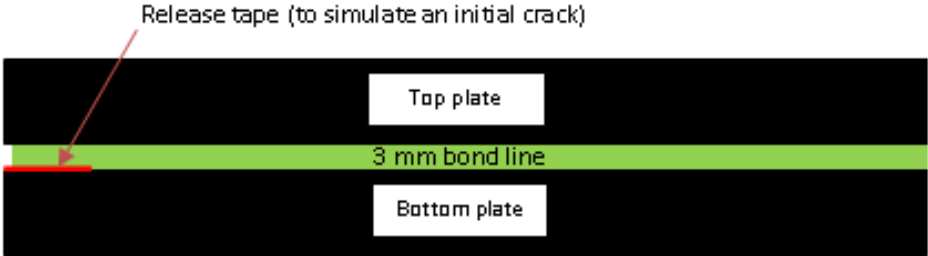


Figure 84 Finished DCB specimen with initial “crack”.

Table 7 shows the mode I initial fracture toughness for the 2 interfaces tested. A significant decrease in fracture toughness is observed with the laminate thickness of 23 mm.

Table 7 Mode I test results for interfaces.

Thickness of laminate, mm	10	23
Fract. init. toughness, kJ/m ²	0.3	0.22
Char. value, kJ/m ²	0.21	0.16

7.4.4 Analytical model of fracture mechanics for trailing edge

This section presents an analytical model able to predict the strength of a trailing edge joint a failure mode related to cracking in the laminate-adhesive interface. The model can cope with various loading, e.g. presence of prying moment and in plane force together – as a trailing edge naturally subjected to. The analytical model will be benchmarked against the tests.

Geometry and loads:

An illustration of a trailing edge joint is shown in Figure 85. The angle between the two laminates is denoted α and the thickness of each beam is denoted h_1 and h_2 . At each beam end (section cuts at points A and B), sectional loads in terms of axial loads P , transverse shear loads Q , and bending moments M are present. A crack with a sharp crack tip at point C is assumed to be present in the interface between the lower beam and the adhesive bond. The

crack could also have been located between the upper laminate and the adhesive bond. However, this crack location can be described by reversing the upper and lower beams including loads at points *A* and *B*.

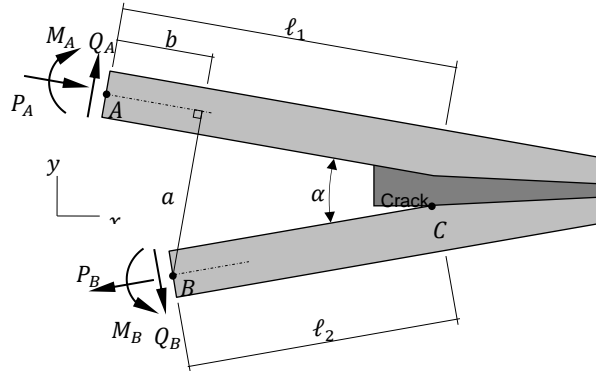


Figure 85 Trailing edge with sectional loads.

Equilibrium equations

From static equilibrium of forces and moments at points *A* and *B* in Figure 85, the following equilibrium equations are established

$$\begin{aligned} P_{A,x} - P_{B,x} + Q_{A,x} + Q_{B,x} &= 0 \\ -P_{A,y} - P_{B,y} + Q_{A,y} - Q_{B,y} &= 0 \\ -M_A + M_B - P_A a - Q_A b &= 0 \end{aligned} \quad (3)$$

with sectional load components

$$\begin{aligned} P_{i,x} &= P_i \cos(\alpha/2), & P_{i,y} &= P_i \sin(\alpha/2), & i &= A, B \\ Q_{i,x} &= Q_i \sin(\alpha/2), & Q_{i,y} &= Q_i \cos(\alpha/2), & i &= A, B \end{aligned} \quad (4)$$

Assuming the sectional loads P_A , Q_A , and M_A are known, the sectional loads at point *B* can be determined by solving the linear system of equations

$$\begin{bmatrix} -\cos(\alpha/2) & \sin(\alpha/2) & 0 \\ -\sin(\alpha/2) & -\cos(\alpha/2) & 0 \\ 0 & 0 & 1 \end{bmatrix} \begin{bmatrix} P_B \\ Q_B \\ M_B \end{bmatrix} = \begin{bmatrix} -P_A \cos(\alpha/2) - Q_A \sin(\alpha/2) \\ P_A \sin(\alpha/2) - Q_A \cos(\alpha/2) \\ M_A + P_A a + Q_A b \end{bmatrix} \quad (5)$$

such that

$$\begin{bmatrix} P_B \\ Q_B \\ M_B \end{bmatrix} = \begin{bmatrix} P_A(2 \cos^2(\alpha/2) - 1) + 2Q_A \cos(\alpha/2) \sin(\alpha/2) \\ Q_A(2 \cos^2(\alpha/2) - 1) - 2P_A \cos(\alpha/2) \sin(\alpha/2) \\ M_A + P_A a + Q_A b \end{bmatrix} \quad (6)$$

It is noticed that for non-parallel beams ($\alpha \neq 0$), axial loads (P_A, P_B) cannot exist without the presence of shear loads (Q_A, Q_B) and vice versa, i.e. you cannot have the one without the other. However, for parallel beams ($\alpha = 0$), the axial and shear forces become independent, i.e. you can have only one of them.

Sectional loads in front of crack tip

The trailing edge joint with section cuts of each beam just in front of the crack tip at point C is illustrated in Figure 86.

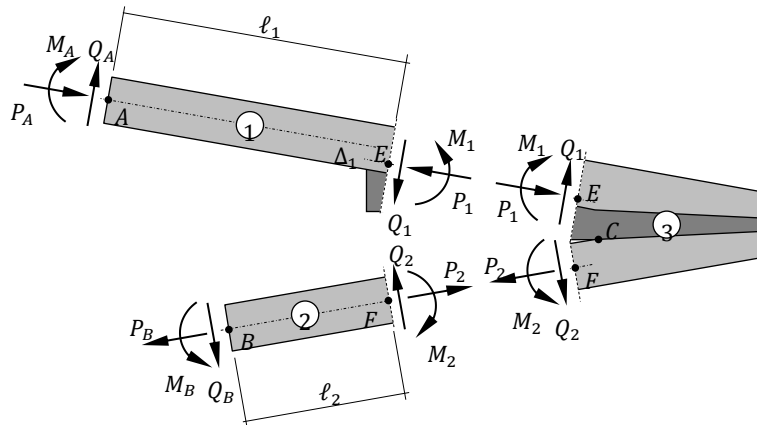


Figure 86: Sectional loads of beam each beam just in front of the crack tip at point C .

Static equilibrium of forces and moments at of parts ① and ②, see Figure 86, gives the following relations

$$\begin{aligned} M_1 &= M_A + Q_A \ell_1 + P_A \Delta_1, & P_1 &= P_A, & Q_1 &= Q_A \\ M_2 &= M_B + Q_B \ell_2, & P_2 &= P_B, & Q_2 &= Q_B \end{aligned} \quad (7)$$

Fracture mechanics

The strength of the trailing edge joint is governed by crack growth that can be predicted by a fracture criterion on the form

$$G = \Gamma \quad (8)$$

where G is the energy release rate (the energy present to initiate crack growth) and Γ is the crack resistance of the material interface. The crack resistance Γ is a material property that depends on the loading mode of the crack, i.e. the resistance against peel and shear loading is different.

Analytical calculation of energy release rate

In this section a simplified mechanical model of the trailing edge is presented based on Hutchinson & Suo (1992). Assuming the strength of a trailing edge joint is governed by the bending moments and the peel forces just in front of the adhesive, the mechanical model shown in Figure 87 can be used to describe the problem. The model consists of two (parallel) laminates that are joined together by an adhesive layer as illustrated in Figure 87. The three-layer model includes a crack between the adhesive and one of the laminates. The cracked

laminates are loaded by bending moments and axial forces at the free beam edges. It should be noticed that transverse and out of plane shear forces are not considered in the model.

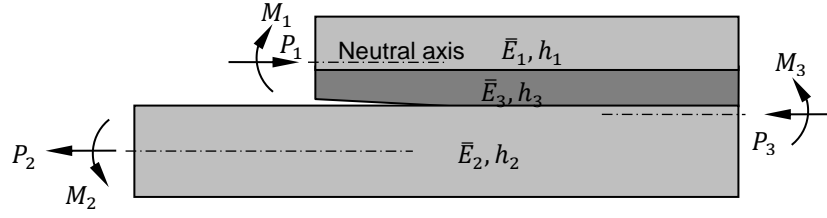


Figure 87: Analytical model of fracture mechanics representing the trailing edge loading

The energy release rate for the problem is derived and summarized below

$$G = \frac{1}{2} \left(\frac{M_1^2}{D_1} + \frac{M_2^2}{D_2} - \frac{M_3^2}{D_3} \right) + \frac{1}{2} \left(\frac{P_1^2}{A_1} + \frac{P_2^2}{A_2} - \frac{P_3^2}{A_3} \right) \quad (9)$$

where D_i and A_i are the bending and axial stiffness of beam ends $i = 1, 2, 3$.

A trailing edge is characterized by a free end with no edge loads, i.e. $M_3 = 0$ and $P_3 = 0$. In this case, the energy release rate of equation (9) reduces to

$$G = \frac{1}{2} \left(\frac{M_1^2}{D_1} + \frac{M_2^2}{D_2} \right) + \frac{1}{2} \left(\frac{P_1^2}{A_1} + \frac{P_2^2}{A_2} \right) \quad (10)$$

The bending stiffness and axial stiffness are defined as

$$D = \frac{1}{3} \sum_{i=1}^n (y_{i+1}^3 - y_i^3) \bar{E}_i, \quad A = \sum_{i=1}^n (y_{i+1} - y_i) \bar{E}_i \quad (11)$$

where y is the distance from the neutral axis to the position of material layers. Dimensionless parameters stiffness parameters are introduced

$$\eta = \frac{h_1}{h_3}, \quad \Sigma = \frac{\bar{E}_1}{\bar{E}_3} \quad (12)$$

Using parameters η and Σ the axial stiffness of beam ends #1 and #2 can be written

$$A_1 = \bar{E}_1 h_1 + \bar{E}_3 h_3 = \bar{E}_1 h_1 \left(1 + \frac{1}{\Sigma \eta} \right), \quad A_2 = \bar{E}_2 h_2 \quad (13)$$

and

$$D_1 = \frac{I}{\Sigma} \bar{E}_1 h_1^3, \quad D_2 = \frac{\bar{E}_2 h_2^3}{12} \quad (14)$$

with

$$I = \Sigma \left[\left(\Delta - \frac{1}{\eta} \right)^2 - \left(\Delta - \frac{1}{\eta} \right) + \frac{1}{3} \right] + \frac{\Delta}{\eta} \left(\Delta - \frac{1}{\eta} \right) + \frac{1}{3\eta^3}, \quad \Delta = \frac{1 + 2\Sigma\eta + \Sigma\eta^2}{2\eta(1 + \Sigma\eta)} \quad (15)$$

7.4.5 Benchmark of analytical model against trailing edge tests

The previously described method is used to calculate the strength of the tested specimens. Since there is no axial loading in the tested specimens and the moment on beam 3 is zero, the energy release rate from equation (10) yield to

$$G = \frac{1}{2} \left(\frac{M_1^2}{D_1} + \frac{M_2^2}{D_2} \right) \quad (16)$$

After calculation of the beam respective bending stiffness, the energy release rate is found. The critical moment M_c for which the fracture toughness equals the energy release rate is given by the equation (17).

$$M_c = \sqrt{\frac{\Gamma}{G}} \quad (17)$$

Table 7 gives the interface fracture toughness for 10 and 23 mm thick laminate. The tested specimens have a laminate thickness of 10 and 20 mm, so the fracture toughness for the 20 mm thick laminate is linearly interpolated from Table 7.

After calculations, a rather good match between the results from analytical model (denoted M_c in Table 8) and mean test values M_{Mean} is obtained.

Table 8 Critical prying moment.

Configuration	M_{Char} [N. mm/mm]	M_{Mean} [N. mm/mm]	M_c [N. mm/mm]	Rel M_{Mean}/M_c [%]
h1/t1	600	850	735	15%
h1/t2	694	927	763	21%
h2/t2	819	1702	1657	3%

This study has demonstrated that it is possible to use simplified fracture mechanical model of fracture mechanics to predict the strength of a blade bond line. The tested configuration where only prying moment at the crack tip was applied somewhat differs from real loading in the blade. To get the strength of the trailing edge joint subjected to complex loading, testing the fracture toughness with different mode mixities is required. Alternatively, the Mode I value can be used, which is conservative as it is lower than mode II and III.

7.4.6 Impact of the crack front shape on fatigue strength

The trailing edge in its present configuration has not been tested in fatigue. But another specimen was designed to study the influence of crack front shape. The designed specimen is illustrated in Figure 88.a in its pure laminate configuration and Figure 88.b using sandwich material in the base plate.

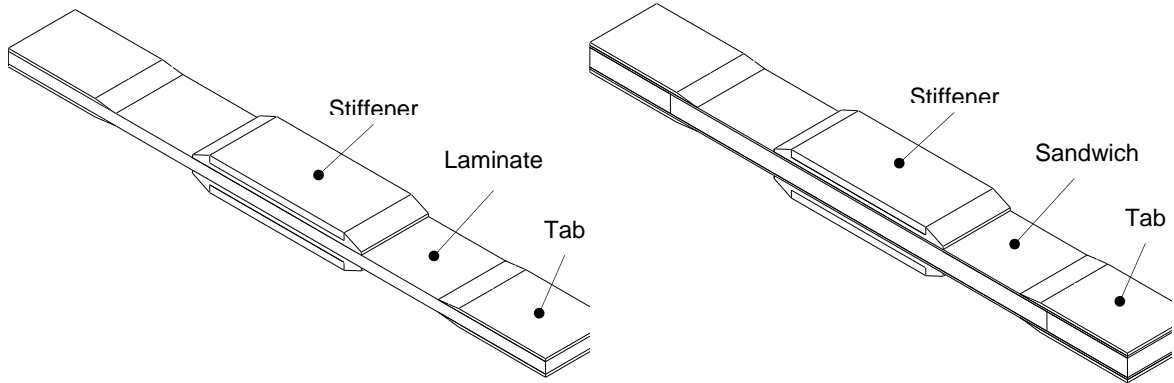
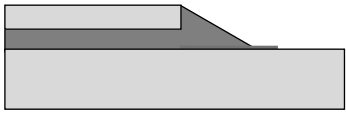
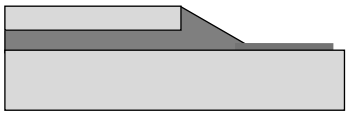
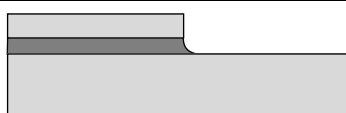


Figure 88.a. Laminate specimen.

Figure 88.b. Sandwich specimen.

Different test series have been performed. Series A1, A2, B1 and B3 are shown in this report. The letter A denotes the full laminate specimen whereas the letter B is for the sandwich specimen. Some specimens have a pre-crack whereas others do not. The pre-crack is made by using slip-foil.

Table 9. Shape of the crack front for the different test series.

Shape	Glue shape	Slip foil	Test series
	Chamfered	Long	A2, B1
	Chamfered	Short	A1
	Fillet	None	B3

The failure criterion for the fatigue test is 15 mm crack length. When the crack has developed with 15 mm, the specimen is considered to be failed. No further precision is given in the geometric and test specification since the purpose here is to illustrate the effect of different crack front shapes using a qualitative approach.



Figure 89 Full base laminate, short pre-crack, A1.



Figure 90 Full base laminate, long pre-crack, A2.



Figure 91 Sandwich base plate, long pre-crack, B1.



Figure 92 Sandwich base plate, no pre-crack, B3.

The critical energy release rate is calculated with bilayer Suo-Hutchinson's model. Looking at Figure 93, it is clear that static fracture toughness is greatly impacted by crack length and front. This is in accordance with a previous study found in Eder & Bitsche (2014).

All test results from different crack front and length configurations converge in fatigue. A reason for that could be that the crack growth during initiation phase becomes insignificant when the specimen is subjected to a high number of cycles. Specimens B3 which have a rounded fillet at the crack front show higher strength at low number of cycle to eventually get to the same level as A1, A2 and B1 after $1E5$ cycles. An important parameter not to be disregarded is the crack length for which the specimen fails and for which the test is stopped. In these tests, the length was set to 15 mm, and a different crack length would have led to different design curve. The decision of crack length to be reached before the test is stopped should be wisely chosen based on the size of the specimen e.g. if the crack get too long, loads are redistributed and energy release rate is non-constant. Crack length should also take into account the geometry of the component for which the design values are used.

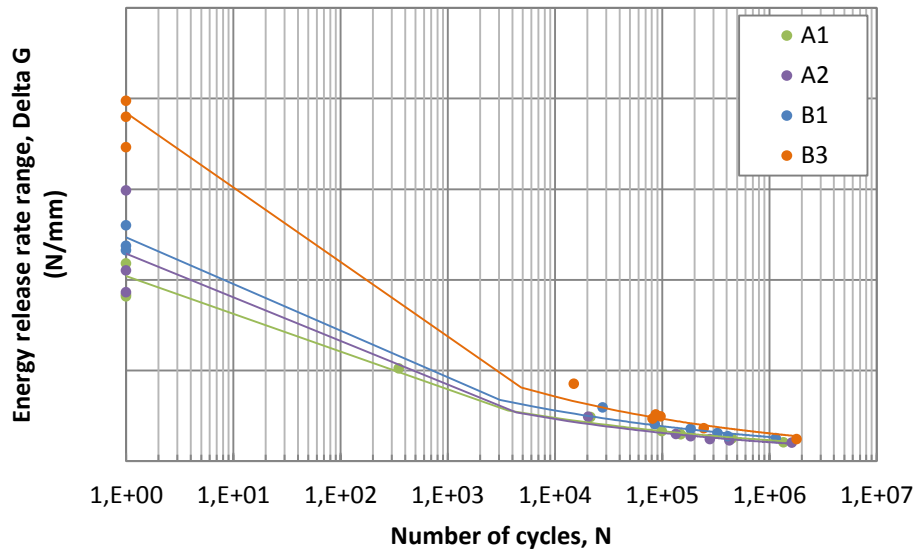


Figure 93 Energy release rate and fitting curve for different configuration of crack front – series A1, A2, B1, B3.

7.4.7 Conclusion

Based on the trailing edge component tests performed by LM Wind Power the following conclusion can be drawn:

- The failure mode of a trailing edge joint loaded in tension was found to be debonding between the adhesive and a shell laminate
- Once the crack has started propagating, it keeps growing in the same adhesive / shell interface
- In tension loading, increasing the thickness of the adhesive and the laminate shells will increase the static strength of the trailing edge joint.

The effect of laminate thickness on the interface fracture toughness between adhesive and shell laminate was investigated on a DCB specimen loaded in mode I. Results show that the fracture toughness is reduced with a thick shell laminate.

The mode I fracture toughness obtained from the DCB tests was used in a fracture mechanical model of fracture mechanics to predict the prying moment to failure of the trailing edge component tests and the error was within 3 to 21 % depending on the test series. This shows that the static strength of a trailing edge joint can be predicted using simple analytical models combined with fracture toughness test results. The loading condition of a trailing edge joint in a blade will however differ from a pure mode I crack loading. To cope with different mode mixity, different combinations of mode I and II can be tested and used according to the mode mixity observed in the blade joint. A conservative approach can also be used where the mode I fracture toughness can be used instead of a mixed mode value, since Mode II and III fracture toughness is higher than mode I.

A method for transforming the joint loads is given. This can be useful when the joint loads are extracted away from the crack tip, e.g. using a finite element model, and have to be recalculated in a new location.

Specimens consisting in a base laminate on which a stiffener was bonded have been tested in tension in static and fatigue. A mixed mode between mode I and II was tested, and it can be concluded that:

- In static, the crack front shape has a significant influence on the fracture toughness
- In fatigue, the crack front shape has only a minor impact on the critical energy release rate range

8. Discussion

Experimental blade tests conducted showed that a controlled loading routine is essential for both accuracy and repeatability. The applied loading scheme proved to comply with both but had other disadvantages such as slow convergence causing extensive testing times and strong fluctuations in the loading paths between target values. Both of which are not desirable because of relaxation effects during the test and because of possible path dependence effects in structural behaviour. Therefore, a controller based loading scheme would be recommended for future blade tests. The PI-controller should enable a smooth loading scheme which avoids strong fluctuations and which arrives at the target loads within a reasonable time.

The developed small displacement measurement system proved to be an essential means to investigate the trailing edge deformation behaviour of the investigated blade. The SDMS offers a wide variety of different applications because of its versatility. The developed automated image processing software proved to be reliable and robust algorithm. One of the striking advantages of the AIPS is the access to the source code in comparison to limitations caused by restricted access to commercially available measurement systems (black box issue).

SDMS measurements revealed that the trailing edge opens and closes for different loading directions. In the present report it could be shown experimentally that the trailing edge opened under +30 degree loading and closed under -30 degree loading. These insights were an essential starting point for further investigations which eventually led to a deep understanding of trailing edge deformation behaviour on a theoretical level. The SDMS measurements agreed well with numerical results. Especially Mode-I agreed pretty well whereas Mode-II deformations showed higher deviations. Mode-III deformations were rather small. This does not necessarily mean that Mode-III ERRs were not present but is mainly attributed to much higher panel stiffness in the out-of-plane direction. In other words the presence of a specific modal deformation close to the flow front of the adhesive joint infers to the presence of a corresponding modal ERR. Conversely, the absence of such a modal deformation does not necessarily infer to the absence of the corresponding modal ERR.

The SDMS and the AIPS were used to measure the trailing edge deformation between 10m and 16m. The ASMs and the optical measurements show excellent agreement. It can clearly be

seen that a wave occurs in the trailing edge at already low loading levels. This wave is caused by geometrically nonlinear effects right at the beginning where its amplitude increases until failure occurs. Failure was buckling induced debonding of the trailing edge joint which occurs at around 14m. Judging from videos failure was not initiated directly at the peak but at some offset away towards the tip. It is also noteworthy to say that the pressure side panel was damaged before occurrence of debonding because of strong local curvatures caused by the buckling wave. This damage was not accounted for in the numerical analysis presented which presumably led to an overestimation of the wave amplitude. The occurrence of the buckling wave at early load stages can have a significant influence on the fatigue life of the trailing edge joint. Considering the fact that the amplitude increase exponentially as a function of the load level an even more rapid increase of the ERRs in the trailing edge joint can be expected for small changes of loads.

The fiber brag strain sensor setup proved to be a reliable and efficient means to measure strains in wind turbine blades. The sensors were pretty easy to align and to install when compared to ordinary electrical resistance strain gauges. The adopted sensor array proved its capability to pick up the buckling wave due to a variation of the longitudinal strain measured parallel to the trailing edge. However, a considerable noise level in the measurement data was found in the fine resolution measurement line. Steep strain gradients seemed to be unreasonable as the peaks were determined by the position of the sensors. Later it was found that the noise of the strain measurements were not associated with the measurement system but rather with the location of the sensors on the blade. Sensors that were coincidentally located in the pure laminate were much more coherent and less noisy than those located within the sandwich core area. It is deemed that the noise level is associated with local imperfections in the measurement substrate where the presence of local imperfections and stress concentrations is more likely in the sandwich core area. The fact that ordinary resistance strain gauges that were at some places mounted adjacent to the fiber brags did not show this issue to the same extent was interesting. One reason could be that the gauge length of the conventional strain gauges is larger and the measurements less sensitive to local imperfections. One solution could be to increase the gauge length which currently measures approx. 4mm to 8mm or more. Moreover, the dependency of the strain values on the fiber direction of the composite material needs to be scrutinised as a strong dependency is rather likely. The experimental findings also have an implication to strain measurements taken in operating blades as e.g. part of a structural health monitoring system. Care should be taken by directly using measurements in a stress damage criterion as strain levels might be over- or under-estimated significantly as a matter of local strain concentrations on a micro level.

Local buckling analysis conducted on two different models showed that local buckling can have a significant influence on the integrity of adhesively bonded joints. Once local buckling is present in the trailing edge pretty much all fracture modes appear depending on the location along the wave. A consistent generic prediction of the prevailing mode mixity becomes rather complex close to being impossible. Moreover, ERR levels appear to have high local peaks next to and in the trailing buckling wave. Numerical analysis of ERRs as a function of different crack lengths showed that fracture transverse to the trailing edge is potentially unstable which is somewhat consistent with experimental observations. Furthermore, it could be shown numerically that a crack in the trailing edge can still have Mode-I ERRs when the panel closes due to the invert scissors effect provided that the crack is long enough.

Buckling analysis on a full 3D model of the SSP34 blade showed that the model could predict the failure area surprisingly accurate. It needs to be emphasised that the buckling analysis did deliberately not incorporate any imperfections that were imposed to the model. Buckling analysis of blades is not straight forward and imposing imperfections as function of previously obtained Eigenmodes can lead to arbitrary results. It could be shown that with a selective choice of a combination of Eigenmodes arbitrary results can be obtained. Even more alarmingly, Eigenmodes calculated at early load stages might significantly differ from those occurring close to failure. On the other hand application of imperfections by moving the nodes according to the Eigenmodes might lead to the wrong prediction of the actual failure load and failure mode. It was also found that the numerical solutions are quite sensitive to the slightest imperfections i.e. amplitude of imperfections.

The fact that the numerical model predicted the experimentally observed buckling wave well can be attributed to imperfections being already present in the model. This is not referring to modelling inaccuracies but rather referring to the blade geometry where different airfoil geometries are morphed into each other using surface spline techniques. The changes in geometry from a circular section in the root into an airfoil at the tip necessarily brings along transitions from one geometry into the other which can be seen as an inherent imperfection already present right from the beginning. Of course these effects are being super imposed by manufacturing tolerances and deviations from the ideal surface.

Full 3D numerical analysis showed that failure of the pressure side panels at 14m was present even before the trailing edge debonded. Furthermore, distinct Mode-I, II and Mode-III ERR peaks were found to be present in certain loading directions. It was shown that the trailing edge joint of the SSP34 features high ERR levels for bending moment vector directions in the second quadrant which is consistent with other investigations.

The DCB tests conducted on three different flow front geometries showed that mitigation of the singularity due to rounded flow front shapes increases the initiation fracture energy. On the other hand in 50% of the investigated cases the crack initiated in the rounded region and propagated a long way in the adhesive. Considering the low critical ERR of the adhesive compared to interface cracks this behaviour is considered unsatisfactory. Moreover, crack growth in the adhesive was unstable. Conversely, in cases with a strong singularity the cracks were forced to initiate in the interface. The cracks typically kinked into the biax interface where it continued to propagate. In this case large scale fibre bridging was observed which led to stable crack propagation. From that it could be counter intuitively inferred that a strong singularity that ensures interface cracks exhibiting large scale fibre bridging should be preferred.

Although the layup architecture and the adhesive type was the same as that one used in the SSP34 blade significant differences between sub-component tests and full scale blade tests could be observed. That is to say that large scale fibre bridging could hardly be observed during the blade tests whilst fibre bridging was predominantly present in DCB tests. Fibre bridging is a desired feature of composite materials which should be utilised. Future research should therefore focussed on utilisation of fibre bridging on full scale.

The slice approach offers a computationally efficient alternative to full scale fracture analysis of adhesive joints in blades. High levels of detail and mesh resolution can be achieved without compromising the computation time. The slice approach enabled deep insights into the fracture behaviour of all typical adhesive joints present in a wind turbine blade. The slice models could be used to investigate the influence of different design parameters such as panel thickness, camber, cap width, web height on ERRs and mode mixities. Furthermore, critical load directions could be established which could facilitate future fracture analyses. To be more precise, once governing load cases are linked to the single adhesive joints, fracture analysis could be conducted more efficiently as the focus can directly be put on the important aero elastic load cases.

With the slice modelling approach it was possible to relate the camber of the trailing edge panels to the magnitude of ERRs in pre-cracks present in the adhesive of the trailing edge joint. The pre-cracks were deliberately put into the adhesive in order to avoid bi-material interface problems. Secondly, the brittleness of the adhesive justifies application of the VCCT which follows linear elastic fracture mechanics. This assumption is of course arbitrary and does not reflect all cases but represents a conservative worst case situation. One has to bear in mind that literature on ERRs in wind turbine blades is quite tacit and the slice modelling approach represents the attempt of shedding some light onto a complex situation.

In the fracture analysis results presented in this report all cracks were assumed to be transversely orientated. Moreover, cracks in the slice approach are assumed to extend over the entire span of the blade since the underlying assumption implies that all cross sections are equal. Clearly both assumptions are a simplification of a real situation where the cracks are very likely to change their direction of propagation. As observed in the blade test, cracks in the trailing edge might initiate in the transverse direction but then propagate in the longitudinal direction of the blade. Such behaviour should be part of future investigations.

Another drawback of the slice approach is that the influence of taper and twist are disregarded and that effects originating from local buckling cannot be simulated. These effects can only be captured by a full 3D model with all its implications. In this way it seems reasonable to use the slice approach for general investigations and 3D models for detailed analysis of specific problems that cannot be captured by the slice model.

It needs to be emphasised that the slice model is suitable for more advanced fracture analysis techniques such as cohesive zone modelling which could be the basis for a more in-depth fracture analysis of bi-material interface cracks and fibre bridging effects. In a nutshell the findings of numerical fracture mechanics concerning the trailing edge joint can be summarised as follows:

- Mode-I and Mode-II ERRs of transverse cracks are mainly associated to in-plane cross section warping deformation itself associated to geometric nonlinear effects. These geometric nonlinear effects are mainly caused by bending moments.
- Mode-III ERRs of transverse cracks are mainly associated with out of plane warping deformations mainly caused by shear forces and torsional moments. Mode-III effects can accurately be predicted with linear models.

- Considering the fact that the critical Mode-I ERR is significantly lower than that of the other modes emphasises the importance to consider geometric nonlinear cross section deformations in fracture analysis of wind turbine blades.

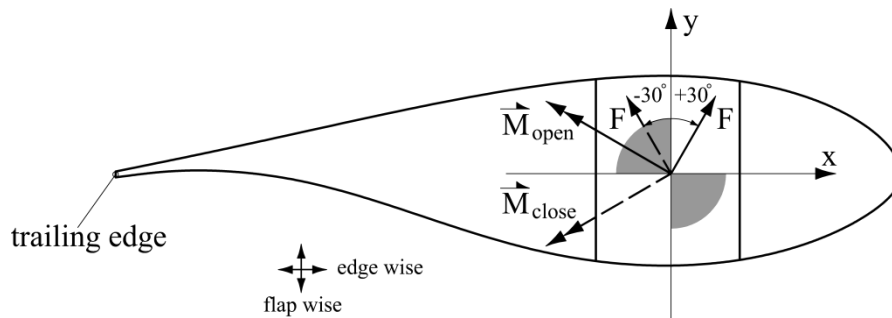


Figure 94 General trailing edge deformation behaviour depicted on the example of the 70m section. Trailing edge opens and closes depending on the direction of bending. (taken from Eder & Bitsche (2015))

The analytical model presented in this report showed that the trailing edge opening is caused by moments of eccentricity induced by axial forces present in the trailing edge panels. Generally speaking it can be said that bending moment vectors within the second and fourth quadrant are causing Mode-I ERRs in transverse trailing edge cracks whereas bending moment vectors in the other quadrants generally lead to a closing of the trailing edge panels (see Figure 94)

References

Publications from current project

Bennett, J., Branner, K., Bitsche, R.D. & Kim, T., Quick Method for Aeroelastic and Finite Element Modeling of Wind Turbine Blades, In: Proceedings of ASME Turbo Expo 2014: Turbine Technical Conference and Exposition, GT2014, June 16-20, 2014, Düsseldorf, Germany

Bitsche, R. D., Belloni, F., & Eder, M.A. (2015). A quantitative investigation of geometrically nonlinear effects in a realistic wind turbine blade cross section. *Composite Structures*, under publication.

Branner, K., Comparing Computational Methods and Full-Scale Tests for Ultimate Failure of Blades, Invited, International Conference on Future Technologies for Wind Energy, Laramie, Wyoming, October 7-9, 2013.

Branner, K. & Berring, P., Compressive Strength of Thick Composite Panels, in: Proc. of 32nd Risø International Symposium on Materials Science, 5-9 September 2011, Roskilde, Denmark.

Branner, K., Berring, P., Gaiotti, M. & Rizzo, C.M., Comparison of Two Finite Element Methods with Experiments of Delaminated Composite Panels, in: Proc. of 18th International Conference of Composite Materials (ICCM), 21-26 August 2011, Jeju Island, Korea.

Eder, M. A. & Bitsche, R.D. (2014). Fracture analysis of adhesive joints in wind turbine blades. *Wind Energy*. DOI: 10.1002/we.1744

Eder, M.A. & Bitsche, R.D. (2015). A qualitative analytical investigation of geometrically nonlinear effects in wind turbine blade cross sections. *Thin Walled Structures*, accepted.

Eder, M.A., Bitsche, R.D., Nielsen, M. & Branner, K. (2014). A Practical Approach to Fracture Analysis at the Trailing Edge of Wind Turbine Rotor Blades, *Wind Energy*, DOI: 10.1002/we.1591.

Haselbach, P.U., Belloni, F., & Eder, M.A. (2015). Energy release rates in the adhesive trailing edge joint of a wind turbine rotor blade. *Renewable Energy*, under publication.

Høgh, J., Waldbjørn, J., Stang, H., Berggreen, C., Wittrup-Schmidt, J. & Branner, K., Static Strain and Deformation Controlled Testing of Composite Beams, *CompTest 2013*, 6th International Conference on Composites Testing and Model Identification, 22-24 April 2013, Aalborg University, Denmark.

Jensen, F.M., Sørensen, J.D., Nielsen, P.H., Berring, P. & Flores, S., Failures in Trailing Edge Bondlines of Wind Turbine Blades, in: Proc. of 32nd Risø International Symposium on Materials Science, 5-9 September 2011, Roskilde, Denmark.

Mollineaux, M., Balafas, K., Branner, K., Nielsen, P.H., Tesauro, A., Kiremidjian, A. & Rajagopal, R. (2014). Dam-age Detection Methods on Wind Turbine Blade Testing with Wired and Wireless Accelerometer Sensors, In: Proceedings of EWSHM - 7th European Workshop on Structural Health Monitoring, July 8-11, 2014. La Cité, Nantes, France

Roczek-Sieradzan, A., Nielsen, M., Branner, K., Jensen, F.M. & Bitsche, R.D., Wind Turbine Blade Testing under Combined Loading, in: Proc. of 32nd Risø International Symposium on Materials Science, 5-9 September 2011, Roskilde, Denmark.

Rosemeier, M., Berring, P. & Branner, K., Non-linear Ultimate Strength and Stability Limit State Analysis of a Wind Turbine Blade, Wind Energy, accepted with minor revisions.

Shmueli, J., Eder, M. A., & Tesauro, A. (2015). A versatile stereo photogrammetry based technique for measuring fracture mode displacements in structures. Precision Engineering, 39(5), 38-46. DOI: 10.1016/j.precisioneng.2014.07.004

Sørensen, J.D., Branner, K. & Toft, H.S., Milestone 6: Recommendations for future sub component tests. EUDP: Experimental Blade Research – Phase 2 (EBR2). Report: Aalborg University & DTU, October 2013.

Sørensen, J.D. & Toft, H.S. Modeling of uncertainties for wind turbine blade design. Proc. ICOSSAR2013, New York, 2013.

Sørensen, J.D. & Toft, H.S., Modeling of uncertainties and framework for reliability analysis of wind turbine blades. EUDP: Experimental Blade Research – Phase 2 (EBR2). Report: Aalborg University & DTU, August 2014.

Tesauro, A., Eder, M. A., & Nielsen, M. (2014). Measurement of local relative displacements in large structures. Journal of Strain Analysis for Engineering Design, 49(5), 301-314. DOI: 10.1177/0309324713519622

Toft, H. S., Branner, K., Mishnaevsky, L. J., & Sørensen, J. D. (2013). Uncertainty modelling and code calibration for composite materials. Journal of Composite Materials, 47(14), 1729-1747. DOI: 10.1177/0021998312451296

Waldbjørn, J., Høgh, J., Stang, H., Berggreen, C., Wittrup-Schmidt, J. & Branner, K. Hybrid Testing of Composite Structures with Single Axis Control, ICCM19, 19th International Conference on Composite Materials, July 28 – August 2, 2013, Montreal, Canada.

Other publications

Hutchinson, J. D., & Suo, Z. (1992). Mixed Mode Cracking in Layered Materials. Advances in Applied Mechanics , 63-191.

L.G. Brazier (1927) On the Flexure of Thin Cylindrical Shells and other 'Thin' Sections, Proc. R. Soc. Lond. Ser. A, 116 (1927) 104–114.

Appendix A Manufacturing the trailing edge specimens

The trailing edge specimens are made following these steps:

- Glass layers are placed on a flat mould, and infused with resin. 2 different plates are made, so that the different series could have a laminate thickness corresponding to the specifications in Table 5.
- The laminate plates are grinded at the areas where adhesive will be applied.
- The plates are bonded together using an assembly device described in the Figure 95 and Figure 96.
- Once the bonding process is completed, the joined laminate plates are post-cured in accordance with the recommendations of the adhesive supplier.
- The joint laminate plates are sliced to a width of 50 mm, and any sharp edge coming from the saw is removed by hand grinding.

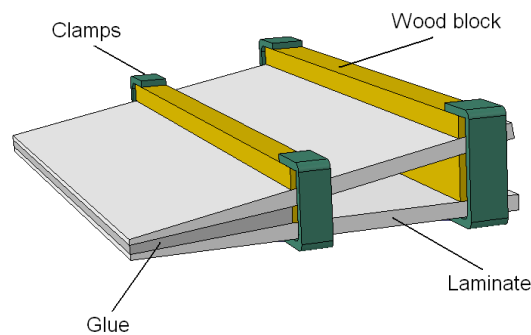


Figure 95: Assembly of up and downwind part of the trailing edge.

Slip foil is placed around the wooden block, so that any remaining piece of wood on the specimens can be avoided, see Figure 96.

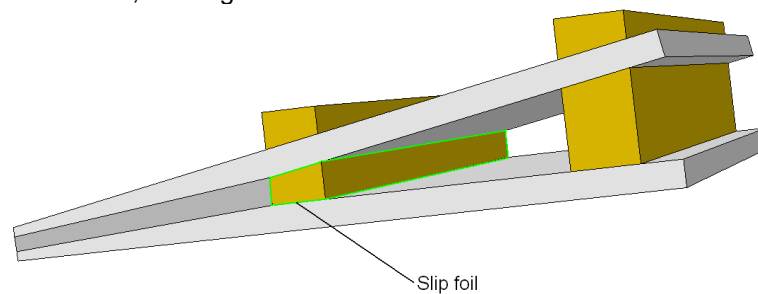


Figure 96: Slip foil around the wood block.

Appendix B Trailing edge test setup and methodology

For each specimen, the prying moment is calculated as following:

Moment arm:
$$a_{Fracture} = a - LVDT_{Fracture}$$

Prying moment:
$$M = F \times a_{Fracture}$$

Prying moment pr. width:
$$M_w = M/w$$

where:

F Tensile force.

w Specimen width

a Moment arm. Note that the distance is measured to the inside end of the bond line. The moment arm will change during loading, therefore it is important to measure the moment arm at the time when the fracture / critical load are achieved, see $a_{Fracture}$.

LVDT Transducer that will measure the horizontal movement of the TE during test

$a_{Fracture}$ The moment arm calculated by subtracting the movement measured by the LVDT from the measured moment arm before test

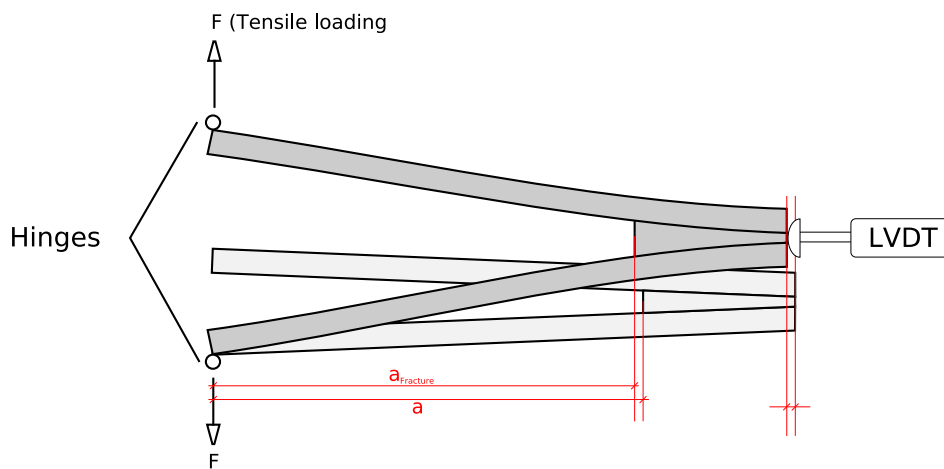


Figure 97: Test setup and measurement of the moment arm to failure



Figure 98: Test setup with LVDT and camera

Appendix C Trailing edge test results

Table 10. Static test results, test series h1/t1

Specimen ID.	F [N]	a_{Fracture} [mm]	w [mm]	Moment [N. mm/mm]
h1/t1/1	237	154.91	50.22	731
h1/t1/2	242	154.67	50.10	747
h1/t1/3	279	153.41	50.25	852
h1/t1/4	291	153.84	50.24	891
h1/t1/5	341	154.22	50.13	1049
h1/t1/6	289	155.26	50.13	895
h1/t1/7	255	153.97	50.26	781

Table 11. Static test results, test series h1/t2

h1/t2/1	340	154.23	50.25	1044
h1/t2/3	322	153.38	50.25	983
h1/t2/3	-	-	-	-
h1/t2/4	297	154.57	50.06	917
h1/t2/5	320	154.87	50.08	990
h1/t2/6	280	154.69	50.12	864
h1/t2/7	249	154.06	50.12	765

Table 12. Static test results, test series h2/t2

h2/t2/1	795	146.99	50.30	2323
h2/t2/2	696	149.89	50.28	2075
h2/t2/3	543	150.80	50.33	1627
h2/t2/4	516	151.74	50.15	1561
h2/t2/5	540	152.49	50.22	1640
h2/t2/6	512	151.07	50.29	1538
h2/t2/7	375	151.10	50.25	1128

Table 13. Static test results for all 3 test series, with mean value, standard deviation and char. value.

Test series	Mean value [N. mm/mm]	Std. dev	Char. val [N. mm/mm]
h1/t1	850	110.2	599.8
h1/t2	927	100.8	693.7
h2/t2	1702	389.7	818.9

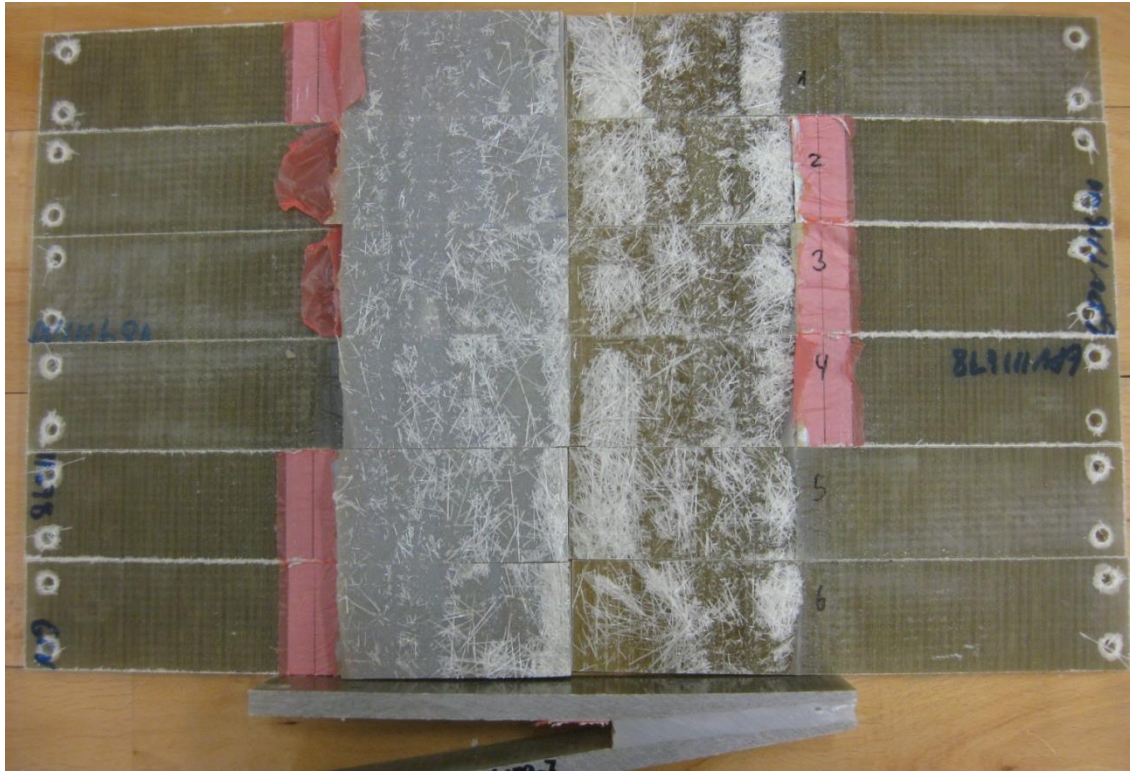


Figure 99: Failed specimens of the series 6478, test series h_1/t_1 , $\alpha = 10^\circ$, $t = 10\text{mm}$, $h = 10\text{mm}$

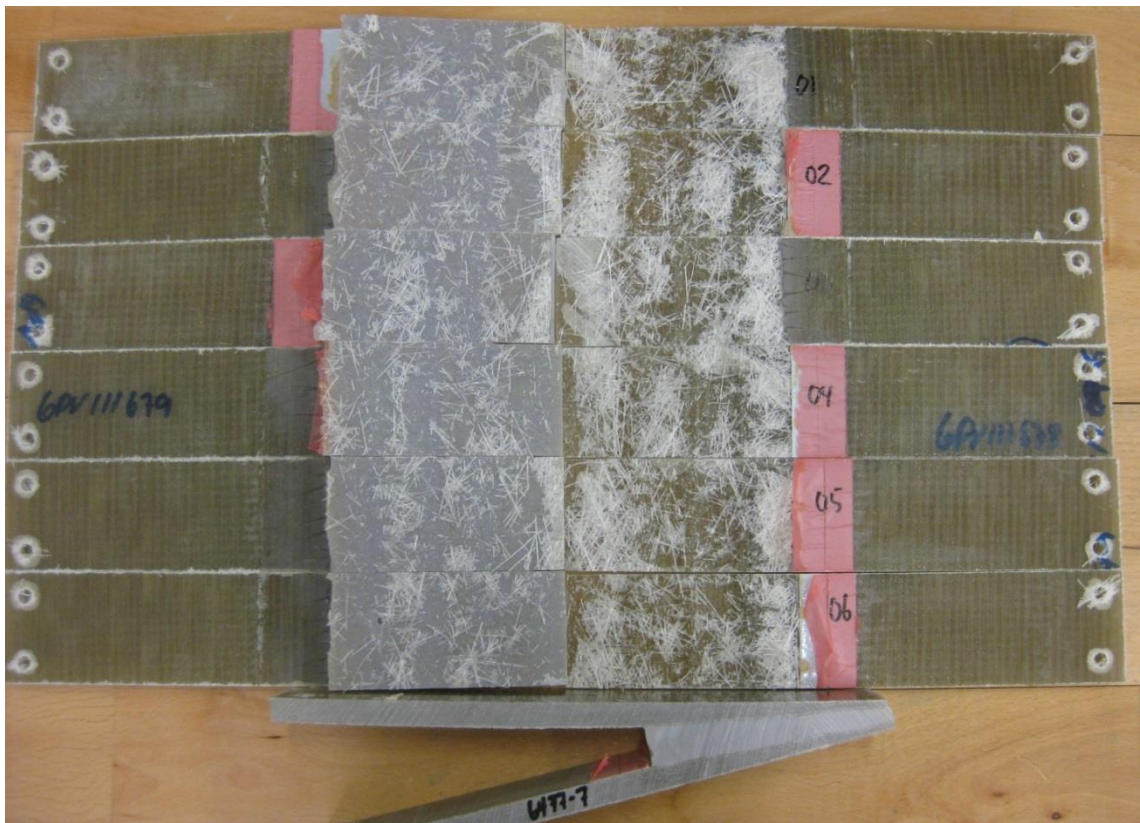


Figure 100: Failed specimens of the series 6477, test series h_1/t_2 , $\alpha = 15^\circ$, $t = 15\text{mm}$, $h = 10\text{mm}$

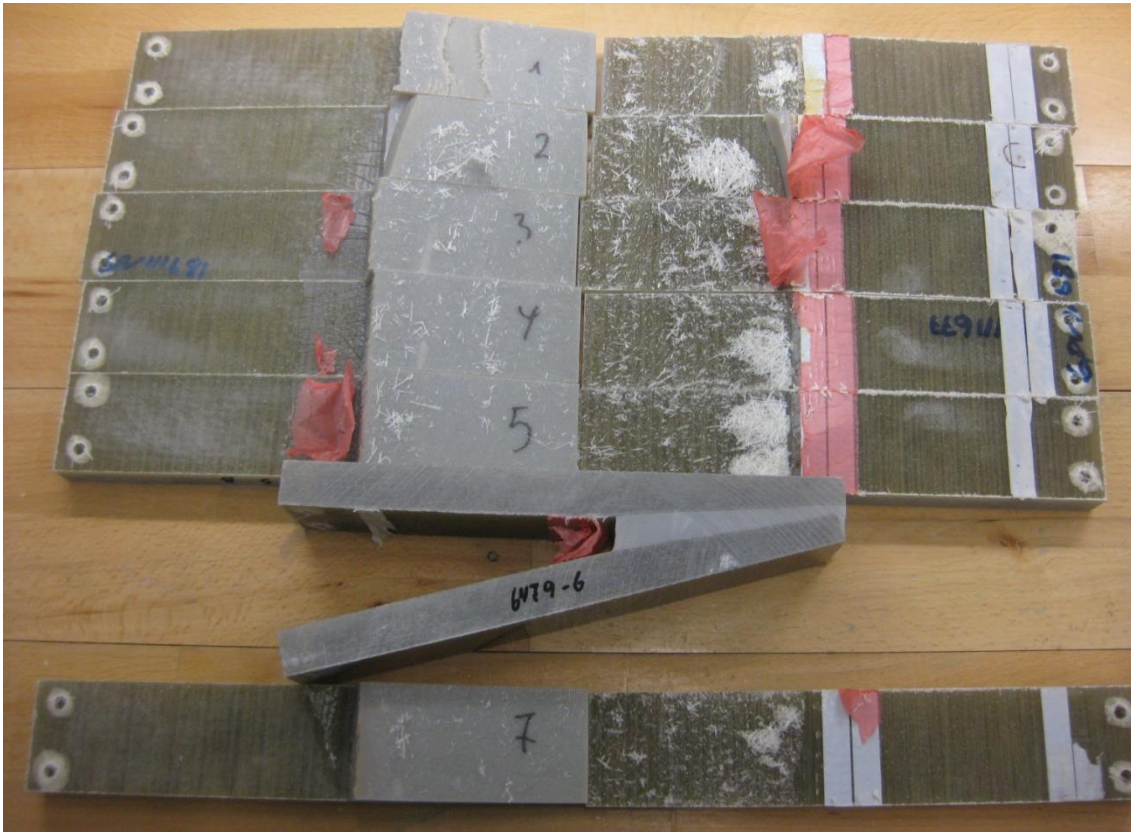


Figure 101: Failed specimens of the series 6479, test series h_2/t_2 , $\alpha = 15^\circ$, $t = 15\text{mm}$, $h = 20\text{mm}$

Acknowledgements

Magda Nielsen and Angelo Tesauro, former colleagues at DTU Wind Energy, are highly acknowledged for being in charge of the first two full-scale tests performed in the project. Also former colleague Find Mølholt Jensen is acknowledged for his major contribution to the application for this project.

The following persons have contributed to the project and their contributions are highly appreciated.

LM Wind Power A/S: Torben Lindby, Hank McShane, Cornelis van Beveren & Adrien Corre

SSP Technology A/S: Claus Burchardt, Flemming Sørensen & Christopher Stanley

Vestas Wind Systems A/S (until 2012): Tomas Vronsky & Jakob Wedel-Heinen

DNV GL AS: Christer Eriksson, Dayton Griffin, Tomasz Sieradzan, Ole Kjær, Bente

Vestergaard, Amilcar Quispitupa & Thomas Karl Petersen

Dong Energy: Bernt Pedersen & Jacob Kronborg Andersen

Blade Test Centre A/S: Carsten Skamris

Bladena ApS: Find Mølholt Jensen, Mikkel Lagerbon & Andrei Buliga

Baumer A/S: Anders Rosborg Hjulmann, Martin Jørgensen & Michael Weigel

German Aerospace Center (DLR): Alexander Kling & Tobias Wille

Swerea SICOMP AB: Sören Nilsson

Aalborg University: John Dalsgaard Sørensen & Henrik Stensgaard Toft

DTU Mechanical Engineering: Christian Berggreen & Jacob Herold Høgh

DTU Wind Energy (alphabetic order): Andreas Waage Borgen, Angelo Tesauro, Basel

Hayatleh, Christen Malte Markussen, Christian Pavese, Claus Brian Munk Pedersen, Erik

Vogeley, Federico Belloni, Gilmar Ferreira Pereira, Jan Sjølin, Jonas Kreutzfeldt Heininge,

Jonathan Shmueli Alvarado, José Pedro Blasques, Kim Branner, Magda Kirstine Nielsen,

Mahmoud Jabbari, Malcolm Mcgugan, Martin A. Eder, Per Hørlyk Nielsen, Peter Berring, Philipp

Ulrich Haselbach, Robert David Bitsche, Taeseong Kim, Thomas Buhl, Tom Løgstrup Andersen

& Vladimir A. Fedorov

Sorry if anybody is forgotten.

DTU Wind Energy is a department of the Technical University of Denmark with a unique integration of research, education, innovation and public/private sector consulting in the field of wind energy. Our activities develop new opportunities and technology for the global and Danish exploitation of wind energy. Research focuses on key technical-scientific fields, which are central for the development, innovation and use of wind energy and provides the basis for advanced education at the education.

We have more than 240 staff members of which approximately 60 are PhD students. Research is conducted within nine research programmes organized into three main topics: Wind energy systems, Wind turbine technology and Basics for wind energy.

Danmarks Tekniske Universitet

DTU Vindenergi
Nils Koppels Allé
Bygning 403
2800 Kgs. Lyngby
Telephone 45 25 25 25

info@vindenergi.dtu.dk
www.vindenergi.dtu.dk